1986

I. State-selected study of ion-molecule reactions using tandem molecular beam photoionization mass spectrometry; II. Absolute spin-orbit-state excitation cross sections for the reactions Ar+(2P3/2) + Ar(1S0) and Ar+(2P3/2) + N2(X~, v=0)

Jian-dong Shao
Iowa State University

Shao, Jian-dong

I. STATE-SELECTED STUDY OF ION-MOLECULE REACTIONS USING TANDEM MOLECULAR BEAM PHOTOIONIZATION MASS SPECTROMETRY. ii. ABSOLUTE SPIN-ORBIT-STATE EXCITATION CROSS SECTIONS FOR THE REACTIONS ARGON ION-2P(3/2) + ARGON-1S(0) AND ARGON ION-2P(3/2) + NITROGEN(X(TILDE),V = 0)

Iowa State University PH.D. 1986

PLEASE NOTE:

In all cases this material has been filmed in the best possible way from the available copy. Problems encountered with this document have been identified here with a check mark __✓__.

1. Glossy photographs or pages _____
2. Colored illustrations, paper or print _____
3. Photographs with dark background _____
4. Illustrations are poor copy _____
5. Pages with black marks, not original copy _____
6. Print shows through as there is text on both sides of page _____
7. Indistinct, broken or small print on several pages ✓
8. Print exceeds margin requirements _____
9. Tightly bound copy with print lost in spine _____
10. Computer printout pages with indistinct print _____
11. Page(s) _____ lacking when material received, and not available from school or author.
12. Page(s) _____ seem to be missing in numbering only as text follows.
13. Two pages numbered _____. Text follows.
14. Curling and wrinkled pages _____
15. Dissertation contains pages with print at a slant, filmed as received ✓
16. Other _____

_____

_____

I. State-selected study of ion-molecule reactions using tandem molecular beam photoionization mass spectrometry

II. Absolute spin-orbit-state excitation cross sections for the reactions $Ar^+(^2P_{3/2}) + Ar(^1S_0)$ and $Ar^+(^2P_{3/2}) + N_2(\tilde{X},v=0)$

by

Jian-dong Shao

A Dissertation Submitted to the
Graduate Faculty in Partial Fulfillment of the
Requirements for the Degree of
DOCTOR OF PHILOSOPHY

Department: Chemistry
Major: Physical Chemistry

Approved:

Members of the Committee:

Signature was redacted for privacy.

In Charge of Major Work

Signature was redacted for privacy.

Signature was redacted for privacy.

For the Major Department

Signature was redacted for privacy.

For the Graduate College

Iowa State University
Ames, Iowa

1986

TABLE OF CONTENTS

ACKNOWLEDGEMENTS

I would like to acknowledge a few of the many individuals to whom I am indebted for helping me in my long march toward an academic goal.

As my major professor, Dr. Cheuk-yiu Ng has guided and supported me through all my years at Iowa State University. Not only have I received academic knowledge from him, but the striving spirit as well. I am deeply indebted to Dr. Bernard C. Gerstein for his encouragement and empathy, especially during my first semester in the graduate college. His kindness and concern helped tide me over the most difficult time. Many thanks also to Dr. Klaus Ruedenberg for his patience and understanding. I can depend on him for help and inspiration when I have academic problems. I am grateful to Harold Skank for leading me into the computer hardware world. Without the knowledge gained from him, I would not have been able to automate the experimental system and to carry out the projects so efficiently. Also thanks to George Steininger and John Sauke for always being available for support. Especially I thank Eldon Ness, who not only gave me his best work, but also was a genius in providing ideas to overcome many difficulties which otherwise seemed insurmountable.

Dr. Bing-lin Young deserves more thanks than I ever can give. He not only made my study here possible, but also, with his wife, Theresa, provided sincere concerns and helps during my difficult time.

There are no words which can express my gratefulness to my parents for their loving, concerning, guiding, and encouraging. They always inspire me to do my best by pointing out the bright side of life and the future,

especially when I was depressed.

I want to express my heartfelt gratitude to my wife, Yao Chen, for her understanding and support throughout all my years. The time she has saved me and the love she has devoted to me have made my academic achievements possible.

GENERAL INTRODUCTION

The observation of ion-molecule reactions with mass spectrometers goes back as early as 1916 when Dempster[1] reported the observation of H_3^+ from the reaction $H_2^+ + H_2$. But the event which really spurred the study of ion-molecule reactions was the discovery of the reaction

$$CH_4^+ + CH_4 \longrightarrow CH_5^+ + CH_3$$

by Tal'roze and Lyubimova,[2] Stevenson and Schissler,[3] and Field et al.[4] independently in the early 1950s. Since then the investigation of ion-molecule reactions has been carried on quite actively, both experimentally and theoretically. Especially in the last 20 years, based on much-improved equipment, the emergence of new technologies and the rapid increase of computing speed, the interest in ion-molecule collision has spread very rapidly.

In the early stages of the development of interest in ion-molecule reactions, all studies were aimed at the measurement of rate constants. Starting from the conventional mass spectrometer, in which the ionization chamber served as the reaction gas cell, new instrumentation was designed or adapted specially for the study of collision reactions: pulsed source reactor[5], flowing afterglow technique[6], ion cyclotron resonance mass spectrometer,[7,8] tandem mass spectrometer[9,10] etc.

Since the 1960s, development of advanced technologies has made it possible to probe a rate process directly at the microscopic, molecular

level either experimentally or theoretically. Among them the most important are the molecular beam technique,[11] the vacuum ultraviolet (VUV) light source,[12-15] the laser as light source and probing measure[16], the coincidence technique,[17] and improved computer hardware and software.

Since the late 1970s studies of state-selected ion-molecule reaction have expanded rapidly, especially with the application of the coincidence technique. Even though the early studies were limited by the single cell arrangement, many significant results have been published about symmetric ion-molecule reactions[18-20] at low collision energies. An example is the study of the symmetric charge transfer reaction

$$O_2^+ + O_2 \longrightarrow O_2^+ + O_2$$

for different vibrational energy levels done by Baer et al.[19]

To extend the state-selected study into unsymmetrical ion-molecule collisions and to observe the effects of higher collision energies, a double cell experimental arrangement coupled with threshold electron-secondary ion coincidence (TESICO) was developed by Tanaka et al.[21] They studied the reaction

$$Ar^+(^2P_{3/2,1/2}) + H_2 \longrightarrow ArH^+ + H$$

Since low ion collection efficiency is inherent to their apparatus, their direct measurements were limited to relative cross sections.

In 1981, Anderson et al.[22] achieved no less than 98% ion collection efficiency by using the radio frequency (rf) octopole ion guide technique. They were able to measure the absolute total cross sections for state-selected reactions in a gas cell separated from the photoionization region. However, the lack of primary mass analysis in their apparatus, in contrast with the single cell experiment, prevented them from studying symmetric ion-molecule reactions. For example, the reaction

$$H_2^+ + H_2 \longrightarrow H_3^+ + H$$

can not be studied because of the formation of H_3^+ in the photoionization region.

By combining a VUV light source, molecular beam, and rf octopole ion guide techniques with tandem mass spectrometry, we have developed a photoionization tandem mass spectrometer. The first quadrupole mass filter (QMF) removes all the undesired ions produced in the photoionization region, and therefore makes it possible to measure absolute total cross sections for either symmetric or unsymmetric ion-molecule reactions. With this apparatus we have studied several state-selected ion-molecule reactions[23] (appears in Section II. and III. of Part I. herein) using collision energies up to E_{lab} = 280 eV:

$$H_2^+(v) + H_2(v'=0) \longrightarrow H_3^+ + H$$

$$Ar^+(^2P_{3/2,1/2}) + N_2(v=0) \longrightarrow N_2^+ + Ar$$

$$N_2^+(v) + Ar(^1S_0) \longrightarrow Ar^+ + N_2$$

Recently, we constructed a constructed a triple-quadrupole double-octopole photoionization mass spectrometer. With a specially designed experimental procedure, we were able to measure absolute cross sections for state-to-state collision induced energy transfer, such as (appears in Part II. herein)

$$Ar^+(^2P_{3/2}) + N_2(v=0) \longrightarrow Ar^+(^2P_{1/2}) + N_2$$

The advantage of this apparatus is the high ion collection efficiency for primary ions and product ions formed in both reaction gas cells. The internal state distributions of ions from the first reaction gas cell are then probed by further reacting with a neutral gas in the second reaction gas cell. Therefore, two sequential ion-molecule reactions can be conducted at one time and the corresponding absolute total cross sections can be measured. The first QMF is used to filter undesired ions produced in the photoionization region. The second QMF is used to select reactant ions for the ion-molecule reaction conducted in the second reaction gas cell. Hence this apparatus can be used to study both symmetric and asymmetric ion-molecule reactions.

The recent development of the capability to measure absolute total cross sections of state-selected and state-to-state ion-molecule reactions is only the beginning of a new chapter in the study of ion-molecule reactions. An accumulated data base of absolute total cross sections will

provide a good basis for the development of theoretical studies of state-selected and state-to-state ion-molecule reaction, which in turn will result in a better understanding of the reaction dynamics of ion-molecule interactions as a whole.

An expected further development is the coupling of the tandem mass spectrometer-rf octopole ion guide technique with the coincidence technique, and laser light source and laser probe in order to prepare the primary ion in a specific state and to measure the final state distribution directly.

References

1. A. J. Dempster, Phil. Mag. 31, 438 (1916).
2. V. L. Tal'roze and A. K. Lyubimova, Dokl. Akad. Nauk SSSR 86, 909 (1952).
3. D. P. Stevenson and D. O. Schissler, J. Chem. Phys. 23, 1353 (1955).
4. F. H. Field, J. L. Franklin, and F. W. Lampe, J. Am. Chem. Soc. 79, 2419 (1957).
5. V. L. Tal'roze and E. L. Frankevich, Zh. Fiz. Khim. 34, 2709 (1960).
6. F. C. Fehsenfeld, A. L. Schmeltekopf, P. D. Goldan, H. I. Schiff, and E. E. Ferguson, J. Chem. Phys. 44, 4087 (1966); P. D. Goldan, A. L. Schmeltekopf, F. C. Fehsenfeld, H. I. Schiff, and E. E. Ferguson, J. Chem. Phys. 44, 4095 (1966);
7. D. Wobschall, J. R. Graham, and D. P. Malone, Phys. Rev. 131, 1565 (1963).
8. L. R. Anders, J. L. Beauchamp, R. C. Dunbar, and J. D. Baldeschwieler, J. Chem. Phys. 45, 1062 (1966).

9. E. Lindholm, in Ion-Molecule Reactions in Gases, (Advances in Chemistry Series), ed. P. J. Ausloos (Washington, D. C.: American Chemical Society, 1966), pp. 1-19.

10. G. F. Giese and W. B. Maier, J. Chem. Phys. 39, 739 (1963).

11. Z. Herman, J. Kerstetter, T. L. Rose, and R. Wolfgang, J. Chem. Phys. 46, 2844 (1967).

12. K. Watanabe and E. C. Y. Inn, J. Opt. Soc. Am. 43, 32 (1953).

13. K. Watanabe, W. C. Walker and G. L. Weissler, J. Appl. Phys. 24, 1318 (1953).

14. K. Watanabe, Phys. Rev. 91, 1155 (1954).

15. J. A. R. Samson, Techniques of Vacuum Ultraviolet Spectroscopy, (New York: John Wiley & Sons, 1967).

16. N. G. (Ed.) Basov, Lasers and Their Applications in Physical Research, (New York: Consultants Bureau, 1979).

17. T. Baer, "State selection by photoion-photoelectron coincidence," in Gas Phase Ion Chemistry, ed. M. T. Bowers (New York: Academic Press, 1979), p. 153.

18. L. Squires, and T. Baer, J. Chem. Phys. 66, 4001 (1976).

19. T. Baer, P. T. Murray, and L. Squires, J. Chem. Phys. 68, 4901 (1978).

20. I. Koyano and K. Tanaka, J. Chem. Phys. 72, 4656 (1980).

21. K. Tanaka, J. Durup, T. Kato, and I. Koyano, J. Chem. Phys. 74, 5561 (1981).

22. S. L. Anderson, F. A. Houle, D. Gerlich, and Y. T. Lee, J. Chem. Phys. 75, 2153 (1981).

23. J. D. Shao and C. Y. Ng, J. Chem. Phys. 84, 4317 (1986).

EXPLANATION OF THESIS FORMAT

This thesis is separated into two parts. Part I is divided into three sections according to the ion-molecule reaction being studied. Part II has only one section, and is also formated as in Part I. Each section is an independent article prepared in a format ready for submission for publication. The experimental apparatus is described in detail in section I, and the specific operating conditions of the apparatus are presented in a brief experimental description in each section. A detailed description of the modified experimental apparatus is presented in Part II. The figures, tables, references and appendixes cited in each section refer only to those contained in that section. Some selected computer programs and the block diagram of the computer system are compiled in APPENDIX A and B at the end of this thesis.

PART I.

STATE-SELECTED STUDY OF ION-MOLECULE REACTIONS USING THE TANDEM MOLECULAR BEAM PHOTOIONIZATION MASS SPECTROMETRY

SECTION I.

A VIBRATIONAL STATE-SELECTED STUDY OF THE REACTION $H_2^+(v_0') + H_2(v_0''=0) \longrightarrow H_3^+ + H$ USING THE TANDEM PHOTOIONIZATION MASS SPECTROMETRY AND RADIO FREQUENCY ION GUIDE METHODS

Introduction

The simplicity of the reaction between H_2^+ and H_2 makes it a system of fundamental importance to molecular reaction dynamics. The $H_2^+ + H_2$ reaction and its isotopic variations have been investigated by nearly all accessible experimental techniques.[1-43] In spite of its apparent simplicity, the reaction is rich in chemistry. Combining the results of previous experimental and theoretical[44-45] studies, a qualitative picture about the $H_2^+ + H_2$ reaction has emerged. At low center-of-mass collision energies ($E_{c.m.}$), the major product channel is the formation of $H_3^+ + H$ which has the cross sections close to the predictions of the Langevin-Gioumousis-Stevens (LGS) model. In principle, the H_3^+ formation can result from the proton and the hydrogen atom transfer mechanisms. The isotopic substitution experiments[9,12,13] show that the cross sections for nominal proton and hydrogen atom transfer reactions are similar. This observation is interpreted to be the result of rapid charge equilibrium between the reactants H_2^+ and H_2, prior to H_3^+ formation. The $H_3^+ + H$ channel is

believed to proceed with a direct mechanism.[9,12-14,47-49,56] As $E_{c.m.}$ is increased, the cross section for H_3^+ formation decreases rapidly with concomitant increase in the cross section for charge transfer, indicating that the $H_3^+ + H$ and charge transfer channels are competing processes. At $E_{c.m.}>5$ eV, charge transfer, which is mainly governed by long range interactions, becomes the dominant product channel. In addition to the $H_3^+ + H$ and charge transfer channels, the formation of $H^+ + H + H_2$ is also a viable process where $E_{c.m.}$ is greater than the dissociation energy of H_2^+. In general, the cross section for the collision induced dissociation channel is much smaller[7,34] than those for the $H_3^+ + H$ and charge transfer channels.

Recently, several reliable theoretical calculations on the $H_2^+ + H_2$ system have been reported.[45-47] Stine and Muckerman have applied a variant[48] of the trajectory surface hopping (TSH) method[57] on H_4^+ valence bond diatomic-in-molecules (DIM) potential energy surfaces and have carried out extensive calculations[47] on the $H_2^+(v_0'=0,3,6;J_1=2) + H_2(v_0''=0;J_2=1)$ system at $E_{c.m.}=0.25$, 0.5, 1.0, 3.0, and 5.0 eV. The TSH model has been found to be successful in predicting absolute total cross sections for the reaction $H^+ + D_2$.[58] Combining the quasiclassical trajectory approach and a newly developed Fourier transform method, Baker and Schatz[45] have calculated cross sections for the $H_3^+ + H$ channel at $E_{c.m.}<1$ eV with an emphasis on the product H_3^+ rotational and vibrational distributions. State-to-state cross sections for the $H_2^+ + H_2$ charge transfer interactions have been calculated by Lee and DePristo[46] for $E_{c.m.}\geq 8$ eV using the semiclassical energy conserving trajectory (SECT) formulation.

As a model system, it is important to observe quantitative agreement between experimental measurements and theoretical predictions on the $H_2^+ + H_2$ system. Detailed state-selected cross-sectional data for the $H_2^+ + H_2$ charge transfer reaction over a wide $E_{c.m.}$ range have been obtained recently by Liao, Liao, and Ng.[2,3] The vibrational state distributions for the H_2 product ions resulting from the charge transfer collisions between H_2^+ (v_0'=0 or 1) and H_2 (v_0''=0) at $E_{c.m.}$=2-16 eV have been determined by Liao and co-workers.[3,59] The results of these experiments have been found to be in satisfactory agreement with the SECT theoretical predictions of Lee and DePristo.[46]

The first state-selected experiment on the reaction

$$H_2^+(v_0') + H_2(v_0''=0) \longrightarrow H_3^+ + H \qquad (1)$$

was performed by Chupka, Russell, and Refaey.[25] Vibrational state-selected total cross sections, $\sigma(v_0')$, for reaction (1) at $E_{c.m.}$<1 eV also were measured by Koyano and Tanaka[8] and van Pijkeren et al.[1] using the photoion-photoelectron coincidence technique. In all these experiments, both photoionization and reaction took place in a single gas cell. Due to a continuous potential drop across the gas cell, the collision energy was ill-defined. Cross sections thus obtained are phenomenological cross sections and represent velocity averages over the microscopic cross sections. In order to compare experimental results with theoretical predictions, appropriate conversion of phenomenological cross sections to microscopic cross sections is necessary. However, there are severe

limitations on the accuracy to which microscopic cross sections can be derived by these means.[60]

Recently, Anderson et al.[7] combined the photoionization and the guide beam technique[61] and measured the microscopic total cross sections for several isotopic $H_2^+ + H_2$ reactions for $v_0'=0-4$ over the $E_{c.m.}$ range of 0.23-6.1 eV. However, because of the high intensity of H_3^+ background produced at the photoionization source, they were not able to study reaction (1).

In an effort to obtain accurate microscopic state-selected total cross sections for reaction (1) over a wide $E_{c.m.}$ range, we have developed a new tandem photoionization mass spectrometer. The experimental setup is similar to that used by Anderson et al.,[7] except that a quadrupole mass filter is used to reject H_3^+ background formed at the photoionization region. The experimental results at $E_{c.m.}=0.04-15$ eV are presented here and compared with previous experimental and theoretical findings.

EXPERIMENTAL

The apparatus essentially consists of a 0.2m vacuum ultraviolet (VUV) monochromator (McPherson 234), a discharge lamp, a tungsten photoelectric VUV light detector, two quadrupole mass filters (QMF), a radio frequency (rf) octopole ion guide, a reaction gas cell, a supersonic free jet production system, and a variant of the Daly scintillation ion detector.[62-64]

The detailed cross-sectional view of the tandem photoionization mass spectrometer, showing the differential pumping arrangement, is depicted in Fig. 1. The vacuum system is partitioned into four chambers: the photoionization chamber (1), the QMF chamber (6), the rf octopole chamber (7), and the detector chamber (13). These chambers are connected only through small apertures. Each of these chambers is evacuated by a separate pumping system which is described below.

The reactant H_2^+ ions are prepared by photoionization of a H_2 free jet produced by supersonic expansion through a quartz nozzle (2) at a stagnation pressure of $\leq$200 Torr. The nozzle has a diameter of ~50μm and is positioned ~1 cm from the photoionization region. A quartz nozzle is used in order to reduce the disturbance on the electric field in the photoionization region. The ion exit aperture of the photoionization region is covered by a high (90%) transmission gold grid to minimize the field penetration into the photoionization region from the adjacent focusing ion lenses. The photoionization chamber, pumped by a freon-trapped 6 in. diffusion pump (DP), maintains a pressure of ~1.5×10^{-5} Torr during the

Figure 1. Cross-sectional view of the tandem photoionization mass spectrometer. (1) Photoionization region, (2) quartz nozzle, (3) to freon-trapped 6 in. diffusion pump (DP), (4) the first quadrupole mass filter (QMF), (5) to liquid-nitrogen (LN_2)-trapped 6 in. DP, (6) the first QMF chamber, (7) the ratio frequency (rf) octopole ion guide chamber, (8) the reaction gas cell, (9) the rf octopole ion guide, (10) auxiliary molecular beam port, (11) to LN_2-trapped 4 in. DP, (12) the second QMF, (13) detector chamber, (14) to LN_2-trapped 2 in. DP, (15) photomultiplier tube, (16) plastic scintillator window, (17) aluminum ion target

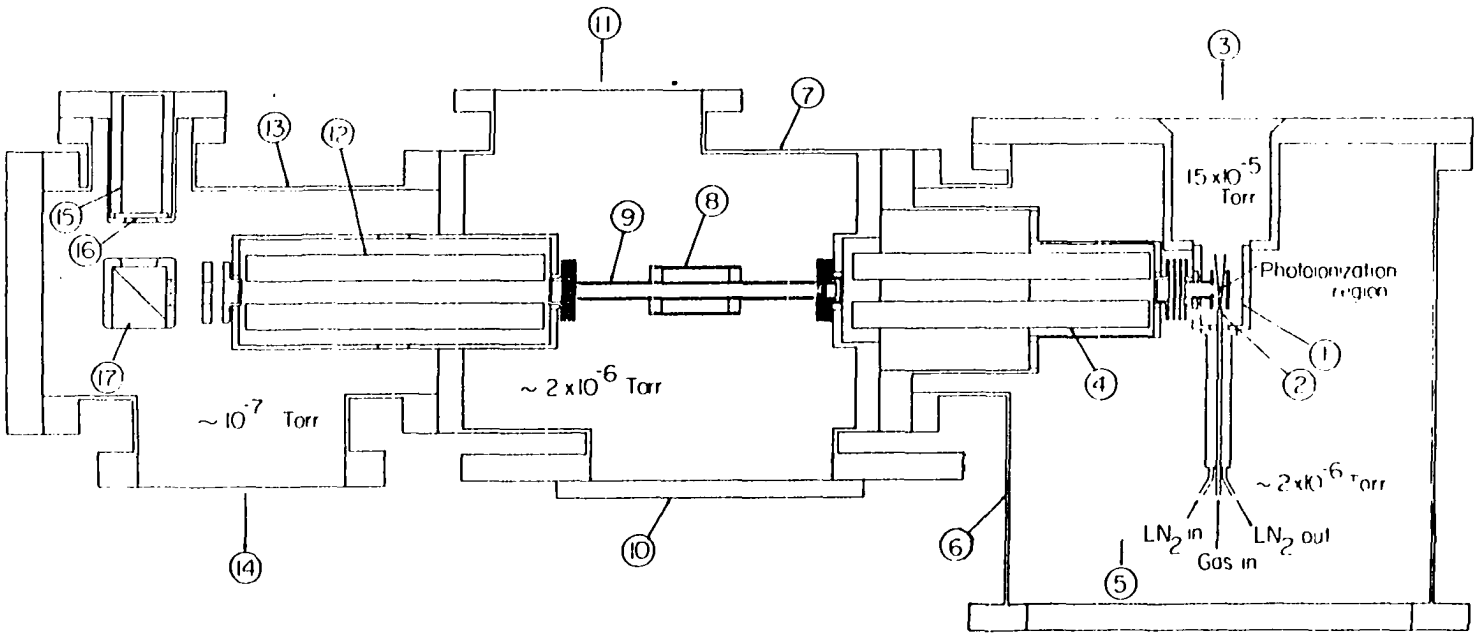
11
3
7
13
12
15
16
9
8
15 x10^-5 Torr
Photoionization region
17
~ 10^-7 Torr
~ 2 x10^-6 Torr
4
1
2
~ 2x10^-6 Torr
14
10
6
LN2 in
Gas in
LN2 out
5

experiment.

The reactant H_2^+ ions, together with H_3^+ background ions formed at the photoionization region, are extracted perpendicular to the H_2 beam. By tuning the first QMF (4) to the mass of H_2^+ (m/z=2), the H_3^+ background is completely rejected and a pure reactant H_2^+ beam is selected to enter the rf octopole ion guide (9). The first QMF chamber is pumped by a liquid-nitrogen (LN_2) trapped 6 in. DP and has a pressure of ~$2X10^{-6}$ Torr.

The rf octopole ion guide is constructed of eight molybdenum rods, with a diameter of 1.59 mm and a length of 17 cm, symmetrically spaced in a circle of 1 cm diameter. Since the trapping efficiency of a given ion in the octopole ion guide depends on the applied rf and rf peak voltage (V_0), it is important to be able to maximize the collection efficiency of a product ion by varying the rf and V_0. The rf power source used here consists of a signal generator and an rf linear power amplifier. Using an impedance matching network, the rf in the range of 5-24 MHz is applied to the octopole ion guide. The maximum value of V_0, which can be delivered by the rf power source, depends on the rf. For the low mass H_3^+ and H_2^+ ions, an rf of ~23 MHz is used, and the value for V_0 can be varied up to ~300 V. We find that 180 V is sufficient to attain ~99% collection efficiency[65] for H_2^+ and H_3^+. The collection efficiency is carefully optimized at each $E_{c.m.}$ except at $E_{c.m.}$=0.25 eV, where a collection efficiency of 98.5% is obtained.

The 7 cm long reaction gas cell (8) is positioned at the center of the ion guide. The reaction gas cell and the octopole are connected to the same dc potential. We find experimentally that the collision energy can be

altered due to field penetration from the gas cell into the octopole ion guide when the gas cell and the octopole are at different dc potentials.

Since the sections of the octopole ion guide outside of the reaction gas cell are fully exposed to the pumping system of the octopole ion guide chamber, the density of reactant H_2 in these regions is nearly two orders of magnitude lower than that of the reaction gas cells. Thus, the intensity of H_3^+ formed along the octopole ion guide outside of the reaction gas cell is expected to be negligibly small.

The electrostatic field between the ion lenses at both ends of the octopole ion guide is usually set up such that the product ions formed in the reaction gas cell are directed toward the second QMF (12) where the intensities of H_2^+ and H_3^+ are measured. In such an arrangement, we estimate that the error on the collision energy due to field penetration to the reaction gas cell from the focusing ion lenses is estimated to be less than 0.1 eV. The lower collection efficiency observed at $E_{c.m.}$=0.25 eV is attributed to the fact that some of the backward scattered H_3^+ ions are lost because an effective retarding voltage cannot be applied to ion lens at the entrance of the octopole ion guide.

The two QMFs used in this apparatus have the same design. They are constructed of four stainless steel rods, have a diameter of 1.9 cm and a length of 21 cm, and are symmetrically held in a circle of 3.55 cm diameter. The resolution of the second QMF is set to give flat-top structures for the mass 2 and mass 3 peaks. Such a resolution setting ensures that the transmission factors for the H_2^+ and H_3^+ are the same.

The rf octopole ion guide chamber is evacuated by a 4 in. LN_2-trapped DP, has a base pressure of ~$1X10^{-7}$ Torr, and is maintained at ~$2X10^{-6}$ Torr during the experiment. The pressure of H_2 in the reaction gas cell is ~$1X10^{-4}$ Torr and is monitored with a Baratron manometer (MKS model 315 HS-1).

Previous experimental studies show that $\sigma(v_0')$ for reaction (1) at low collision energies are large. It is expected that low energy H_2^+ ions produced by charge transfer may further react with H_2 in the reaction gas cell to give background H_3^+. At $E_{c.m.} \leq 5$ eV, we find that the H_3^+ product intensity is linearly proportional to the H_2 gas cell pressure in the range of $(0.1\text{-}2.5)X10^{-4}$ Torr indicating that H_2^+ ion intensities produced by secondary processes are not significant in comparison with those formed by the primary reaction. The intensity of H_3^+ clearly deviated from linearity only when the H_2 gas cell pressures are $>3X10^{-4}$ Torr. Within experimental uncertainties, the H_3^+ ion intensities observed at $E_{c.m.} \geq 6$ eV can also be fitted by a straight line in the H_2 gas cell pressure range of $(0.2\text{-}2)X10^{-4}$ Torr. Since the H_3^+ ion intensities observed at $E_{c.m.} \geq 6$ eV and at H_2 gas cell pressures $<5X10^{-5}$ Torr are very low and have high uncertainties, the linear fits at $E_{c.m.} \geq 6$ eV may not be unique.

In order to obtain estimates of the error bounds for $\sigma(v_0')$, we have replaced H_2 by D_2 in the octopole gas cell and measured the formation of D_3^+ as H_2^+ ions enter the reaction gas cell at various $E_{c.m.}$. The D_3^+ are most likely formed by the secondary reaction $D_2^+ + D_2$ in the reaction gas cell subsequent to the charge transfer reaction between H_2^+ and D_2. The fact that D_3^+ can be distinguished from H_2D^+ and D_2H^+ allows realistic

estimates for the extent of secondary reactions taking place in the reaction gas cell at different $E_{c.m.}$. Based on these measurements, we estimate that the contribution by secondary reactions to the observed intensity of H_3^+ is $\leq$10% at $E_{c.m.} \leq 1$ eV and up to ~40% at $E_{c.m.}$~15 eV. The values for $\sigma(v_0')$ at $E_{c.m.} \geq 2$ eV measured here possibly represent upper bounds. Values for $\sigma(v_0')$ at $E_{c.m.}$=6, 8, 10 ,12, and 15 eV may be 25%-40% too high.

The vibrational dependences for $\sigma(v_0')$ measured at high $E_{c.m.}$ (>1 eV) are also expected to be affected by secondary gas cell reactions. At the $E_{c.m.}$ range of 1-5 eV, we find that the vibrational dependence of $\sigma(v_0')$, deduced from the photoionization efficiency (PIE) spectra of H_3^+, is independent of H_2 gas cell pressure in the range of $(0.2\text{-}2)\times10^{-4}$ Torr. Figures 2(a), 2(b), and 2(c) show the PIE spectra for H_3^+ observed at $E_{c.m.}$=4 eV and H_2 gas cell pressures of 0.2, 1, and 2.3×10^{-4} Torr, respectively. With the exception of minor details, which are attributable to poor counting statistics at low H_2 gas cell pressures, the spectra shown in Fig. 2(a)-2(c) are essentially superimposable. Due to the very low signals observed for H_3^+ at $E_{c.m.} \geq 6$ eV and low gas cell pressures it is not feasible to examine the H_2 gas cell pressure effect on the vibrational energy dependence of $\sigma(v_0')$ at H_2 gas cell pressures below 5×10^{-5} Torr. The relative values for $\sigma(v_0')$ at the $E_{c.m.}$ range of 6-15 eV vary by ~10% when the H_2 gas cell pressure is changed from 0.5 to 2×10^{-4} Torr. These observations suggest that secondary reactions have a lesser effect on the vibrational energy dependences of $\sigma(v_0')$ than on the absolute values for $\sigma(v_0')$. If the cross sections for charge transfer and H_3^+ formation at a

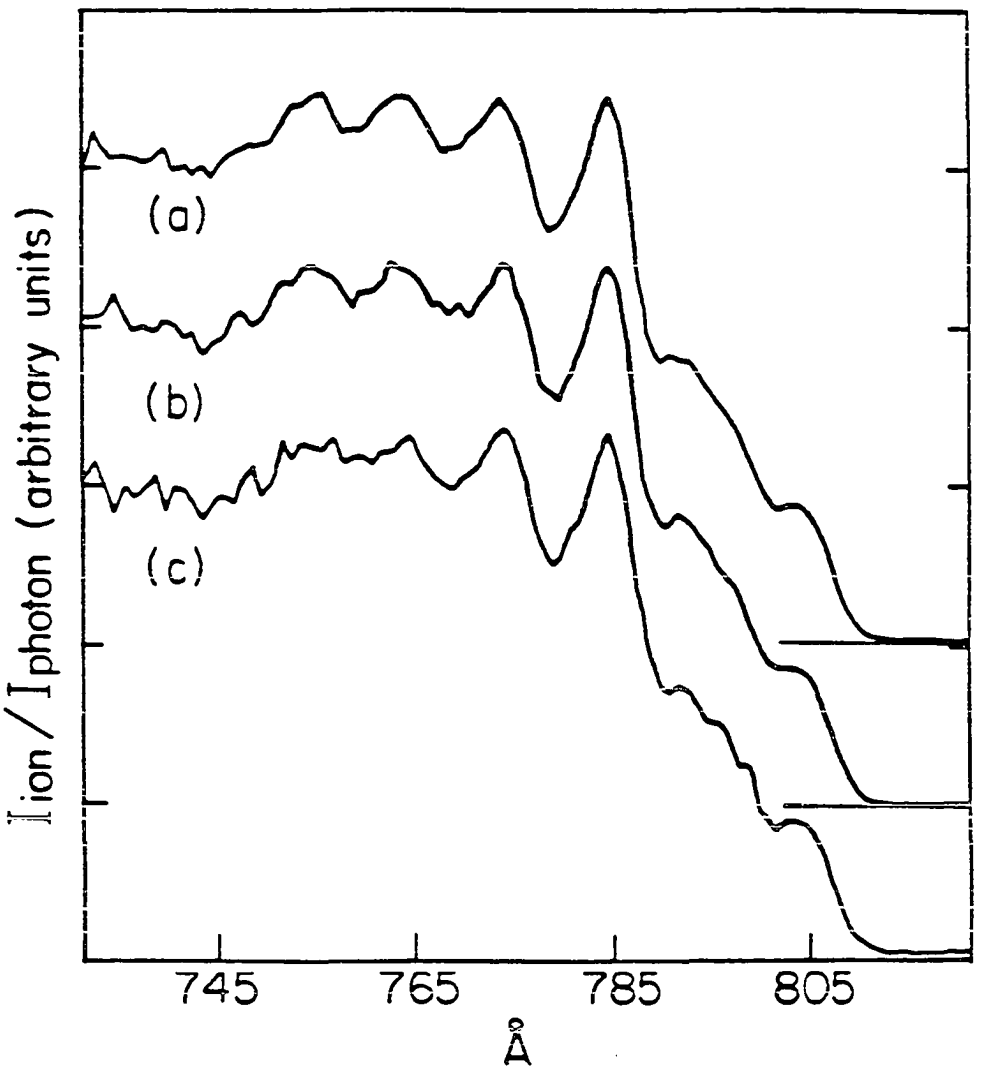

Figure 2. PIE curve for the H_3^+ product ions formed at $E_{c.m.}$ = 4 eV and at H_2 gas cell pressures of (a) 2 x 10^{-4} Torr, (b) 1 x 10^{-4} Torr, and (c) 0.2 x 10^{-4} Torr

given $E_{c.m.}$ have similar vibrational dependences, the errors for the relative cross sections of reaction (1) will be suppressed. We believe the relative standard deviations for the relative values of $\sigma(v_0')$, $v_0'=0-4$, at $E_{c.m.}$ ranges 1-5 and 6-15 eV contributed by secondary reactions in the gas cell are $\leq$10% and $\leq$20%, respectively.

The H^+ ion intensities observed at the $E_{c.m.}$ range of interest here are nearly within the noise level and are significantly lower than the intensities for H_3^+. This observation is consistent with the previous measurements[7] that the cross section for the collision induced dissociation channel is $\leq$1.5 $\AA^2$. The low H^+ intensities in comparison to those for H_3^+ also eliminate the possibility for the secondary collisional dissociation of product H_3^+ in the reaction gas cell as a source of error for $\sigma(v_0')$.

The ion detector chamber is pumped by a LN_2-trapped 2 in. DP and has a pressure of ~1X10^{-7} Torr. The ion detector is a variant of the Daly scintillation ion detector[62-64] and consists of a photomultiplier tube (15), a scintillator window (16), and a polished stainless steel box (17). The ion entrance aperture of the stainless steel box is covered by a 90% transmission gold grid. During the experiment, the aluminum ion target and the stainless steel box assembly is floated at -20 kV, while the photomultiplier holder and the scintillator window are held at the ground potential. In this arrangement, the observed dark noise of the ion detector is ~1 count/s. Using a different voltage arrangement, the scintillating detector can detect negative ions.

The grating employed in this study is a Jobin Yvon 1200 lines/mm MgF_2 coated holographic grating (J-20 VUV) blazed at 1600 $\AA$. Using ~100 μm

entrance and exit slits, the wavelength resolution achieved is 4.5 Å (FWHM), similar to that used by Anderson et al.[7] The tungsten photoelectric detector is used in the electron loss mode to transfer the photon flux into current which is then measured by a picoammeter (Keithley model 602). The analogue output of the picoammeter is converted into digital signals by a voltage-to-frequency converter and the digital signals are then counted. The PIE curves presented in this experiment have been corrected for the photoelectric yield of tungsten.[66] The design of the discharge lamp and the differential pumping arrangement of the windowless light source monochromator assembly are the same as described in Refs. 68. The helium Hopfield continuum is used as the light source. The observed intensity of reactant H_2^+ ion is ~10^5 counts/s.

The laboratory collision energy (E_{lab}) is defined by the difference in potential between the photoionization region and the reaction gas cell. Due to the finite height (~4 mm) of the photon beam in the photoionization region and the finite repeller field applied to the repeller, the reactant H_2^+ beam arriving at the reaction gas cell has a spread in kinetic energy. The kinetic energy resolution (ΔE) is proportional to the potential difference of the repellers (ΔV) and can be determined by the retarded field method. Figures 3(a) and 3(b) show the reactant H_2^+ ion beam intensities measured as a function of the retarding voltage applied to the octopole ion guide at ΔV=2 and 1 V, respectively. The ΔE value for ΔV=2 is $\pm$0.6 eV and that for ΔV=1 is $\pm$0.3 eV. At E_{lab}=10-30 eV, ΔV is set at 1.0 V in this experiment. Since the ΔV values used are $\leq$0.4V at E_{lab}<10 eV, the corresponding ΔE values are expected to be $\leq\pm$0.12 eV. The most serious

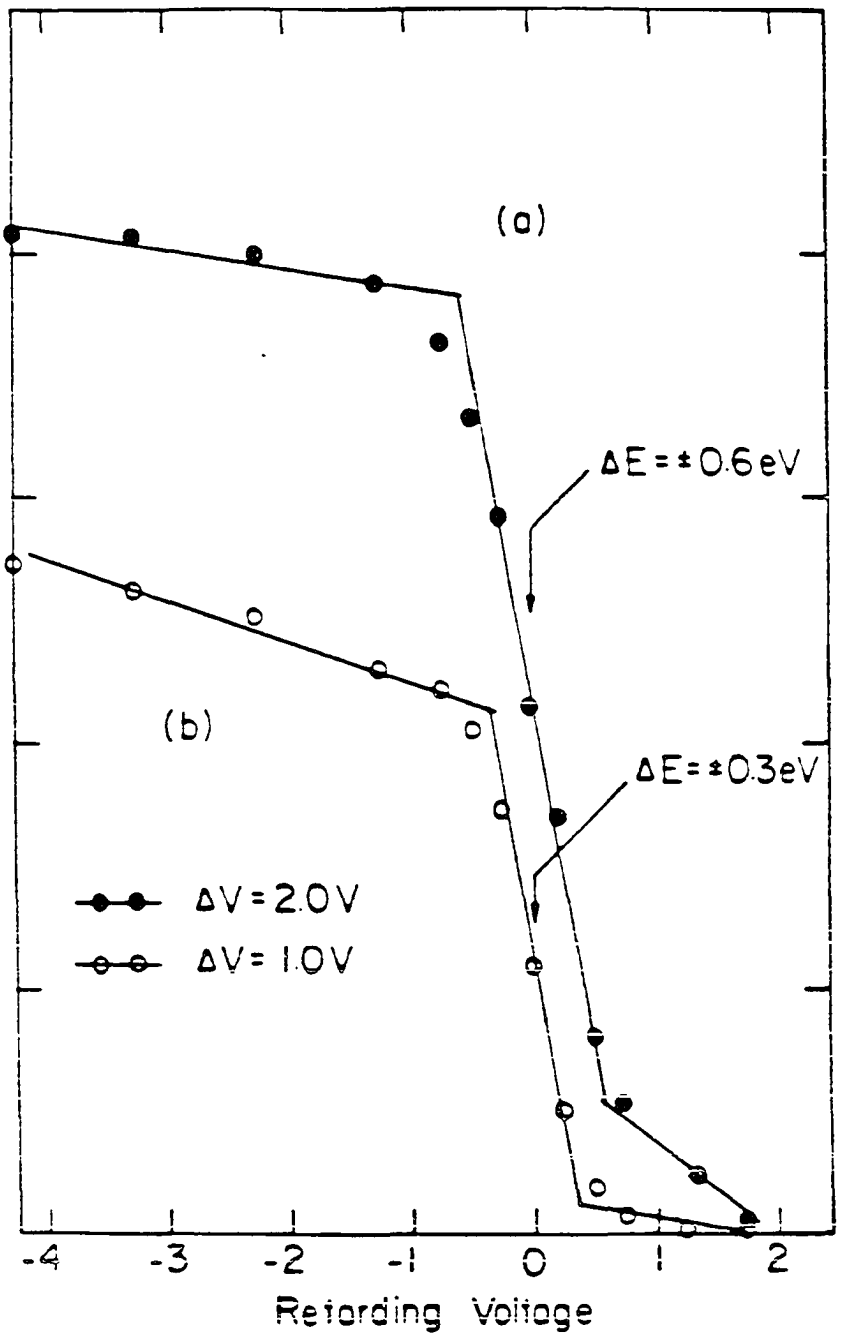

Figure 3. Retarding potential energy curves for the reactant H_2^+ ion beam. (a) Potential difference between the repeller ΔV = 2.0 V. (b) ΔV = 1.0 V

factor, which affects ΔE in an ion beam gas cell experiment such as this, is due to the random thermal motion of the neutral H_2 reactant molecules in the gas cell. This effect has been discussed in detail recently.[3,7,68] In order to eliminate the random thermal motion or the Doppler broadening effect, it is necessary to replace the reaction gas cell with a supersonic molecular beam. A molecular beam can be introduced in the octopole ion guide in the future by coupling a molecular beam source to the auxiliary molecular beam port (10). However, due to the unknown beam density at the reaction region, the molecular beam method is only suitable for relative cross section measurements.

The data acquisition and operation of the apparatus are controlled by minicomputer (LSI11/23) and are fully automatic. The results presented here are based on at least three independent measurements at each $E_{c.m.}$.

RESULTS AND DISCUSSION

Figure 4 compares the PIE curves for the reactant H_2^+ and product H_3^+ ions obtained at $E_{c.m.}$=0.04-15 eV. The PIE curves for H_2^+ are obtained when the reaction gas cell is empty. Since the relative standard deviations for these PIE data are less than 2%, the PIE data for H_2^+ and H_3^+ are connected by solid or dashed lines, respectively. The PIEs of the product H_3^+ and reactant H_2^+ ions in the region of 790-805 Å, which corresponds to the formation of reactant H_2^+ in the ground vibrational state, are normalized to have the same values. The PIE spectrum for H_3^+ at thermal energy ($E_{c.m.}$=0.04 eV) is obtained by measuring the PIE for H_3^+ formed at the photoionization region with the repeller voltage in the photoionization region maintained at a negligibly small value ($\leq$0.05 V). These comparisons clearly show that as v_0' is increased $\sigma(v_0')$ for reaction (1) at $E_{c.m.}$=0.04, 0.25, 0.46, 10, and 15 eV are inhibited by vibrational excitations of the reactant H_2^+ while those at $E_{c.m.}$=1, 2, 3, and 5 eV are enhanced.

The work of Chupka and co-workers[69-71] shows that because of the dominance of autoionization with $\Delta v=-1$, H_2 ions produced by autoionization are formed predominantly in the highest possible vibrational state. The wavelength resolution used in this study is not sufficient to resolve the detailed autoionization structure. Thus, vibrational distribution of H_2^+ formed in a given wavelength interval depends on the contributions by autoionization as well as direct ionization. Using the high resolution PIE spectrum for H_2^+ obtained by Dehmer and Chupka,[71] Anderson et al.[7] have

Figure 4. The comparisons of PIE curves for the H_3^+ product ions (——) formed at the $E_{c.m.}$ range of ~0.04-15 eV with that for the $H_2^+(v_0')$ reactant ion (– –)

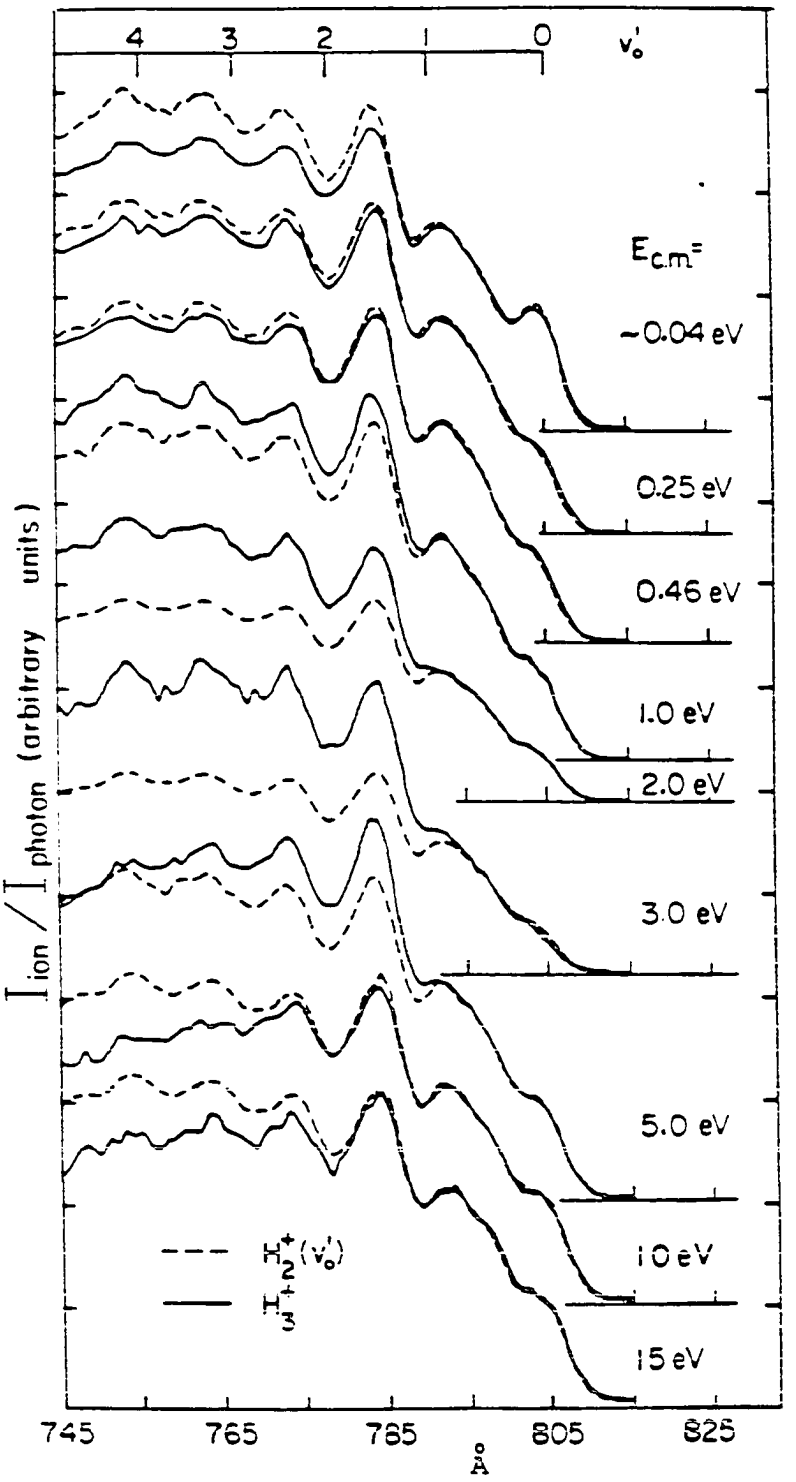
4
3
2
1
0
v_o'
$E_{c.m.}$=
~0.04 eV
0.25 eV
0.46 eV
1.0 eV
2.0 eV
3.0 eV
5.0 eV
10 eV
15 eV
I_{ion} / I_{photon} (arbitrary units)
$H_2^+(v_o')$
H_3^+
745
765
785
805
825
Å

estimated the ratio of H_2^+ produced by direct photoionization to that produced by autoionization. This ratio, together with the assumption that the vibrational distributions of H_2^+ formed by direct photoionization are governed by Franck-Condon factors for transitions from $H_2(X^1\Sigma_g^+,v) \longrightarrow H_2^+(X^2\Sigma_g^+,v_0')$, allows Anderson et al. to deduce the vibrational distributions of H_2^+ resulting from photoionization in the wavelength region (745-805 Å) corresponding to the first five vibrational intervals. Since the wavelength resolution used here is similar to that employed by Anderson et al., the same procedures and vibrational distributions of reactant H_2^+ as reported by Anderson et al.[7] are used to deconvolute the experimental data.[72]

The previous studies of reaction (1) have been limited to $E_{c.m.}$<1 eV. Figures 5(a)-5(f) show the relative total cross sections, $\sigma(v_0')/\sigma(v_0'=0)$, where v_0'=0-4, at $E_{c.m.}$=0.04, 0.25, 0.46, 0.5, 0.75, and 1.0 eV, deduced in this study. The experimental results obtained by Koyano and Tanaka and van Pijkeren et al.[1] are included in Figs. 5(a), 5(c), and 5(f). The relative cross sections at thermal energy reported by van Pijkeren et al. are found to be in good agreement with those determined here [Fig. 5(a)], indicating that the vibrational distributions of H_2^+ used in the deconvolution are reliable. At $E_{c.m.}$=0.46 eV, the results of both Koyano and Tanaka, and this study, show vibrational inhibition on $\sigma(v_0')$. Although the values for $\sigma(v_0')/\sigma(v_0'=0)$, where v_0'=1-3, obtained by Koyano and Tanaka appear to be lower than those deduced here [Fig. 5(c)], the two results are within experimental uncertainties. In a single chamber experiment,[8,25] the uncertainty in collision energy ΔE becomes greater as $E_{c.m.}$ is increased.

Figure 5. Relative total cross sections $\sigma(v_0')/\sigma(v_0'=0)$ for reaction (1) at $E_{c.m.}$ = 0.04–1 eV plotted as a function of vibrational quantum number v_0'. (•) This work; (x) mean values of proton and atom transfer (Ref. 7); (o) Ref. 1; (Δ) Ref. 47; (⊡) Ref. 45; (+) Ref. 8

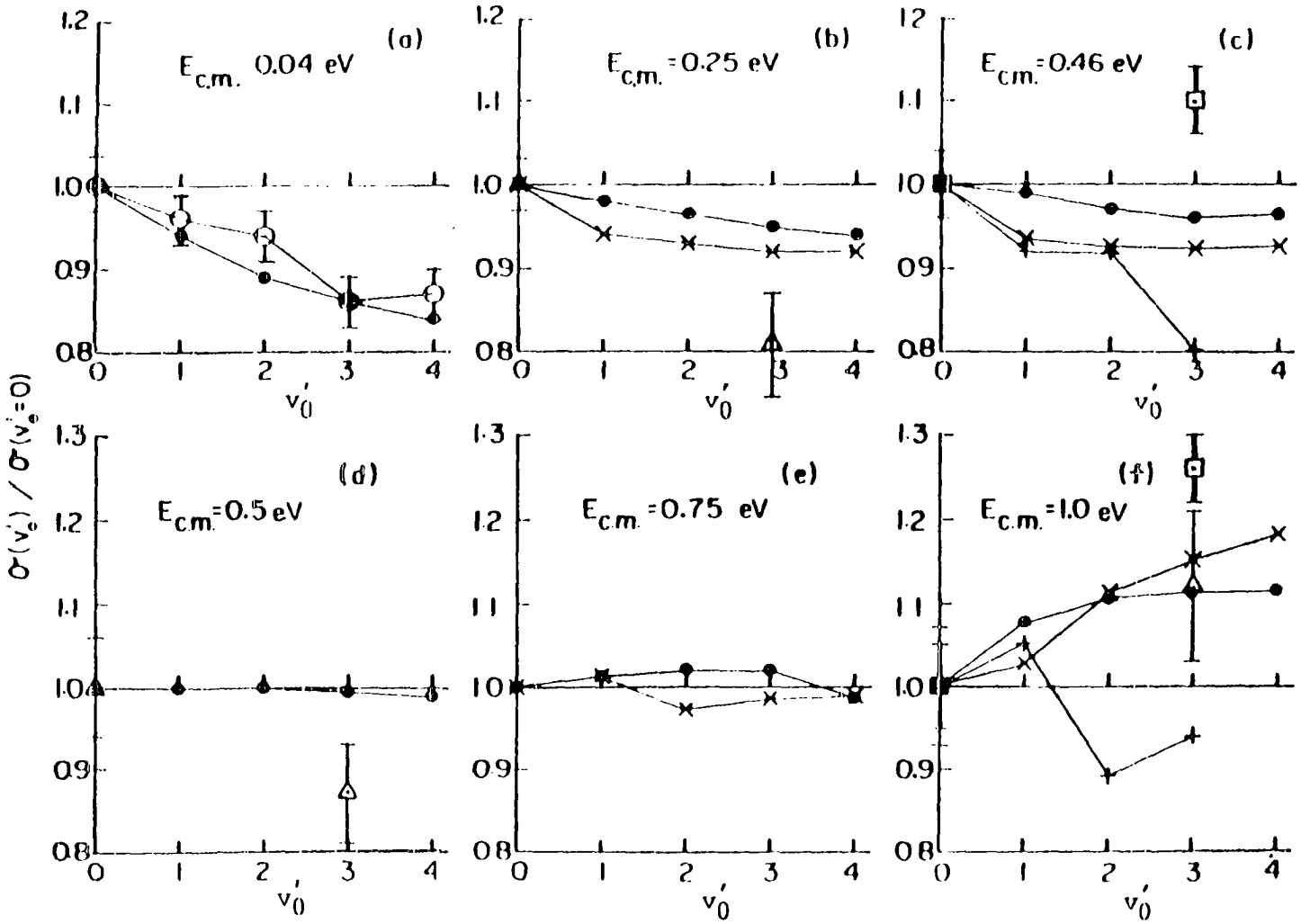
(a)
E c.m. 0.04 eV
(b)
E c.m. = 0.25 eV
(c)
E c.m. = 0.46 eV
(d)
E c.m. = 0.5 eV
(e)
E c.m. = 0.75 eV
(f)
E c.m. = 1.0 eV
σ(v'0) / σ(v'0=0)
v'0

In Fig. 5(f), the experimental results at an average $E_{c.m.}$ of 0.93 eV obtained by Koyano and Tanaka are compared to those at $E_{c.m.}$= 1.0 eV found in the present study. The difference in collision energy of the two sets of results is within the uncertainties in $E_{c.m.}$ of both experiments. The results of Koyano and Tanarka show that the values for $\sigma(v_0')$, where v_0'=2 and 3, are slightly lower than that for $\sigma(v_0'=0)$, contrary to the observation of this experiment. A recent state-selected study using the crossed ion-neutral beam method[3] shows qualitatively that vibrational excitations of the reactant H_2^+ ions have a negligible effect on $\sigma(v_0')$ at $E_{c.m.}$=1 eV. Since the collection efficiency for H_3^+ is poor, their results are less accurate than those reported here.

Absolute cross sections for the reactions

$$H_2^+(v_0') + D_2 \longrightarrow D_2H^+ + H \qquad (2)$$

$$D_2^+(v_0') + H_2 \longrightarrow D_2H^+ + H \qquad (3)$$

have been measured by Anderson et al.[7] The formation of D_2H^+ by reaction (2) and (3) are referred to as the nominal proton and atom transfer reactions, respectively. If an electron hops repeatedly between H_2^+ and H_2 in the reaction channel prior to the formation of H_3^+,[7,13,47-49] the value for $\sigma(v_0')$ of reaction (1) should be in accord with the mean value of the total cross sections for reaction (2) and (3). We have obtained the mean values of the total cross sections for the nominal proton and atom transfer reactions by scaling the experimental results plotted in Fig. 3 of Ref. 7. The mean values for $\sigma(v_0')/\sigma(v_0'=0)$, where v_0'=0-4, at $E_{c.m.}$=0.23, 0.43,

0.77, and 1.1 eV of proton and atom transfers are in good agreement with those determined in this experiment, as shown in Figs. 5(b), 5(c), 5(e), and 5(f), respectively. This observation gives strong support for the rapid charge hopping interpretation.

For $E_{c.m.} \leq 1$ eV, the results of two theoretical calculations are available to compare with the experimental data. Trajectory calculations by Stine and Muckerman[47,48] and by Eaker and Schatz[45] provide only $\sigma(v_0')$, where $v_0'=0$ and 3, for reaction (1). Their results, including the standard deviations, are shown in Figs. 5(b), 5(c), 5(d), and 5(f). The fact that only a finite number of trajectories were sampled in their calculations causes large uncertainties in the theoretical results. Taking into account the uncertainties of the calculated and experimental values, the theoretical predictions of Stine and Muckerman at $E_{c.m.}=0.25$, 0.5, and 1.0 eV are in agreement with the experimental measurements. At $E_{c.m.}=0.46$ eV, the calculations of Eaker and Schatz predict vibration enhancement for $\sigma(v_0')$, whereas the experimental values show the opposite trend. Their value of 1.2[6] for $\sigma(v_0'=3)/\sigma(v_0'=0)$ at $E_{c.m.}=0.93$ eV is higher than the experimental value of 1.12.

The experimental values for $\sigma(v_0')/\sigma(v_0'=0)$, where $v_0'=0$–4, measured over the $E_{c.m.}$ range of 2–15 eV are plotted in Figs. 6(a)–6(i). Similar to the observation in Fig. 4, vibrational enhancement for $\sigma(v_0')$ reaches a maximum near $E_{c.m.}=3$ eV. As $E_{c.m.}$ is further increased in the range of 3–15 eV the values for $\sigma(v_0' \geq 0)$ decrease steadily with respect to $\sigma(v_0'=0)$. At $E_{c.m.}=12$ and 15 eV, $\sigma(v_0')$ is found to decrease monotonically as a function of v_0'. The relative values for $\sigma(v_0')$, $v_0'=0$ and 3, at $E_{c.m.}=3$ and 5 eV,

obtained by the TSH calculations of Stine and Muckerman also agree with the experimental findings [Figs. 6(b) and 6(d)].

The mean values for $\sigma(v_0')/\sigma(v_0=0)$ of proton and atom transfers at $E_{c.m.}$=2.1, 2.77, 4.1, 5.1, and 6.1 eV obtained by Anderson et al. are also included in Figs. 6(a)-6(e) to compare with the results observed at $E_{c.m.}$=2,3,4,5, and 6 eV in this study. The relative values for $\sigma(v_0')$ of reaction (1) and those for the mean cross sections of reactions (2) and (3) exhibit similar functional dependences on v_0'. Nevertheless, the two sets of data show better agreement at $E_{c.m.}$=0.25-1 eV [Figs. 5(b), 5(c), 5(e)_, and 5(f)] than at $E_{c.m.}$=2-6 eV. The collision time of a scattering event is expected to be shorter when the collision takes place at a higher collision energy. Since a finite length of time is needed for an electron to jump from H_2 to H_2^+ in the H_2^++H_2 collision, the shorter collision time at high $E_{c.m.}$ will limit the number of electron jumps between H_2 and H_2^+ at the entrance channel. The fact that charge equilibrium cannot be maintained at high $E_{c.m.}$ at the entrance channel prior to the formation of H_3^+ is probably the primary reason for the different vibrational dependences observed for $\sigma(v_0')/\sigma(v_0'=0)$ of reaction (1) and the relative mean cross section for reactions (2) and (3). The results of Anderson et al. show that the cross section for reaction (2) and (3) are similar and have similar vibrational dependences at low $E_{c.m.}$, whereas at high $E_{c.m.}$, the cross sections for atom and proton transfers are quite different. The behaviors of the cross sections for atom and proton transfers at various $E_{c.m.}$ can also be rationalized by the charge hopping argument presented above.

The relative vibrational state-selected total cross sections for the $H_2^+ + H_2$ charge transfer reaction at $E_{c.m.}$=2,4,8,and 16 eV obtained by Liao, Liao, and Ng[3] are included in Figs. 6(a), 6(c), 6(f), and 6(i), respectively. The vibrational enhancements for the cross sections of charge transfer at $E_{c.m.}$=2,4,and 8 eV are greater than those observed for $H_3^+ + H$ channel. The vibrational dependence of the $H_2^+ + H_2$ charge transfer reaction at these collision energies is in qualitative agreement with the Franck-Condon factors for the ionization transitions H_2 ($\tilde{X}^1\Sigma_g^+$, v=0) → H_2^+($\tilde{X}^2\Sigma_g^+$, v_0'=0-4), indicative of a predominantly long range electron jump mechanism. The Franck-Condon factor patterns are not observed for the vibrational dependence of $\sigma(v_0')$for reaction (1). It is interesting to find that the relative cross section at $v_0' \geq 1$ for both charge transfer and H_3^+ formation decrease with respect to that at v_0'=0 as $E_{c.m.}$is increased in the range of 4-15 eV.

The TSH calculation reveals that the critical impact parameter for charge transfer is larger than that for H_3^+ formation, and is relatively independent of collision energy.[47] The latter decreases with increasing $E_{c.m.}$. Baker and Schatz[45] have given a rationalization for the observed vibrational dependence of $\sigma(v_0')$ in the low and intermediate collision energy range ($E_{c.m.}$<3 eV). They note that from their trajectory results, the probability of nonreactive charge transfer increases as v_0' is increased, but at the same time the maximum impact parameter leading to H_3^+ formation is larger. The vibration inhibitions for $\sigma(v_0')$ observed at $E_{c.m.} \leq 0.5$ eV indicate that the first effect is more important. In the intermediate $E_{c.m.}$ range of 1-3 eV, the vibrational enhancements for $\sigma(v_0')$ can be attributed to the dominance of the second effect. An increase in

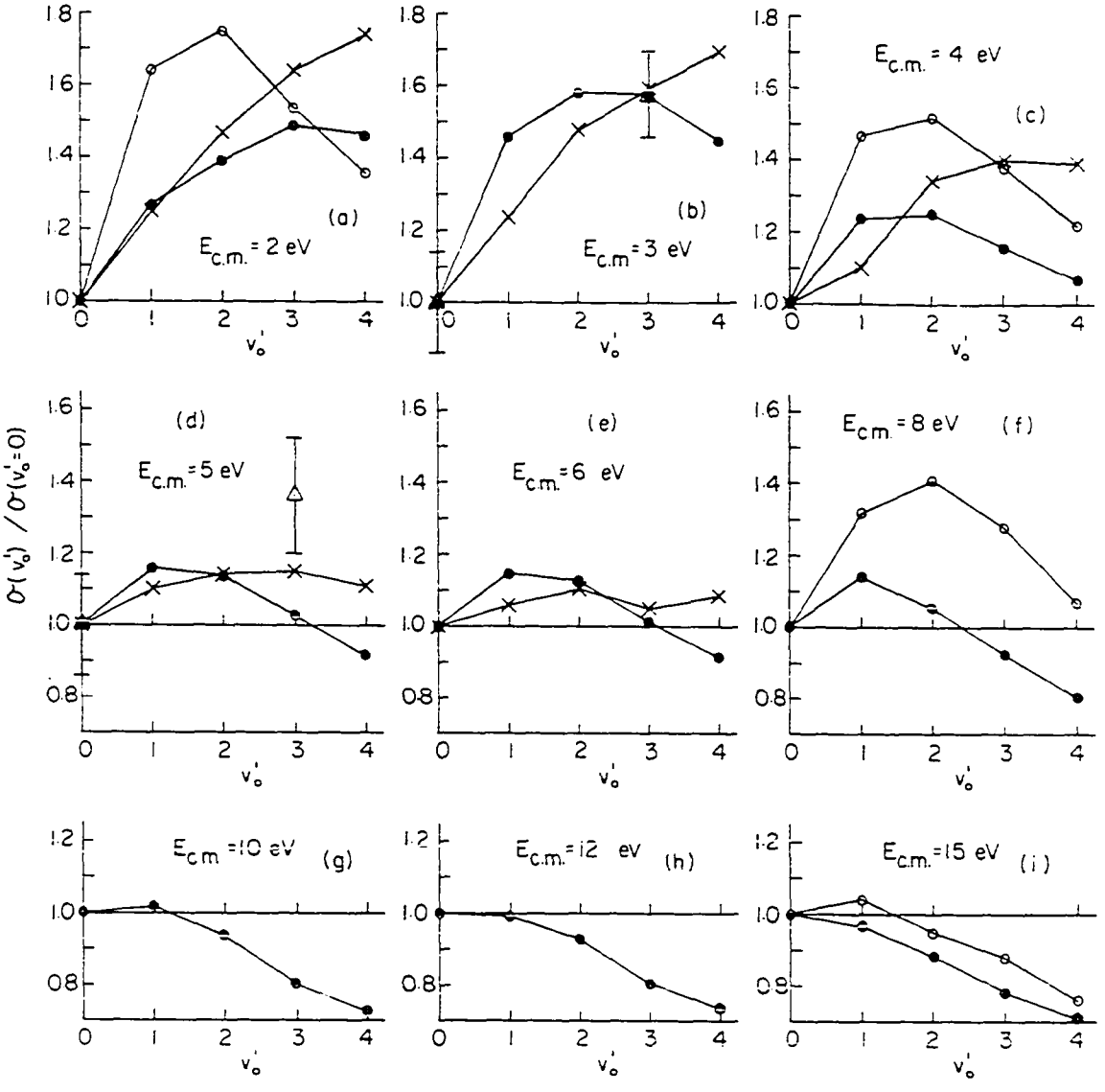

Figure 6. Relative total cross sections $\sigma(v_0')/\sigma(v_0'=0)$ for reaction (1) at $E_{c.m.}$ = 2-15 eV plotted as a function of vibrational quantum number v_0'. (●) This work; (×) mean values of proton and atom transfer (Ref. 7); (○) relative total cross sections for the $H_2^+ + H_2$ charge transfer reaction (Ref. 3); (Δ) Ref. 47

reagent vibrational excitation is expected to favor H_3^+ formation by providing more translational energy for the products to overcome the product centrifugal barriers. For a direct proton transfer reaction, the vibrational excitations of the reactant H_2^+ ions should facilitate the H_2^+ bond breaking and enhance the formation of H_3^+.

At $E_{c.m.} \geq 2$ eV, collision induced dissociation becomes energetically allowed. These processes have the major contribution from low impact parameter collisions. The most recent quasiclassical trajectory calculation of the $(H_2+D_2)^+$ system by Eaker and Muzyka[44] shows that collision induced dissociations for impact parameter <1 bohr often are caused by perpendicular collisions of the diatoms. Their calculation also reveals that a significant amount of collision induced dissociations occurs for larger impact parameter collisions which involve the further dissociation of highly rotational excited triatom. They comment that the fall off of vibrational enhancement for H_3^+ formation form 4 eV to higher $E_{c.m.}$ is due to the increase in collision induced dissociation upon vibrational excitation of H_2^+.

The SECT theoretical calculations of Lee and DePristo,[46] which have been shown to be in satisfactory agreement with the experimental results,[3] predict a similar behavior for the charge transfer cross sections over the $E_{c.m.}$ range of 4-16 eV, i.e., the values for $\sigma(v_0'>0)$ decrease with respect to $\sigma(v_0'=0)$as $E_{c.m.}$ is increased [Figs. 6(c)-6(i)]. Since the SECT calculations have not taken into account the collision induced dissociation and H_3^++H channels, the observed decrease of the charge transfer cross sections for $v_0' \geq 1$ with respect to that for $v_0'=0$ with increasing $E_{c.m.}$ cannot be explained by the above argument.

The absolute value for $\sigma(v_0'=0)$ at a given $E_{c.m.}$ is determined by the relation

$$\sigma(v_0'=0)=-(1/nl)\ln[1-(i/I_0)] \qquad (4)$$

here, i is the intensity for product H_3^+, which has been corrected for background H_3^+ formed outside the reaction gas cell using the same procedures described in Ref. 61. I_0 is the measured intensity of reactant $H_2^+(v_0'=0)$ when the reaction gas cell is empty; n and l represent the density of H_2 in the reaction gas cell and the length of the gas cell, respectively. The measured values for (v_0'), v=0 and 3 over the $E_{c.m.}$ range of 0.25–15 eV are plotted in Fig. 7. The absolute values for $(v_0'=3)$ are obtained by scaling the values for $(v_0'=0)$ using the corresponding relative cross sections for $v_0'=0$ and 3. Due to the poor relative kinetic energy resolution ($\Delta E/E_{lab}$) and the low reactant H_2^+ ion intensity at very low $E_{c.m.}$, it is difficult to measure $\sigma(v_0')$ with accuracy at $E_{c.m.}<0.25$ eV. The most difficult problem encountered in measuring $\sigma(v_0')$ at very low $E_{c.m.}$ is that some of the backward scattered H_3^+ ions cannot be redirected towards the detector because a sufficiently high retarding voltage cannot be applied to the ion lens at the entrance of the octopole ion guide.

Table I summarizes values for $\sigma(v_0')$, where $v_0'=0$ and 3, at the $E_{c.m.}$ range of 0.25–5 eV, obtained by previous theoretical and experimental studies and compares them with those determined here. The uncertainties for $\sigma(v_0')$ measured here have taken into account the estimated errors due to secondary gas cell reactions. The experimental and theoretical values for $\sigma(v_0')$ at $E_{c.m.}=0.5$ and 1.0 eV are in good agreement. With the exception of

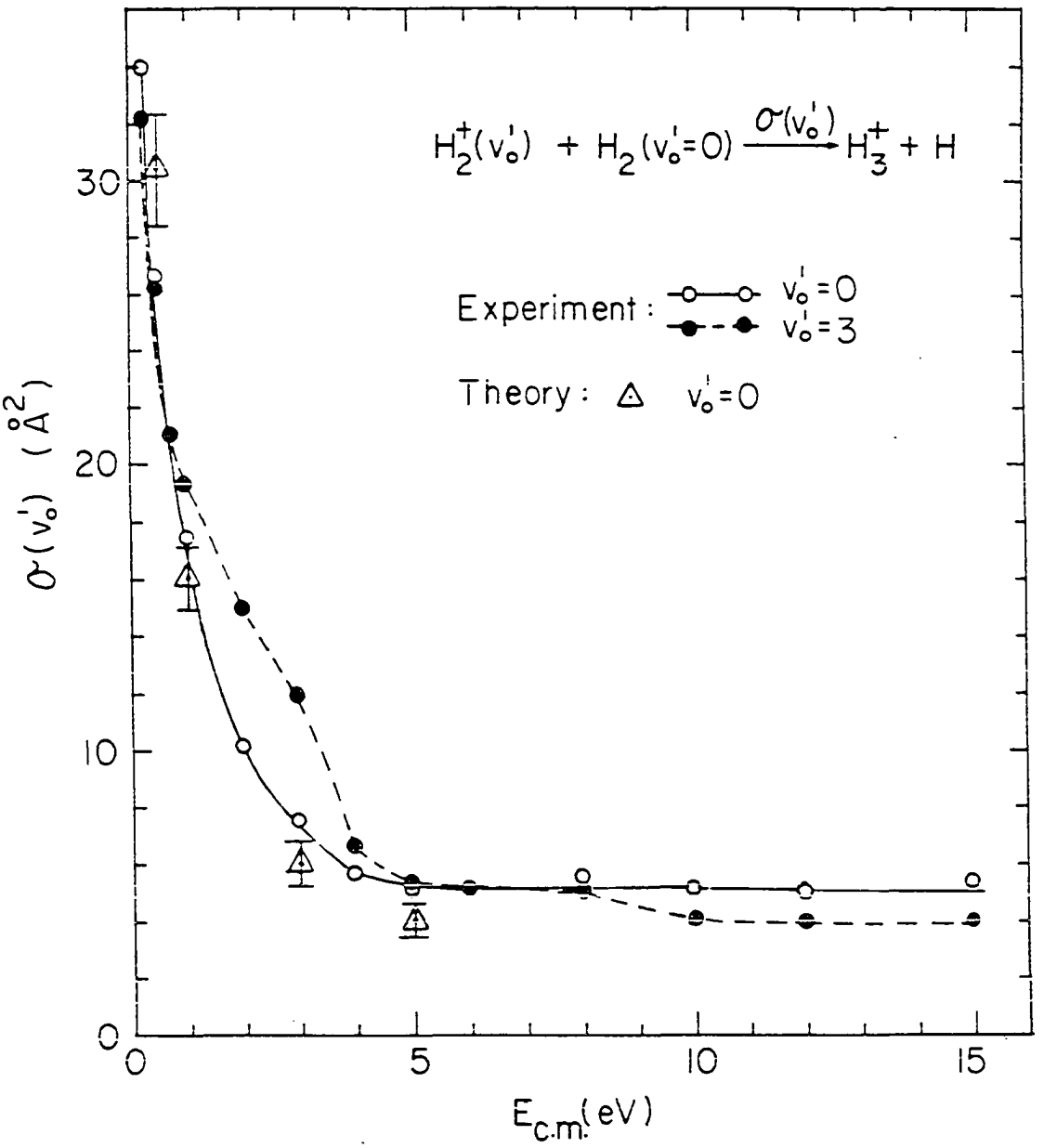

Figure 7. Absolute vibrational-state-selected total cross sections $\sigma(v_0')$, $v_0' = 0$ and 3, for reaction (1) plotted as a function of $E_{c.m.}$. Experiment (this work): (o) $\sigma(v_0'=0)$; (o) $\sigma(v_0'=3)$. Theory (Ref. 47): (Δ) $\sigma(v_0'=0)$

Table I. Total cross sections for the reaction H_2^+ (v_0' = 0 or 3) + $H_2(v_0'' = 0) \rightarrow H_3^+ + H$

		$\sigma(v_0')$ (Å^2)					
		Experimental		Theoretical			
$E_{c.m.}$ (eV)[a]	v_0'	This work	Ref. 8[b]	Ref. 47	Ref. 45	ES[c]	LGS[d]
0.25	0	34.0 ± 4.0	...	47.8 ± 1.4	...	46.4 ± 2.0	30.5
	3	32.3 ± 4.0	...	38.8 ± 2.2	...	37.4 ± 2.0	30.5
0.5	0	26.6 ± 2.0	24.3 ± 1.5[e]	30.6 ± 1.7	30.6 ± 1.4[e]	30.6 ± 1.4	21.5
	3	26.3 ± 2.0	19.5 ± 2.0[e]	26.7 ± 1.7	33.7 ± 1.4[e]	26.4 ± 2.0	21.5
1.0	0	17.4 ± 1.5, 2.5	16.9 ± 1.5[f]	16.0 ± 1.1	18.3 ± 0.8[f]	16.6 ± 1.1	15.2
	3	19.3 ± 1.5, 2.5	16.2 ± 1.5[f]	18.8 ± 1.7	23.0 ± 0.8[f]	18.5 ± 1.4	15.2
3.0	0	7.5 ± 0.8, 1.6	...	5.8 ± 0.8	...	6.5 ± 0.6	8.8
	3	11.8 ± 0.8, 1.6	...	9.3 ± 1.1	...	9.6 ± 0.8	8.8
5.0	0	6.1 ± 0.6, 2.0	...	3.9 ± 0.6	...	3.7 ± 0.3	6.8
	3	6.3 ± 0.6, 2.0	...	5.3 ± 0.8	...	5.06 ± 0.6	6.8

[a]Center-of-mass collision energy.

[b]These values are obtained by scaling the values plotted in Fig.7 of Ref. 8.

[c]Results of the TSH calculation obtained by Eaker and Schatz (Ref. 74).

[d]Values calculated using the Langevin-Gioumousis-Stevens Model.

[e]Values for $E_{c.m.}$ = 0.46 eV.

[f]Values for $E_{c.m.}$ = 0.93 eV.

$\sigma(v_0')$ at $E_{c.m.}$=0.25 eV, the TSH cross sections obtained by Stine and Muckerman[47] are consistent with the experimental cross sections of this study. The fact that the experimental values for $\sigma(v_0')$ are in good accord with the predictions of the LGS model indicates that the dynamics of reaction (1) are governed mainly by the charge induced-dipole interaction.

In the quasiclassical trajectory calculation of Eaker and Schatz[45] the surface hopping part of the dynamics is treated by using an approximation to the usual TSH model. They assumed that the trajectories follow the diabatic surfaces up to a particular intermolecular separation and then the ground adiabatic surfaces thereafter. The DIM surface used by Eaker and Schatz is similar to that of Stine and Muckerman but has a different parameterization of the diatomic potentials. Very recently, Eaker and Schatz[73] have reinvestigated reaction (1) using the same TSH model used by Stine and Muckerman. The results of their recent TSH calculation, which are also listed in Table I, are found to be in good agreement with those obtained by Stine and Muckerman and with the experimental results of this study. Although it has been shown that the previous quasiclassical trajectory calculation can account for the general features of the experimental cross-sectional data,[44,45] the detailed features can be predicted only by the TSH model which includes nonadiabatic surface hopping throughout the reaction.

CONCLUSIONS

We have developed a new tandem photoionization mass spectrometer for state-selected studies of ion-molecule reactions. This apparatus, which combines the merits of photoionization, rf octopole ion guide, and tandem mass spectrometric techniques, is capable of performing absolute state-selected total cross section measurements on simple as well as more complicated ion-molecule reactions over a wide kinetic energy range. Using this apparatus, we have measured the absolute state-selected microscopic total cross sections for reaction (1) over the $E_{c.m.}$ range of 0.25–15 eV. With the exception at $E_{c.m.}$=0.25eV, the absolute values for $\sigma(v_0'=0)$ are in good accord with the semiclassical trajectory calculations of Stine and Muckerman, and Eaker and Schatz. However, the measured relative values for $\sigma(v_0'=0)$ and $\sigma(v_0'=3)$ are found to be in better agreement with the results of the TSH calculations of Stine and Muckerman, which include nonadiabatic surface hopping throughout the reaction. The kinetic energy dependence of $\sigma(v_0')$ at the $E_{c.m.}$ range of 0.25–5 eV is consistent with the prediction of the LGS model, confirming the previous experimental and theoretical findings. This suggests that the dynamics of reaction (1) at low $E_{c.m.}$ is mainly governed by the charge induced-dipole interaction. This experiment, together with the state-selected charge transfer study of Liao, Liao, and Ng provides detailed experimental cross-sectional data for a more thorough comparison with theoretical calculations of the reaction dynamics of $H_2^+ + H_2$ in the future.

References

1. D. van Pijkeren E. Bottjes, J. van Eck, and A. Niehaus, Chem. Phys. 91, 239 (1984).

2. C.-L. Liao, C.-X. Liao, and C. Y. Ng, 103, 418 Chem. Phys. Lett. (1984).

3. C.-L. Liao, C.-X. Liao, and C. Y. Ng, Chem. Phys. 81, 5672 (1984).

4. A. Carrington and R. A. Kennedy, J. Chem. Phys. 81, 91 (1984).

5. S. K. Cole T. Baer, P.-M. Guyon, and T. R. Govers, Chem. Phys. Lett. 109, 285 (1984).

6. F. M. Campbell, R. Browning, and C. J. Latimer, J. Phys. B 14, 3493 (1981).

7. S. L. Anderson, F.A. Houle, D. Gerlich, and Y. T. Lee, J. Chem. Phys. 75, 2152 (1981).

8. I. Koyano and K. Tanaka, J. Chem. Phys. 72, 4858 (1980).

9. P. M. Hierl and Z. Herman, Chem. Phys. 50, 249 (1980).

10. A. Ding, Faraday Discuss. Chem. Soc. 67, 353 (1979).

11. A. Ding and A. Redpath, Proc. I.C.P.E.A.C. 10, 759 (1979).

12. C. H. Douglass, D. J. McClure, and W.R. Gentry, J. Chem. Phys. 67, 4931 (1977).

13. J. R. Krenos, K. K. Lehmann, J. C. Tully, P. M. Hierl, and G. P. Smith, Chem. Phys 16, 109 (1976).

14. A. B. Lees and P. K. Rol, J. Chem. Phys. 61, 4444 (1974).

15. R. N. Stocker and H. Newmann, J. Chem. Phys. 61 385 (1974).

16. L. D. Theard and W. T. Huntress, J. Chem. Phys. 60, 2840 (1974).

17. A. Henglein, J. Chem. Phys. 76, 3883 (1972).

18. R. P. Clow and J. H. Futrell, Int. J. Mass Spectrom. Ion Phys. 8, 119 (1972).

19. W. T. Huntress, D. D. Ellenan, and M. T. Bowers, J. Chem. Phys. 55, 5413 (1971).

20. J. Krenos, P. M. Hierl, J. C. Tully, Z. Herman, and R. Wolfgang, Adv. Mass Spectrom. 5, 213 (1971).

21. L. V. Sumin and M. V. Gurev, Dokl. Akad. Nauk SSSR 193, 858 (1970).

22. M. T. Bowers, D. D. Elleman, and J. King, Jr., J. Chem. Phys. 50, 4787 (1969).

23. T. F. Moran and J. R. Roberts, J. Chem. Phys. 49, 3411 (1968).

24. A. G. Harrison and J. C. J. Thynne, Trans. Faraday Soc. 64, 945 (1968).

25. W. A. Chupka, M. E. Russell, and K. Refaey, J. Chem. Phys. 48, 1518 (1968).

26. R. H. Neynaber and S. M. Trujillo, Phys. Rev. 167, 63 (1968).

27. R. H. Neynaber and S. M. Trujillo, Phys. Rev. 171, 282E (1968).

28. M. Yamane, J. Chem. Phys. 49 4624 (1968).

29. J. Durup and M. Durup, J. Chem. Phys. 64, 386 (1967).

30. J. J. Leventhal, T. F. Moran, and L. Friedman, J. Chem. Phys. 46, 4666 (1967).

31. L. Matus, I. Opauszky, D. Hyatt, A. J. Masson, K. Birkinshaw, and M. J. Henchman, Discuss. Faraday Soc. 44, 146 (1967).

32. L. D. Doverspike and R. L. Champion, J. Chem. Phys. 46 4718 (1967).

33. P. Warneck, J. Chem. Phys. 46, 4718 (1967).

34. D. W. Vance and T. L. Bailey, J. Chem. Phys. 44, 486 (1966).

35. J. H. Furtell and F. P. Abramson, Adv. Chem. Ser. 58, 123 (1966).

36. A. G. Harrison, A. Ivko, and T. W. Shkannon, Can. J. Chem. 44, 1351 (1966).

37. M. Saporoschenko, J. Chem. Phys. 42, 2760 (1965).

38. A. Weingartshofer and E. M. Clarke, Phys. Rev. Lett. 12, 591 (1964).

39. C. F. Giese and W. B. Maier II, J. Chem. Phys. 39, 739 (1963).

40. B. G. Reuben and L. Friedman, J. Chem. Phys. 37, 739 (1962).

41. V. L. Talroze, Izv. Akad. Nauk SSSR Ser. Fiz. 24, 1001 (1960).

42. D. P. Steveson and D. O. Schissler, J. Chem. Phys. 29, 282 (1958).

43. V. H. Gutbier, Z. Naturforsch. Teil A 12, 499 (1957).

44. C. W. Eaker and J. L. Muzyka, Chem. Phys. Lett. 119, 169 (1985).

45. C. W. Eaker and G. C. Schatz, J. Chem. Phys. 89, 2612 (1985).

46. C. Y. Lee and A. E. DePristo, J. Chem. Phys. 80, 1116 (1984).

47. Data of Stine and Muckerman (1980). See J. T. Muckerman, in Theoretical Chemistry, edited by D. Henderson (Academic, New York, 1981).

48. J. R. Stine and J. T. Muckerman, J. Chem. Phys. 68, 185 (1978).

49. J. R. Stine and J. T. Muckerman, J. Chem. Phys. 65, 3975 (1976).

50. T. F. Moran, M. R. Flannery, and K. L. Albritton, J. Chem. Phys. 65, 3172 (1976).

51. M. R. Flannery, J. V. Hornstein, and T. F. MAORAN, Chem. Phys. Lett. 32, 455 (1977).

52. T. F. Moran, M. R. Flannery, and D. L. Albritton, J. Chem. Phys. 62, 2869 (1975).

53. F. A. Wolf and J. L. Haller, J. Chem. Phys. 52, 5910 (1970).

54. D. R. Bates and R. H. G. Reid, Proc. R. Soc. London Ser. A 1, 310 (1969).

55. H. Eyring, J. O. Hirschfelder, and H. S. Taylor, J. Chem. Phys. 4, 479 (1936).

56. S. L. Anderson, T. Hirooka, P. W. Tiedemann, B. H. Mahan, and Y. T. Lee, J. Chem. Phys. 73, 4779 (1980).

57. J. C. Tully and R. K. Preston, J. Chem. Phys. 55, 562 (1971).

58. G. Ochs and E. Teloy, J. Chem. Phys. 61, 4930 (1974).

59. C. L. Liao and C. Y. Ng, J. Chem. Phys. 84, 197 (1985).

60. J. C. Light, J. Chem. Phys. 41, 586 (1964).

61. E. Teloy and D. Gerlich, Chem. Phys. 4, 417 (1974).

62. N. R. Daly, Rev. Sci Instrum. 31, 264 (1960).

63. V. V. Afrosimov, I. P. Gladkovski, Yu S. Gordeev, I. F. Kalinkevich, and N. V. Fedorenko, Sov. Phys. Tech. Phys. 5, 1378, 1389 (1961).

64. E. Chönheit, A. Naturforsch. Teil A 15, 839 (1960).

65. The collecting efficiency for H_3^+ is definded to be $[(I+i)/I_0]x100\%$, where $i(H_3^+)$ is the intensity for product H_3^+ and I_0 and I are the unattenuated and attenuated reactant H_2^+ ion beam intensities, respectively.

66. J. A. R. Samson, Techniques of Vacuum Ultraviolet Spectroscopy (Wiley, New York, 1967), p.231.

67. Y. Ono, S. H. Linn, H. F. Press, M. E. Gress, and C. Y. Ng, J. Chem. Phys. 73, 2523 (1980).

68. K. M. Ervin and P. B. Armentrout, J. Chem. Phys. 83, 166 (1985).

69. W. A. Chupka and J. Berkowitz, J. Chem. Phys. 48, 5226 (1968).

70. W. A. Chupka and J. Berkowitz, J. Chem. Phys. 51, 4244 (1969).

71. P. M. Dehmer and W. A. Chupka, J. Chem. Phys. 65, 2243 (1976).

72. Using the same procedures and vibrational distributions for H_2^+ as reported by Anderson et al., we have reproduced the vibrational dependences of the relative total cross sections for the formation of D_2H^+ by the reaction $H_2^+ + D_2$ obtained by Anderson et al. (Ref. 7).

73. C. W. Eaker and G. C. Schatz, J. Chem. Phys., to be published.

SECTION II.

A VIBRATIONAL STATE-SELECTED STUDY OF THE REACTION $Ar^+(^2P_{3/2,1/2}) + N_2(\tilde{X},v=0) \longrightarrow Ar(^1S_0) + N_2^+(\tilde{X},v')$

Introduction

Partly due to the early controversy in the rate constant measurements for the electron transfer reaction $Ar^+ + N_2$,[1-9] the electron transfer system $[Ar + N_2]^+$ has been the focus of many experimental studies[10-21] in the last few years. The kinetic energy dependences of the rate coefficients for this system obtained in the flow drift tube experiment of Lindinger et al.[11] and the selected ion flow tube study of Smith and Adams[10] reveal that the poor agreement observed in early rate constant measurements for the electron transfer reaction of $Ar^+ + N_2$ can be attributed to the strong kinetic energy dependence of the rate coefficient, the high reactivity of the reverse reactions $N_2^+(v' \geq 1) + Ar$, and the buffer gas effect. The recent study of Federer et al.[22] shows that internal heating of reactant ions can result from collisions of buffer gas with reactant ions at high drift velocities in flow drift tube environments.

The energy level diagram for the $[Ar + N_2]^+$ system is shown in Fig. 1. The formation of $N_2^+(\tilde{X},v'=0)$ by the reaction

$$Ar^+(^2P_{3/2}) + N_2^+(\tilde{X},v=0) \longrightarrow Ar(^1S_0) + N_2^+(\tilde{X},v') \qquad (1)$$

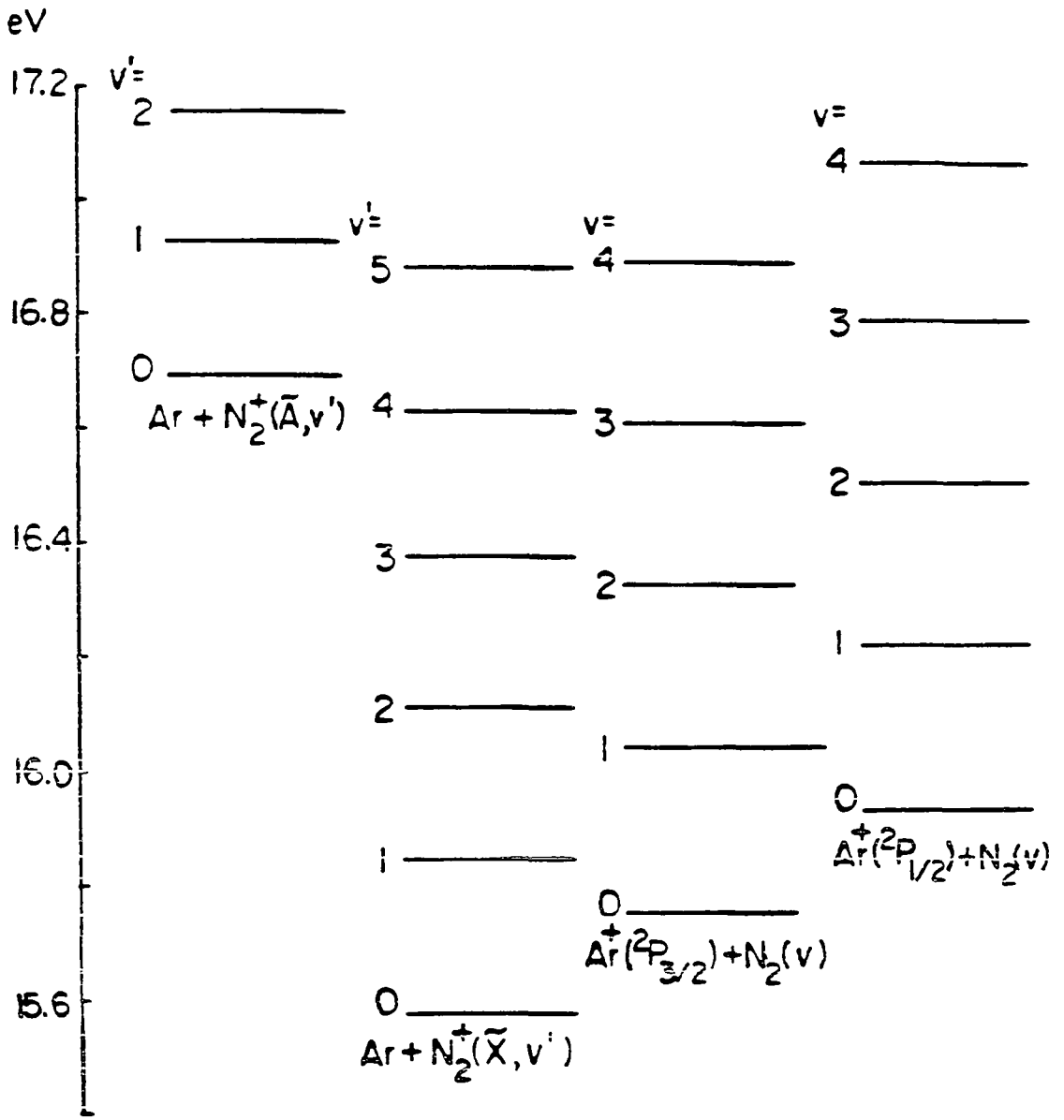

Figure 1. Energy level diagram of the $Ar^+(^2P_{3/2}) + N_2(\tilde{X},v)$, $Ar^+(^2P_{1/2}) + N_2(\tilde{X},v)$, $Ar(^1S_0) + N_2^+(\tilde{X},v')$, and $Ar(^1S_0) + N_2^+(\tilde{A},v')$ states in the asymptotic limits

is exothermic by 0.179 eV, while the production of $N_2^+(\tilde{X},v'=1)$ is endothermic by 0.090 eV. By adding Ar downstream of the flow tube and monitoring the decline of N_2^+ product ions, the studies of Smith and Adams[10] and Lindinger et al.[11] provide evidence that reaction (1) proceeds predominantly (>70%) via the endothermic channel to produce $N_2^+(\tilde{X},v'=1)$ when it is energetically allowed. The Ar^+ reactant ions in both studies were prepared by electron ionization and the complete quenching of $Ar^+(^2P_{1/2})$ in the flow tube was assumed.

The relative spin-orbit-state-selected total cross sections, $\sigma_{3/2}$ and $\sigma_{1/2}$, for reaction (1) and the reaction

$$Ar^+(^2P_{1/2}) + N_2^+(\tilde{X},v=0) \longrightarrow Ar(^1S_0) + N_2^+(\tilde{X},v') \qquad (2)$$

respectively, have been measured over the center-of-mass collisional energy ($E_{c.m.}$) range of 0.2-8 eV using the threshold photoelectron secondary ion coincidence method (TESICO).[12,20] The experimental values for $\sigma_{1/2}/\sigma_{3/2}$ are found to be less than one. However, the $\sigma_{1/2}/\sigma_{3/2}$ ratios determined at $E_{c.m.}$=1.4 and 5.8 eV by Kato, Tanaka, and Koyano[12] are higher than those obtained by Guyon and Govers[20] by approximately a factor of two. This discrepancy is ascribed[23] to the possible occurrence of collisional-induced fine structure mixings in the collision chamber prior to electron transfer. The values for $\sigma_{1/2}/\sigma_{3/2}$ deduced by Liao, Yu, and Ng[19] in a crossed ion-neutral beam experiment are slightly lower than those obtained by Guyon and Govers, and support this speculation. The kinetic energy dependence for $\sigma_{1/2}/\sigma_{3/2}$ in the $E_{c.m.}$ range of 0.41-164.7 eV observed in the crossed ion-neutral beam experiment also exhibits a broad minimum at $E_{c.m.}$=3.3 eV.[19]

Friedrich et al.[17] and Rockwood et al.[18] have measured the angular and kinetic energy distributions of N_2^+ ions formed by reaction (1) at $E_{c.m.}$=1.1, 1.71 and 4.01 eV in a crossed-beam experiment. The Ar^+ reactant ions were prepared by a high pressure electron impact ion source and were assumed to be in the $^2P_{3/2}$ state. At $E_{c.m.}$=1.71 and 4.01 eV, N_2^+ product ions were found to be scattered essentially in the neutral N_2 beam direction with little momentum transfer. This observation is consistent with the findings of previous molecular beam experiments.[24-27] The kinetic energy distributions of product N_2^+ indicate that N_2^+ ions are produced primarily in the v'=1 state with rotational excitation. At $E_{c.m.}$=4.01 eV, the kinetic energy distribution of N_2^+ can also be interpreted to contain a lesser population of N_2^+ in v'=2. However, at $E_{c.m.}$=1.1 eV, Rockwood et al.[18] reported pronounced anisotropic scattering of N_2^+ with considerable excitation into v'=2, 3, and 4 in addition to v'=1. Since their experiment shows that this phenomenon does not occur at higher and lower energies, they suggest that this observation resembles that reported for the reactive scattering of F + H_2. The correlation of quantum-state specificity with angular scattering observed for HF formed by the reaction of F + H_2 at a particular collision energy was interpreted to be the result of a quantum mechanical dynamic resonance.[28-31]

The vibrational and rotational state distributions for N_2^+ resulting from reaction (1) at $E_{c.m.}$=0.24 eV have been measured by Hüwel et al.[16] using the laser-induced fluorescence method. The Ar^+ reactant ions were produced in the flow of neutral buffer gas by Penning ionization from helium metastable atoms. Excited $Ar^+(^2P_{1/2})$ ions initially formed were

assumed to be quickly relaxed by superelastic collisions with the electrons in flow tube plasma.[7,9,10] In that experiment, the Ar^+ ions together with helium buffer gas were allowed to expand through an orifice at the end of the flow tube before intersecting a N_2 beam effusing through a linear array. By extrapolating the ratio of the measured densities for $N_2^+(v'=0)$ to that of $N_2^+(v'=1)$ at $E_{c.m.}=0.24$ eV.

The wealth of experimental information for the $[Ar + N_2]^+$ electron transfer system, especially the state specific cross-sectional data,[12,13,15-19] which have appeared in the literature in the last three years, has stimulated considerable theoretical work on this system.[12,13,15-17,32-35] The semi-classical multiple state studies of Spalburg, Los, and Gislason[33] and Spalburg and Gislason[32] have provided a great deal of insight into this system. The vibrational-state-selected cross sections calculated for the reverse of reaction (1) are found to be consistent with experimental values.[13,15,21] A broad minimum at $E_{c.m.}=4.1$ eV for the kinetic energy dependence of $\sigma_{1/2}/\sigma_{3/2}$ predicted by the theory is also in qualitative agreement with the results of the crossed ion-neutral beam experiment.[19] The calculation of Spalburg and Gislason[32] uses straight line trajectories and estimated potential energy surfaces (PES) for the $[Ar + N_2]^+$ system, assumes that the electronic coupling potential[36] is independent of the molecular orientation, but ignores interactions due to the $\tilde{A}$ state of N_2^+. Most recently, Archirel and Levy[35] have computed ab initio PES for the electronic states $N_2^+(\tilde{X}) + Ar(^1S_0)$, $N_2^+(\tilde{A}) + Ar(^1S_0)$, and $Ar^+(^2P) + N_2(\tilde{X})$ at the linear and perpendicular approaches of Ar to N_2. Parlant and Gislason[34] have used these ab initio

PES in a more accurate semi-classical multi-state calculation and obtained state-to-state total cross sections for the electron transfer reactions of $N_2^+(\tilde{X},v') + Ar(^1S_0)$ and $N_2^+(\tilde{A},v') + Ar(^1S_0)$. The latter calculation has removed most of the approximations made in the previous study.[32] As expected, the measured state-selected cross sections[15,21] for the electron transfer reaction $N_2^+(\tilde{X},v') + Ar(^1S_0)$ are in better agreement with those obtained by Parlant and Gislason. State-to-state cross sections for reactions (1) and (2) should be available from the consideration of microscopic reversibility.

Although discrepancies still exist between various measurements and calculations, the $[Ar + N_2]^+$ electron transfer system has rapidly become one of the most thoroughly investigated atom-diatom reactions. Detailed state-to-state or final product state distribution measurements over a wide collisional energy range are expected to be valuable for further improvements in the theoretical calculation of this model system. We have measured the absolute values for $\sigma_{3/2}$ and $\sigma_{1/2}$ at $E_{c.m.}$=0.25-115.3 eV by using the tandem photoionization mass spectrometer.[37,38] Experimental results are compared to the calculation of Spalburg and Gislason[32] and previous experimental studies.[16-18] Combining the absolute values for $\sigma_{3/2}$ and $\sigma_{1/2}$, the values for $\sigma_{1/2}/\sigma_{3/2}$, and vibrational state distributions of $N_2^+(\tilde{X},v')$ determined using the crossed ion-neutral beam photoionization apparatus,[39-41] absolute state-to-state total cross sections for reactions (1) and (2) have been determined at selected $E_{c.m.}$.

EXPERIMENTAL

The tandem photoionization mass spectrometer used to measure the absolute values for $\sigma_{3/2}$ and $\sigma_{1/2}$ has the same design as that discussed in Section I.

The reactant Ar^+ were prepared by photoionization of an Ar supersonic beam at 783 or 770 Å. The wavelength resolution employed was ~4.5 Å (FWHM). The reactant Ar^+ ions were selected by the first QMF before entering the rf octopole ion guide reaction cell in which Ar^+ ions react with N_2 according to reactions (1) and (2). The N_2 gas cell pressure was ~7 x 10^{-5} Torr. The intensities of reactant Ar^+ and product N_2^+ were selected by the second QMF and then measured by a scintillation ion detector. The rf frequency and V_{pp} applied to the octopole were ~4 MHz and ~280 V, respectively. The collection efficiency for product N_2^+ was carefully optimized at each $E_{c.m.}$. Collection efficiencies of ≥99% were achieved for all $E_{c.m.}$. The ratios of the intensities for product N_2^+ and reactant Ar^+ measured at 783 Å, $I(N_2^+,783\ Å)/I(Ar^+,783\ Å)$, for E_{lab}=0.6, 2.9, 10, 25, 100, and 280 eV are plotted as a function of V_{pp} in Fig. 2. The constant values observed for the ratios at V_{pp}≥180 V indicate that total product N_2^+ collections can be achieved at V_{pp}=180 V. Depending on E_{lab}, we found that as V_{pp} was increased beyond ~400–500 volts, the transmission for the reactant Ar^+ ion beam through the rf octopole ion guide decreased significantly, concomitant with the decrease of product N_2^+ ion intensity. This observation is consistent with the expectation that at a given rf and a sufficiently high V_{pp}, the reactant ions can be deflected out of the octopole. In some cases,

Figure 2. The ratio of the intensities for product N_2^+ and reactant Ar^+ at E_{lab} = 0.6, 2.9, 10, 15, 100, and 280 eV measured at 783 Å, $I(N_2^+, 783\ Å)$, plotted as a function of the radio frequency (rf) peak-to-peak voltage (V_{pp}) applied to the rf octopole gas cell. The measurements were made using the tandem photoionization mass spectrometer

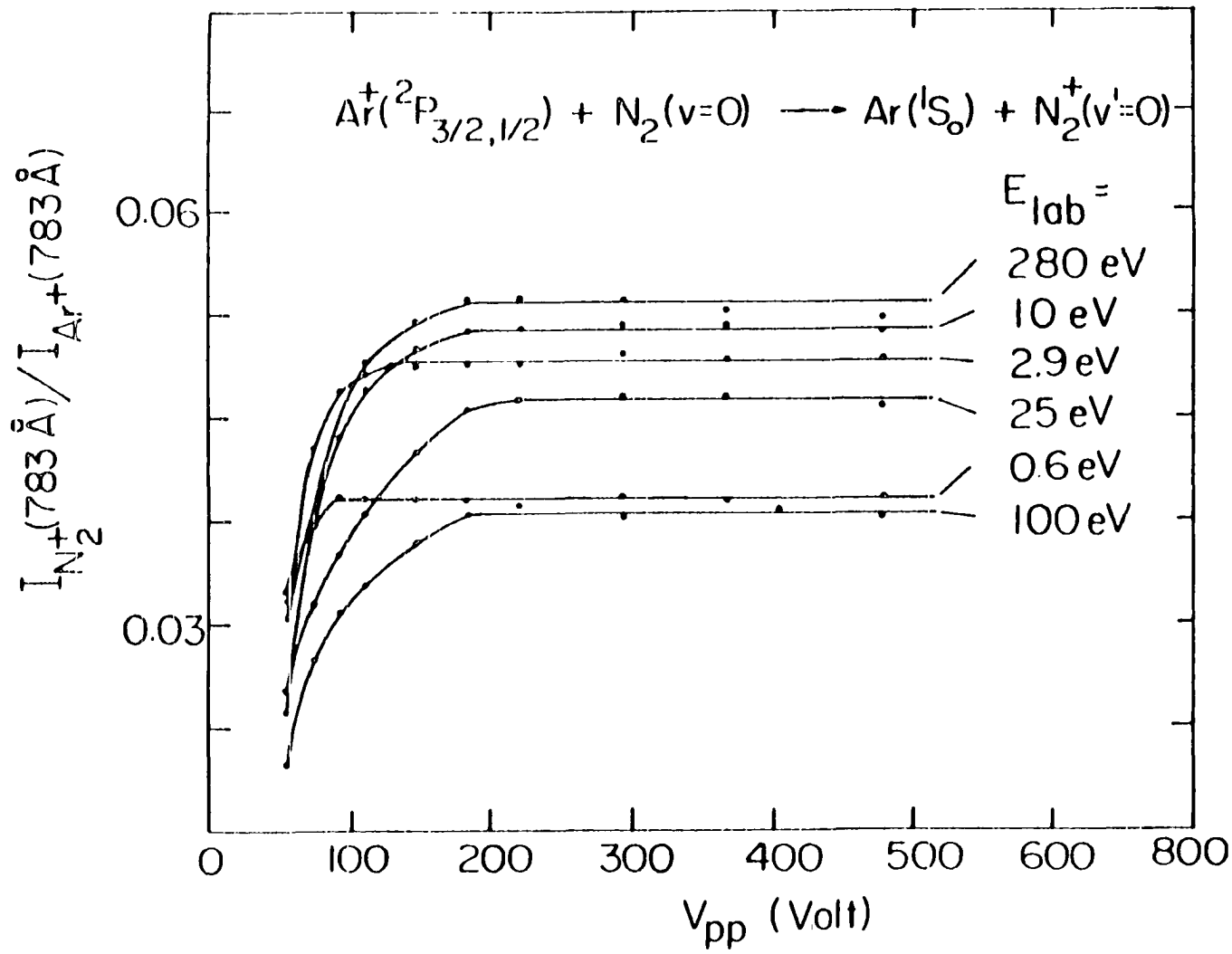
$Ar^+(^2P_{3/2,1/2}) + N_2(v=0) \longrightarrow Ar(^1S_o) + N_2^+(v'=0)$
E_{lab} =
280 eV
10 eV
2.9 eV
25 eV
0.6 eV
100 eV
$I_{N_2^+}(783\,Å) / I_{Ar^+}(783\,Å)$
0.06
0.03
0
100
200
300
400
500
600
800
V_{pp} (Volt)

a decrease in the ratio at high V_{pp} was also observed, indicating that the trapping efficiencies for different ions depend on rf, V_{pp}, and ion energy. The decrease of the ratio for E_{lab}=280 eV in the V_{pp} range of ~350-500 volts is evident in Fig. 2. The value of 280 volts for V_{pp} is approximately at the center of the V_{pp} voltage region for which the values for $I(N_2^+,783$ Å) and $I(Ar^+,783$ Å) were constant and at their highest values for a given E_{lab}.

Figure 3 compares the PIE spectra for the reactant Ar^+ and product N_2^+ ion measured at $E_{c.m.}$=10.3 eV. The Ar^+ spectrum was obtained when the gas cell was empty. The PIE data for the reactant and product ions were normalized to have the same values at 783 Å. The PIE curve for N_2^+ at energies above the IE for $Ar^+(^2P_{1/2})$ is lower than the corresponding PIE curve for Ar^+, indicating that $\sigma_{1/2}$ is lower than $\sigma_{3/2}$ at $E_{c.m.}$=10.3 eV. This observation is in accord with results reported previously.[12,19,20] The ratio for the intensity of product N_2^+ to that of reactant Ar^+ obtained as a function of wavelength is also plotted in Fig. 3. The constant values observed for $I(N_2^+,<775$ Å$)/I(Ar^+,<775$ Å) support the conclusion of the previous photoelectron study[42] that the ratio of the intensities for $Ar^+(^2P_{3/2})$ and $Ar^+(^2P_{1/2})$ formed by photoionization remains constant at photon energies higher than the IE of $Ar^+(^2P_{1/2})$.

The absolute values for $\sigma_{3/2}$ and σ_m at a given $E_{c.m.}$ are determined by the relations

$$\sigma_{3/2} = -(1/nl)\ln[1 - I(N_2^+,783\text{ Å})/I(Ar^+,783\text{ Å})] \quad (3)$$

$$\sigma_{1/2} = 3\sigma_m - 2\sigma_{3/2} \quad (4)$$

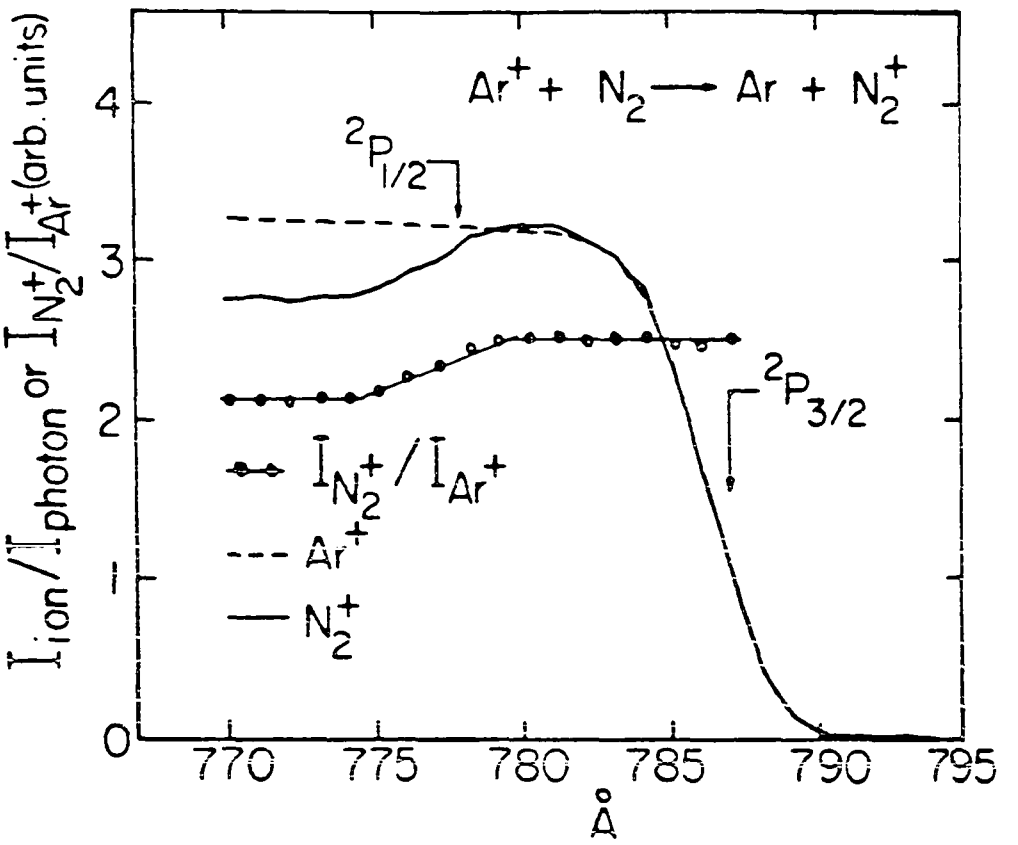

Figure 3. Photoionization efficiency spectra for reactant Ar^+ (--) and product N_2^+ (——) at $E_{c.m.}$ = 10.3 eV measured using the tandem photoionization mass spectrometer. (o o o) the ratio for the intensities of N_2^+ and Ar^+ plotted as a function of wavelength

where σ_m is the total cross section measured for the electron transfer reaction $Ar^+ + N_2$ characteristic of reactant Ar^+ ions produced at 769 Å. Since $Ar^+(^2P_{3/2})$ and $Ar^+(^2P_{1/2})$ are formed at 769 Å with a statistical distribution of 2:1, σ_m is equal to $(2/3)\sigma_{3/2} + (1/3)\sigma_{1/2}$. Under thin target conditions, σ_m can be obtained by the relation

$$\sigma_m = -(1/nl)\ln[1 - I(N_2^+, 769\ \text{Å})/I(Ar^+, 769\ \text{Å})] \qquad (5)$$

RESULTS AND DISCUSSION

Absolute Values for $\sigma_{3/2}$ and $\sigma_{1/2}$

The values for $\sigma_{3/2}$, σ_m, and $\sigma_{1/2}$ over the $E_{c.m.}$ range of 0.25–115.3 eV determined in this experiment are listed in Table I. The experimental uncertainties for $\sigma_{3/2}$ and σ_m are estimated to be $\leq$5% caused mostly by the uncertainties in the N_2 gas cell pressure ($P(N_2)$) measurements. At a given $E_{c.m.}$, the experimental uncertainty for $\sigma_{1/2}$ is approximately three times those for σ_m. This results from the calculation of $\sigma_{1/2}$ using Eq. (4).

Total cross sections for the electron transfer reaction of $Ar^+ + N_2$ have been measured previously[43–51] over a wide range of collision energies. Since results of many of these studies have recently been tabulated and compared to the theoretical results,[32] they are not included in Table I. Most of the previous measurements use electron impact ionization to prepare the reactant Ar^+ ions and the reactant state distributions are unknown. Assuming the Ar^+ ions formed by electron impact ionization to be a two-thirds $^2P_{3/2}$ and one-third $^2P_{1/2}$ mixture, the total cross sections of previous studies can be compared to the values for σ_m obtained here. The measured values for σ_m in the $E_{c.m.}$ range of 0.25–115.3 eV vary from ~ 9–13 Å^2 and are in good agreement with the cross section (~ 10–15 Å^2) reported by Gilbody and Hasted[43] and Galli et al.[44]

The theoretical values for $\sigma_{3/2}$ and $\sigma_{1/2}$ at $E_{c.m.}$=1.2, 4.1, 10.3, and 41.2 eV obtained in the multi-state calculations of Spalburg and Gislason[32] are also listed in Table I. The theory correctly predicts that $\sigma_{3/2}$ is

Table I. Values for $\sigma_{3/2}$, σ_m, $\sigma_{1/2}$, and $\sigma_{1/2}/\sigma_{3/2}$ in the center-of-mass collision energy ($E_{c.m.}$) of 0.2-115.3 eV

			Experimental			
			$\sigma_{1/2}$ (Å^2)		$\sigma_{1/2}/\sigma_{3/2}$	
$E_{c.m.}$ (eV)	$\sigma_{3/2}$ (Å^2)[b]	σ_m (Å^2)[b]	This work[c]	Ref. 19[d]	This work[e]	Ref. 19[e]
0.2	...	...	...	...	...	...
0.25	12.9	10.7	6.7±1.3	6.6±1.1	0.52	0.51
0.6	13.4	11.6	8.1±1.6	5.3±1.1	0.60	0.39
1.2	14.5	12.5	8.5±1.7	4.5±0.9	0.58	0.31
1.4	...	...	...	...	...	0.29
2.1	15.3	12.9	8.1±1.6	4.6±0.9	0.52	0.30
4.1	14.9	12.3	7.2±1.4	3.3±0.7	0.48	0.22
5.8	...	...	...	...	...	0.22
8.0	...	...	...	...	...	0.23
10.3	13.2	11.1	6.7±1.3	3.2±0.6	0.51	0.24
15.2	11.8	10.2	6.8±1.4	3.2±0.6	0.57	0.27
18.0	...	...	...	...	...	...
22.6	10.9	9.2	5.8±1.2	3.0±0.6	0.53	0.28
41.2	10.7	9.0	5.8±1.2	2.9±0.6	0.54	0.27
52.7	11.3	9.8	6.8±1.4	3.2±0.6	0.60	0.28
60.0	...	...	...	...	...	...
82.4	13.9	11.9	7.9±1.6	4.4±0.9	0.57	0.32
115.3	15.3	13.0	8.4±1.7	5.0±1.0	0.56	0.33
120.0	...	...	...	...	...	...

[a]Reference 32.

[b]This work. The experimental uncertainties for $\sigma_{3/2}$ and σ_m are estimated to be ≤5%.

[c]The value for $\sigma_{1/2}$ are calculated using the relation $\sigma_{1/2} = 3\sigma_m - 2\sigma_{3/2}$.

[d]The values fro $\sigma_{1/2}$ are obtained by multiplying the corresponding values for $\sigma_{1/2}/\sigma_{3/2}$ of Ref.19 and $\sigma_{3/2}$ determined here.

[e]The experimental uncertainties are estimated to be ~ 20%.

[f]Values obtained from Fig. 3 of Ref. 12.

[g]Reference 62 of Ref. 32.

[h]Most recent values obtained by Guyon and Govers (Ref. 23).

		Theoretical[a]		
Ref. 20	Ref. 12[f]	$\sigma_{3/2}(\text{Å}^2)$	$\sigma_{1/2}(\text{Å})^2$	$\sigma_{1/2}/\sigma_{3/2}$
...	0.74±0.10	...	...	...
...	...	...	...	...
...	...	...	...	...
...	...	8.3	4.8	0.58
0.31±0.03	0.58±0.06	...	...	...
...	...	...	...	...
...	...	12.1	2.9	0.24
0.32±0.03	0.68±0.10	...	...	...
0.35[g]...	...	...	...	...
...	...	12.3	13.1	0.25
...	...	...	...	...
0.51±0.04[h]	...	...	...	...
...	...	...	...	...
...	...	8.9	5.4	0.61
...	...	...	...	...
0.52±0.05[h]	...	...	...	...
...	...	...	...	...
...	...	...	...	...
0.41±0.04[h]	...	...	...	

greater than $\sigma_{1/2}$. In the intermediate $E_{c.m.}$ range of interest here, the theoretical studies[32,34] reveal that the energy resonance effect is more important than the Franck-Condon factor in governing the magnitude of the electron transfer cross section. The higher values for $\sigma_{3/2}$ have been partly attributed to the close energy resonance of the $Ar^+(^2P_{3/2})$ + $N_2(\tilde{X},v=0)$ and $Ar(^1S_0)$ + $N_2^+(\tilde{X},v'=1)$ states. The strong coupling between $Ar^+(^2P_{3/2})$ + $N_2(\tilde{X},v=0)$ and the electron transfer state is also shown to be responsible for the higher values for $\sigma_{3/2}$.

The experimental cross sections are higher than the theoretical cross sections.[32] The measured values for $\sigma_{3/2}$ at $E_{c.m.}$ = 4.1, 10.3, and 41.2 eV and $\sigma_{1/2}$ at $E_{c.m.}$ = 41.2 eV are in reasonable accord with the theoretical value. However, the experimental values for $\sigma_{3/2}$ at 1.2 and $\sigma_{1/2}$ at 1.2, 4.1, and 10.3 eV are approximately twice the theoretical predictions. Recent studies on the vibrational relaxation of diatomic ions show that the relaxation rate constant depends strongly on binding energy to the collision partner.[52,53] Since the binding energy of the $(Ar \cdot N_2)^+$ complex is ~ 1 eV,[54] the collision complex mechanism is likely to be important at low $E_{c.m.}$. The discrepancy observed between the experimental and theoretical cross section at low $E_{c.m.}$ may be due to the fact that in the theoretical calculation[32] the strong binding energy effect on the reaction dynamics of the system has been ignored.

The variations of $\sigma_{3/2}$ and $\sigma_{1/2}$ as a function of E_{lab} can be seen in Fig. 4. The curve for $\sigma_{3/2}$ exhibits a maximum in the E_{lab} range studied, an observation consistent with the theoretical prediction. However, the experimental maximum is at ~ 5-10 eV instead of that predicted at ~ 10-25

Figure 4. Total spin-orbit-state-selected cross sections, $\sigma_{3/2}$, $\sigma_{1/2}$, for the reaction $Ar^+(^2P_{3/2,1/2}) + N_2(v=0) \rightarrow Ar(^1S_0) + N_2^+(v')$ in the E_{lab} range of 0.6-280 eV. Experimental: (⊡) $\sigma_{3/2}$; (x) $\sigma_{1/2}$ measured using the tandem photoionization mass spectrometer; (o) $\sigma_{1/2}$ obtained by multiplying $\sigma_{3/2}$ of this experiment and $\sigma_{1/2}/\sigma_{3/2}$ measured using the crossed ion-neutral beam arrangement (Ref. 19). Theoretical (Ref. 32): (▮) $\sigma_{3/2}$; (●) $\sigma_{1/2}$

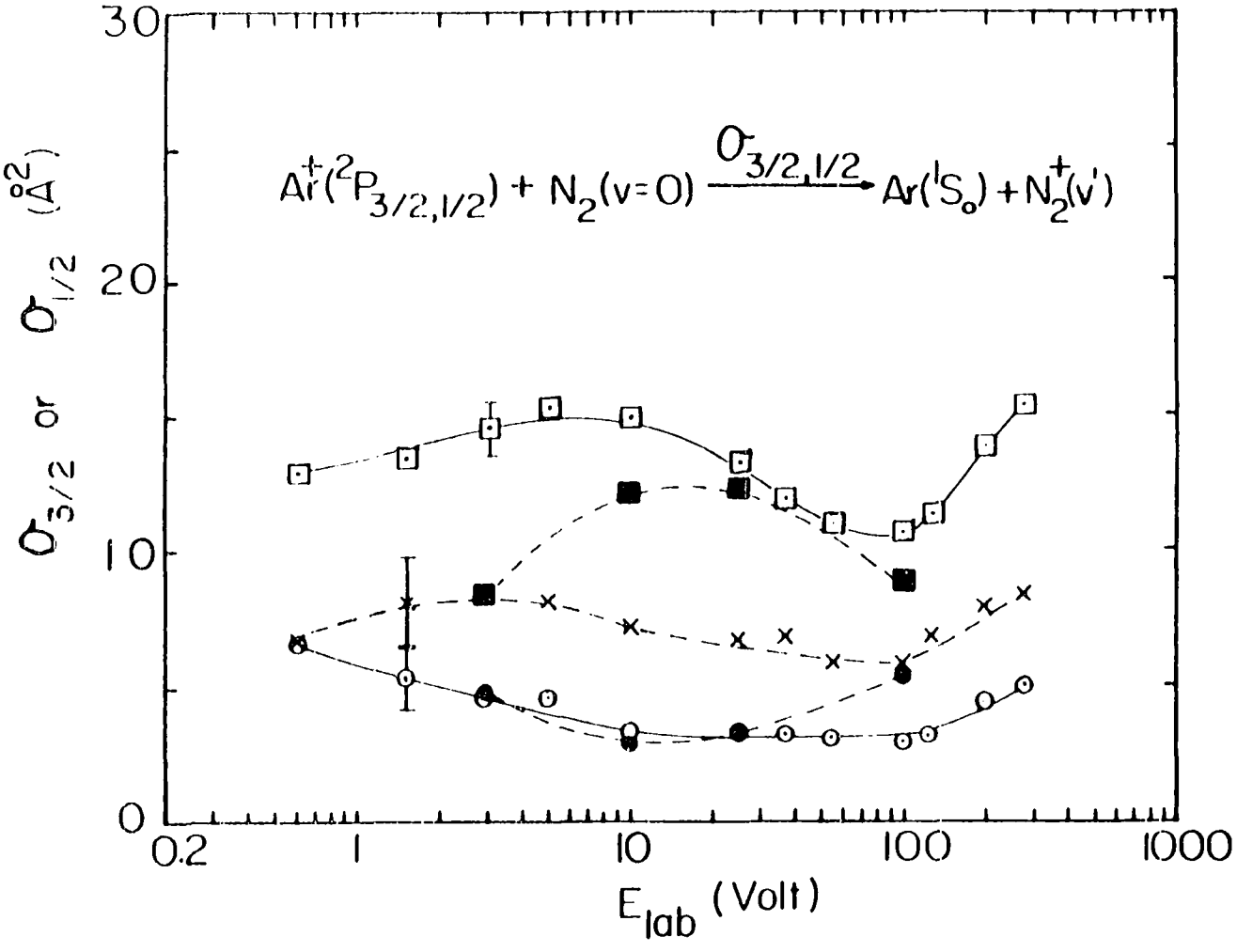
$Ar^+(^2P_{3/2,1/2}) + N_2(v=0) \xrightarrow{\sigma_{3/2,1/2}} Ar(^1S_o) + N_2^+(v')$
$\sigma_{3/2}$ or $\sigma_{1/2}$ ($Å^2$)
30
20
10
0
0.2
1
10
100
1000
E_{lab} (Volt)

eV. The kinetic energy dependence of the cross section for the electron transfer reaction $Ar^+ + N_2$ observed by Mahadevan and Magnuson[49] in the same E_{lab} range also has a maximum, but at E_{lab} ~ 30 eV. The most interesting observation is that the values for $\sigma_{3/2}$ and $\sigma_{1/2}$ reach a minimum at E_{lab} ~ 55–100 eV and then increase as E_{lab} is increased from E_{lab} ~ 100 eV. The increase of the cross section from E_{lab} ~ 60 to 1000 eV has been observed previously by Amme and Hayden.[47]

Previous experimental[16,17] and theoretical[32] studies show that reaction (1) favors the formation of the $Ar(^1S_0) + N_2^+(\tilde{X},v'=1)$ endothermic channel at low E_{lab}. The observed decrease of $\sigma_{3/2}$ from E_{lab} ~ 5–10 eV towards lower E_{lab} is most likely due to the energetic effect.

The $N_2^+(\tilde{X},v'=0) + Ar(^1S_0)$ state is higher than the $Ar^+(^2P_{3/2}) + N_2(\tilde{X},v=0)$ and $Ar^+(^2P_{1/2}) + N_2(\tilde{X},v=0)$ states by 0.98 and 0.77 eV, respectively. These three states are directly coupled in the vibronic Hamiltonian matrix.[34] Therefore, at sufficiently high E_{lab}, product N_2^+ ions of reaction (1) and (2) can be formed efficiently in the $\tilde{A}$ state of N_2^+. Parlant and Gislason[34] point out that the energy spread (FWHM) of the inelastic electron transfer products should be of the order of ~ 2 $\alpha\hbar v_{rel}$, where α = 1.75 $\mathring{A}^{-1}$ for the $[Ar + N_2]^+$ system and v_{rel} is the relative velocity of the colliding pair. The effective coupling range and the collision time can be approximated by $1/\alpha$ and $1/\alpha v_{rel}$, respectively. At E_{lab} = 280 eV, the highest collision energy used in this study, the energy spread of the electron transfer products is estimated to be ~ 0.81 eV which is similar to the potential energy differences between $N_2^+(\tilde{A},v'=0) + Ar(^1S_0)$ and $Ar^+(^2P_{3/2,1/2}) + N_2^+(\tilde{X},v=0)$. Since the energy spread of the

products is expected to be broadened when impulsive vibrational energy transfer is taken into account, we believe that the increases of $\sigma_{3/2}$ and $\sigma_{1/2}$ at E_{lab} > 100 eV are likely the results of populating the $\tilde{A}$ state of N_2^+. The theoretical investigation[34] shows that for a strongly-coupled system such as the $[Ar + N_2]^+$ system, increasing the number of accessible product channels increases the total cross sections for all accessible processes.

The values for $\sigma_{1/2}$ can also be calculated by multiplying the corresponding values for $\sigma_{3/2}$ determined here and $\sigma_{1/2}/\sigma_{3/2}$ determined in the crossed ion-neutral beam experiment.[19] These values for $\sigma_{1/2}$, which are shown in Table I and Fig. 4, are found to be in reasonable agreement with the theoretical predictions.

The Values of $\sigma_{1/2}/\sigma_{3/2}$ and Its Kinetic Energy Dependence

The values for the ratio $\sigma_{1/2}/\sigma_{3/2}$ over the $E_{c.m.}$ range of 0.41-164.7 eV measured using the crossed ion-neutral beam photoionization apparatus have been reported recently by Liao, Xu, and Ng.[19] The results of previous studies[12,19,20] and those of this experiment obtained using the tandem photoionization mass spectrometer at $E_{c.m.}$ = 0.2-115.3 eV are summarized in Table I. The previous findings reveal that the values for $\sigma_{1/2}/\sigma_{3/2}$ determined using the ion beam-gas cell arrangement[12] are higher than those observed in the crossed ion-neutral beam study.[19] The discrepancy is speculated[23] to be caused by secondary reactions in the gas cell experiment. The TESICO values obtained by Guyon and Govers[20] are slightly

higher than those obtained in the crossed ion-neutral study. The instrument of Guyon and Govers employs a crossed ion beam-effusive neutral beam arrangement and essentially maintains thin target conditions. The tandem photoionization mass spectrometer used here has an ion beam-gas cell arrangement. In order to maintain a homogeneous N_2 target gas density and minimize the ion focusing effect on the absolute cross section measurement, it is necessary to have a relatively long gas cell. Although the value for $P(N_2)$ used in the absolute cross section measurements is low, ~ 7 x 10^{-5} Torr, the conversion ratios $I(N_2^+)/I(Ar^+)$ (~ 0.03-0.05) are more than an order of magnitude higher than those observed in the crossed ion-neutral beam experiment.[19] Guyon and Govers found that when the conversion ratio for $Ar^+(^2P_{1/2})$ is increased from 0.008 to 0.012, the value for $\sigma_{1/2}/\sigma_{3/2}$ at $E_{c.m.}$ = 8 eV changes from ~ 0.35 to 0.5.[23] The values for $\sigma_{1/2}/\sigma_{3/2}$ determined here range from 0.48-0.61 and are substantially higher than the corresponding values deduced from the crossed ion-neutral beam study. This observation is consistent with the trend found in previous studies.

Figure 5 depicts the experimental[12,19,20] and theoretical results[32] for the kinetic energy dependence of $\sigma_{1/2}/\sigma_{3/2}$. Kato, Tanaka, and Koyano[12] and Guyon and Govers[20] measured the value for $\sigma_{1/2}/\sigma_{3/2}$ in relatively narrow energy ranges. They found that $\sigma_{1/2}/\sigma_{3/2}$ is nearly independent of E_{lab}, an observation contrary to the theoretical prediction and the experimental results of Liao, Xu, and Ng.[19] Despite the fact that the values for $\sigma_{1/2}/\sigma_{3/2}$ determined using the tandem photoionization mass spectrometer are higher than those found in the crossed ion-neutral beam study, the two sets of data, when plotted as a function of E_{lab}, have a

Figure 5. The values for $\sigma_{1/2}/\sigma_{3/2}$ in the E_{lab} range of 0.2–400 eV. Experimental: (o) Ref. 19; (x) Ref. 20; (●), (⬡) this work; (△) Ref. 12; (+) Most recent values obtained by Guyon and Govers (Ref. 23). Theoretical: (⊡) Ref. 32

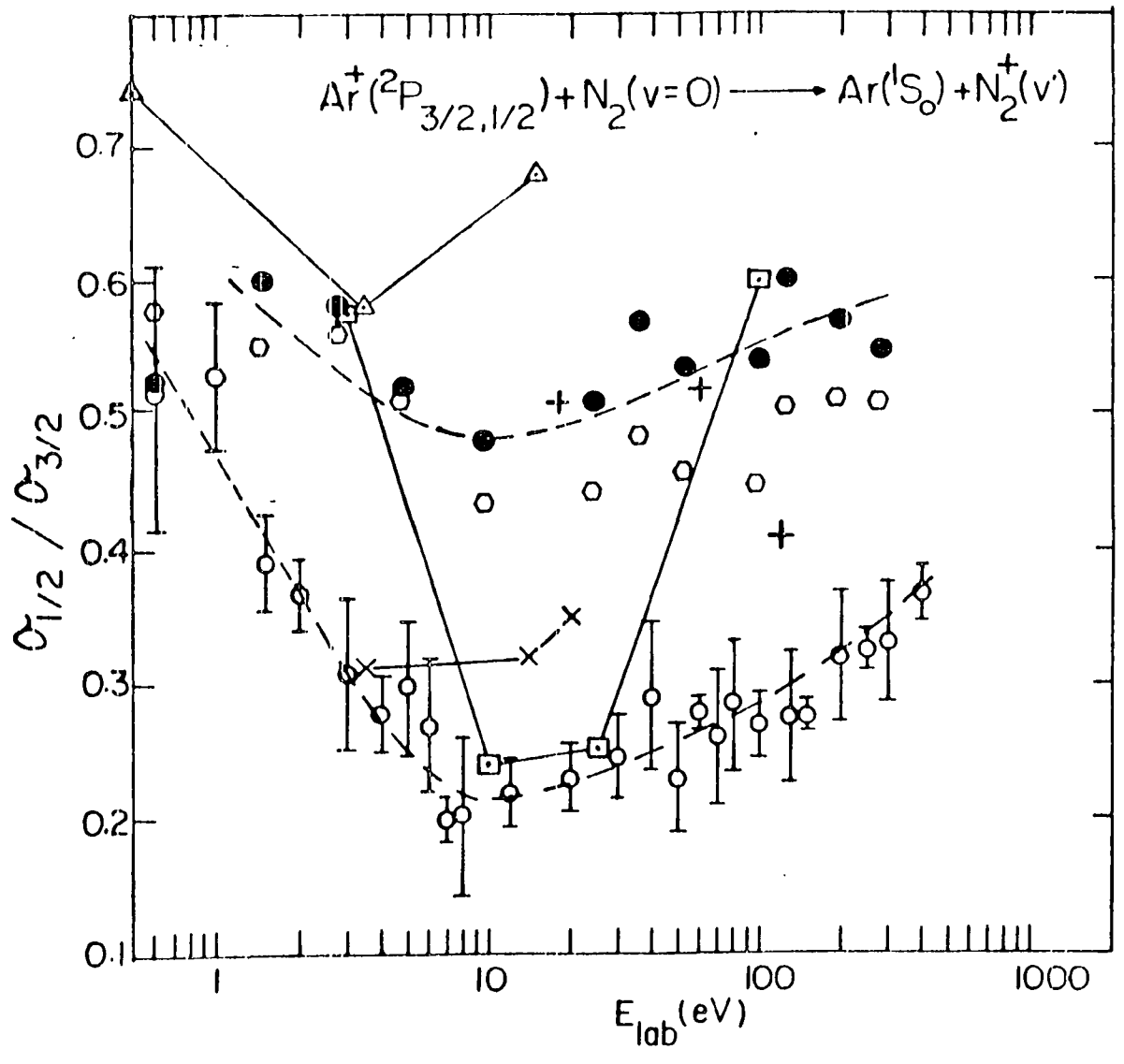
$Ar^+(^2P_{3/2,1/2}) + N_2(v=0) \longrightarrow Ar(^1S_0) + N_2^+(v')$
$\sigma_{1/2} / \sigma_{3/2}$
0.7
0.6
0.5
0.4
0.3
0.2
0.1
1
10
100
1000
E_{lab} (eV)

similar profile showing a broad minimum at E_{lab} ~ 10 eV. This observation is a qualitative support for the theoretical prediction on the kinetic energy dependence of $\sigma_{1/2}/\sigma_{3/2}$. The values for $\sigma_{1/2}/\sigma_{3/2}$ determined using a rf of ~ 20 MHz applied to the octopole gas cell, are also plotted in Fig. 5. Taking into account the experimental uncertainties (~ $\pm$0.1), the values for $\sigma_{1/2}/\sigma_{3/2}$ obtained with rf = 4 and 20 MHz are in agreement. The values for $\sigma_{1/2}/\sigma_{3/2}$ at E_{lab} = 10-15 eV obtained by the crossed ion-neutral beam study are in good agreement with the theoretical[32] results. The discrepancy observed between the experimental[19] and the theoretical values for $\sigma_{1/2}/\sigma_{3/2}$ at higher and lower E_{lab} has been attributed to the estimated PES used in the calculation. Recently, Parlant and Gislason have reported a more accurate calculation on the electron transfer reaction of $Ar^+ + N_2$ using the ab initio PES. The calculation of the state-to-state cross sections for reaction (1) and (2) should be straightforward. It will be interesting to compare results of the new calculation and experimental findings.

Possible N_2 Gas Cell and Background Pressure Effects on the Measured Values for $\sigma_{3/2}$, $\sigma_{1/2}$, and $\sigma_{1/2}/\sigma_{3/2}$

One of the interesting findings of the semi-classical multi-state study is that the cross section, σ_D, for the deexcitation reaction

$$Ar^+(^2P_{1/2}) + N_2(\tilde{X},v=0) \longrightarrow Ar^+(^2P_{3/2}) + N_2 \qquad (6)$$

is found to be large even at low collision energies. The cross section, σ_E, for the excitation process

$$Ar^+(^2P_{3/2}) + N_2(\tilde{X},v=0) \longrightarrow Ar^+(^2P_{1/2}) + N_2 \qquad (7)$$

is predicted to be small at low $E_{c.m.}$ (< 10 eV); but it becomes significant as $E_{c.m.}$ is increased. The calculated values[32] for σ_D and σ_E are listed in Table II. The predicted value (14.5 $\mathring{A}^2$) for σ_D is higher than the experimental value (10.7 $\mathring{A}^2$) for $\sigma_{3/2}$ at $E_{c.m.}$ = 41.2 eV. Although the $Ar^+(^2P_{3/2}) + N_2$ and $Ar^+(^2P_{1/2}) + N_2$ states are not directly coupled, the theoretical study shows that the surprisingly large cross sections for reactions (6) and (7) arise from the mutual interactions of the electron transfer Ar + N_2^+ states with the spin-orbit states of Ar^+.

The spin-orbit transitions induced by the presence of the Ar + N_2^+ electron transfer state provide possible mechanisms for the mixing of the reactant Ar^+ state during the transportation of reactant Ar^+ ions from the photoionization region to the reaction gas cell if the N_2 background pressure in the apparatus is high. When the spin-orbit-state mixing occurs prior to the electron transfer reactions (1) and (2) in the gas cell, the experimental value for $\sigma_{1/2}/\sigma_{3/2}$ will be higher than the true value. Because the background pressure is low (< 5 x 10^{-6} Torr) along the path between the photoionization region and the entrance of the rf octopole gas cell in the tandem photoionization mass spectrometer, the mixing of the reactant Ar^+ state outside of the gas cell should be small. Assuming a value of 15 $\mathring{A}^2$ for σ_D or σ_E, we estimate the conversion between $Ar^+(^2P_{3/2})$ and $Ar^+(^2P_{1/2})$ to be < 2%.

If the N_2 gas cell pressure is high or the gas cell is long, spin-orbit-state mixing can also take place within the gas cell concomitant with

Table II. Theoretical[a] cross sections σ_E[b] and σ_D[c] for collisional-induced spin-orbit transitions

$E_{c.m.}$ (eV)	$\sigma_E(\mathring{A}^2)$	$\sigma_D(\mathring{A}^2)$
1.2	0.02	4.19
4.1	0.44	4.35
10.3	1.98	6.59
41.2	6.63	14.50

[a]Reference 32.

[b]Total cross section for the process $Ar^+(^2P_{3/2}) + N_2(v=0) \rightarrow Ar^+(^2P_{1/2}) + N_2(v')$.

[c]Total cross section for the process $Ar^+(^2P_{1/2}) + N_2(v=0) \rightarrow Ar^+(^2P_{3/2}) + N_2(v')$.

electron transfer. Because of the relatively long gas cell used in this study, it is possible that secondary processes in the rf octopole gas cell may have an effect on the measured values for $\sigma_{3/2}$, σ_m, and $\sigma_{1/2}/\sigma_{3/2}$. We have performed a simple model analysis to examine the effect of reaction (6) and (7) on the absolute cross section measurements (see Appendix). In the model analysis, we consider a beam of reactant Ar^+ ions, all assumed to have the same velocity, is incident on a target of N_2 in the rf octopole gas cell. In addition to reaction (1) and (2), $Ar^+(^2P_{3/2})$ and $Ar^+(^2P_{1/2})$ can undergo spin-orbit transitions according to reactions (6) and (7). The derivation in Appendix shows that the intensities of $Ar^+(^2P_{3/2})$ and $Ar^+(^2P_{1/2})$ at a position x measured with respect to the entrance of the rf octopole gas cell, $I_{3/2}(x)$ and $I_{1/2}(x)$, respectively, can be calculated by Eqs. (A9) and (A10). The product $Ar^+(^2P_{3/2,1/2})$ ions of reactions (6) and (7) are assumed to move along the gas cell with the same velocity as that of the reactant Ar^+ ion beam. If the main contribution to σ_E and σ_D arises from long range interactions as predicted by the theory, the latter assumption is a reasonable one. Assuming 100% collection efficiency for product N_2^+, the total intensity for N_2^+ formed in the reaction gas cell is predicted by Eq. (A11). Using the theoretical values for σ_E and σ_D (Table II) and the experimental values for $\sigma_{3/2}$ and $\sigma_{1/2}$ (column 5 of Table I) as the true cross sections, the variations of the measured values for $\sigma_{3/2}$, σ_m, and $\sigma_{1/2}/\sigma_{3/2}$ as a function of $P(N_2)$ can be calculated by Eqs. (A12) and (3). The experimental values for $\sigma_{1/2}$ used as part of the inputs in the calculation are obtained by multiplying the corresponding experimental

values for $\sigma_{3/2}$ and those for $\sigma_{1/2}/\sigma_{3/2}$ measured by the crossed ion-neutral experiment.[19] The values predicted in the model analysis for $\sigma_{3/2}$, σ_m, and $\sigma_{1/2}/\sigma_{3/2}$ at $P(N_2) = 1 \times 10^{-5}$, 1.1×10^{-4}, 4.6×10^{-4}, 1.0×10^{-3}, and 2.0×10^{-3} Torr are summarized in Table III.

As anticipated, the predicted value for $\sigma_{3/2}$ at $E_{c.m.} = 1.2$ eV remains constant as $P(N_2)$ is increased from 1×10^{-5} to 2×10^{-3} Torr because σ_E is negligible. At a higher $E_{c.m.}$ and a high $P(N_2)$, a finite value of σ_E causes the Ar^+ beam to be richer in $Ar^+(^2P_{1/2})$ as the reactant Ar^+ beam moves along the gas cell and thus the measured value for $\sigma_{3/2}$ is lower than that measured at a lower $P(N_2)$. For example, at $E_{c.m.} = 41.2$ eV, the value of σ_E is 6.6 $\mathring{A}^2$, and the predicted value for $\sigma_{3/2}$ decreases by 1.5 $\mathring{A}^2$ as $P(N_2)$ increases from 1×10^{-5} to 2×10^{-3} Torr. Nevertheless, the variation of $\sigma_{3/2}$ must be considered small for a change of more than two orders of magnitude in $P(N_2)$. Based on this analysis, we believe that the measured values for $\sigma_{3/2}$ (Table I) are reliable.

The value for σ_m is measured by using a reactant Ar^+ beam with a composition of 66.7% in $Ar^+(^2P_{3/2})$ and 33.3% in $Ar^+(^2P_{1/2})$. Although the value for σ_D is predicted to be greater than that for σ_E, as a consequence of substantially higher $\sigma_{3/2}$ than $\sigma_{1/2}$, the model analysis shows that the reactant Ar^+ beam also becomes richer in $Ar^+(^2P_{1/2})$ as it traverses through the rf octopole gas cell at a high $P(N_2)$. This effect is manifested by lower σ_m values at higher $P(N_2)$. Thus the value for $\sigma_{1/2}/\sigma_{3/2}$, calculated by Eq. (3) is highly susceptible to the change in $P(N_2)$. The values for $\sigma_{1/2}/\sigma_{3/2}$ at $E_{c.m.} = 1.2$ and 4.1 eV are found to decrease with increasing $P(N_2)$, while the opposite trends are observed at $E_{c.m.} = 10.3$ and 41.2 eV.

Table III. Predicted variations of the meassured vlues for $\sigma_{3/2}{}^{a}$, $\sigma_m{}^{a}$, and $\sigma_{1/2}/\sigma_{3/2}$ as a function of the N_2 gas cell pressure ($P(N_2)$)

	$E_{c.m.}$ = 1.2eV			$E_{c.m.}$ = 4.1eV		
$P(N_2)$(Torr)	$\sigma_{3/2}(\mathring{A}^2)$	$\sigma_m(\mathring{A}^2)$	$\sigma_{1/2}/\sigma_{3/2}$	$\sigma_{3/2}(\mathring{A}^2)$	$\sigma_m(\mathring{A}^2)$	$\sigma_{1/2}/\sigma_{3/2}$
$1X10^{-5}$	14.5	11.2	0.31	14.9	11.0	0.22
$1.1X10^{-4}$	14.5	11.2	0.31	14.9	11.0	0.22
$4.6X10^{-4}$	14.5	11.1	0.31	14.8	10.8	0.19
$1.0X10^{-3}$	14.5	11.0	0.28	14.8	10.7	0.17
$2.0X10^{-3}$	14.5	10.9	0.26	14.6	10.3	0.12

[a] $\sigma_{3/2}$ and σ_m are equal to $\sigma(X=1)$ and $\sigma(X=0.667)$, respectively, which are calculated using Eq. (B12). In the calculation, the theoretical values for σ_E and σ_D (Table II) and the experimental values for $\sigma_{3/2}$ (column 2 of Table I) and $\sigma_{1/2}$ (column 5 of Table I) are used as the inputs for the true cross sections.

[b] Calculated using the relation $\sigma_{1/2}/\sigma_{3/2} = 3\sigma_m/\sigma_{3/2} - 2$.

$E_{c.m.}$ = 10.3eV			$E_{c.m.}$ = 41.2eV		
$\sigma_{3/2}(\mathring{A}^2)$	$\sigma_m(\mathring{A}^2)$	$\sigma_{1/2}/\sigma_{3/2}$	$\sigma_{3/2}(\mathring{A}^2)$	$\sigma_m(\mathring{A}^2)$	$\sigma_{1/2}/\sigma_{3/2}$
13.2	9.9	0.24	10.7	8.1	0.27
13.2	9.9	0.24	10.6	8.1	0.29
13.0	9.8	0.26	10.2	8.0	0.36
12.8	9.7	0.26	9.8	7.9	0.43
12.4	9.4	0.28	9.2	7.8	0.55

A change by nearly a factor of two for $\sigma_{1/2}/\sigma_{3/2}$ at $E_{c.m.}$ = 4.1 and 41.2 eV is expected when $P(N_2)$ varies from 1 x 10^{-5} to 2 x 10^{-3} Torr. At $P(N_2)$ = 4.6 x 10^{-4} Torr, the mean free path of N_2 is comparable to the length of the rf octopole gas cell. The value of $\sigma_{1/2}/\sigma_{3/2}$ at $E_{c.m.}$ = 41.2 eV with $P(N_2)$ = 4.6 x 10^{-4} Torr is predicted to be 22% higher than that at $P(N_2)$ = 1 x 10^{-5} Torr. It is deceiving to use the mean free path argument to exclude the possible influence of secondary reactions in the measurement of $\sigma_{1/2}/\sigma_{3/2}$. The analysis is based on probably an oversimplified model. The accuracy of the values for σ_E and σ_D used here remains in question, especially values at higher $E_{c.m.}$ where contributions by short range impulsive interactions may be important. The $(Ar \cdot N_2)^+$ complex is strongly bound.[54] At low $E_{c.m.}$, the collision complex mechanism is expected to have a significant effect on σ_D.[52,53] Nonetheless, this simple model analysis reveals that the values for $\sigma_{1/2}/\sigma_{3/2}$ determined here might be less accurate in comparison to those obtained in the crossed ion-neutral beam experiment where the effects of reactions (6) and (7) are small. Similarly, the values for $\sigma_{1/2}$ deduced by multiplying the corresponding experimental values for $\sigma_{3/2}$ reported here and those for $\sigma_{1/2}/\sigma_{3/2}$ reported in Ref. 19 might be more accurate than those measured using the tandem photoionization mass spectrometer.

However, the model analysis does not explain the differences of the values for $\sigma_{1/2}/\sigma_{3/2}$ obtained using the tandem photoionization mass spectrometer and the crossed ion-neutral beam photoionization apparatus. The results of the analysis as listed in Table III indicate that for $P(N_2)$ ~ 7 x 10^{-5} Torr used in the measurements of $\sigma_{3/2}$ and σ_m, reactions (6) and

(7) should have little effect on the values deduced for $\sigma_{1/2}/\sigma_{3/2}$ (and $\sigma_{1/2}$). In view of these observations, we believe that it is not justified to reject the values for $\sigma_{1/2}/\sigma_{3/2}$ (and $\sigma_{1/2}$) determined using the tandem photoionization mass spectrometer.

As pointed out previously, the collection efficiency for electron transfer product ions in a crossed ion-neutral beam experiment is expected to be good. The fact that relative state-selected cross sections for the electron transfer reactions $H_2^+(v') + H_2$[39] and $N_2^+(v') + Ar$[21] determined using the crossed ion-neutral beam photoionization apparatus are in good accordance with results of TESICO experiments[15,52] and reliable theoretical calculations[33,35,53] seems to favor the values for $\sigma_{1/2}/\sigma_{3/2}$ of Ref. 19 over those measured with the ion beam-rf octopole gas cell arrangement. Without doubt the collection efficiency of product N_2^+ in the latter experiment is better than that in the crossed ion-neutral beam experiment. The higher value for $\sigma_{3/2}$ than that for $\sigma_{1/2}$ is partly attributed to the close energy resonance of $Ar^+(^2P_{3/2}) + N_2(\tilde{X},v=0)$ with the $N_2^+(\tilde{X},v'=1) + Ar(^1S_0)$ electron transfer state. It is possible the collection efficiency attained in the crossed ion-neutral beam experiment for product N_2^+ of reaction (1) is slightly higher than that of reaction (2). If this is the case, the values for $\sigma_{1/2}/\sigma_{3/2}$ should be considered as lower bounds. At the present time, we do not have an explanation for the observed differences of values for $\sigma_{1/2}/\sigma_{3/2}$ obtained using the tandem photoionization mass spectrometer and crossed ion-neutral beam photoionization apparatus.

Most recently, Guyon and Govers[23] have obtained values for $\sigma_{1/2}/\sigma_{3/2}$ at $E_{c.m.}$ = 18, 60, and 120 eV (see Table I and Fig. 5). These values are close to those measured using the tandem photoionization mass spectrometer.

Absolute state-to-state total cross sections for reactions (1) and (2)

The vibrational distributions of product $N_2^+(\tilde{X},v')$ formed by reactions (1) and (2) in the $E_{c.m.}$ range of 0.25-41.2 eV have been measured by Liao et al.[56] as part of this experiment with a crossed ion-neutral beam photoionization apparatus. The theoretical values for the fractions of product N_2^+ formed in a vibrational state v' by reactions (1) and (2), $X_{3/2\to v'}$ and $X_{1/2\to v'}$, are obtained by the relations

$$X_{3/2\to v'} = \sigma_{3/2\to v'}/\sigma_{3/2} \tag{8}$$

$$X_{1/2\to v'} = \sigma_{1/2\to v'}/\sigma_{1/2} \tag{9}$$

At $E_{c.m.}$ = 1.2, 4.1, 10.3, and 41.2 eV, it is energetically possible to produce N_2^+ via reactions (1) and (2) in vibrational states $v' \geq 2$. According to the theoretical prediction, the values for $X_{3/2\to v'}$ and $X_{1/2\to v'}$, $v' \geq 3$, are ≤ 0.01 in the $E_{c.m.}$ range of 1.2-41.2 eV. Therefore, Liao et al. analyzed their data with an assumption that charge transfer product $N_2^+(\tilde{X},v')$ ions are only formed in the v' = 0, 1, and 2 states.

The experimental uncertainties for $X_{3/2\to v'}$ deduced in the crossed ion-neutral beam experiment are relatively large. Nevertheless, the experimental results confirm the theoretical prediction that product $N_2^+(\tilde{X},v')$ ions of reactions (1) over the $E_{c.m.}$ range of 1.2-41.2 eV are formed predominantly in the v'=1 state. The semi-classical multi-state studies of Spalburg and Gislason[32] and Parlant and Gislason[34] show that the

high cross section for producing $Ar(^1S_0) + N_2^+(\tilde{X},v'=1)$ is partly due to the close energy resonance of $Ar^+(^2P_{3/2}) + N_2(\tilde{X},v=0)$ and $Ar(^1S_0) + N_2^+(\tilde{X},v'=1)$ and partly because of the strong direct coupling of the two states in the vibronic Hamiltonian matrix. In the intermediate $E_{c.m.}$ range, they find that energy resonance is more important than the Franck-Condon consideration in determining the product state distributions. The observation that the formations of inelastic charge transfer channels $Ar(^1S_0) + N_2^+(\tilde{X},v'=0)$ and $Ar(^1S_0) + N_2^+(\tilde{X},v'=2)$ become more significant as $E_{c.m.}$ increases is consistent with the conclusion found in the symmetric electron transfer reaction of $H_2^+ + H_2$.[39,41]

Combining the experimental values for $\sigma_{3/2}$, $\sigma_{1/2}$, $X_{3/2\to v''}$, and $X_{1/2\to v''}$, absolute state-to-state total cross sections, $\sigma_{3/2\to v''}$ and $\sigma_{1/2\to v''}$, for reactions (1) and (2) are calculated using Eqs. (8) and (9), respectively. As shown in Table IV, the experimental and theoretical values for $\sigma_{3/2\to v''}$, $v' = 0-2$, are in reasonable agreement except at $E_{c.m.} = 1.2$ eV where the experimental value for $\sigma_{3/2\to 1}$ is ~ a factor of 1.5 higher than that predicted by the theory. Theoretical values for $\sigma_{1/2\to v''}$, $v' = 0-2$, at $E_{c.m.} = 0.25$ eV are not available to compare with the experimental results. The values for $\sigma_{1/2\to 2}$ at $E_{c.m.} = 1.2$ and 4.1 eV are crude estimates. Depending on the values for $\sigma_{1/2}$ used (column 4 or 5 of Table I), the estimated values for $\sigma_{1/2\to 2}$ at $E_{c.m.} = 1.2$ and 4.1 eV differ by nearly a factor of two.

Table IV. State-to-state cross sections, $\sigma_{3/2\to v'}$ and $\sigma_{1/2\to v'}$, for the reactions $Ar^+(^2P_{3/2,1/2}) + N_2(\tilde{X},v=0) \to Ar(^1S_0) + N_2^+(\tilde{X},v')$

		Experimental[b]				Theoretical[c]			
$E_{c.m.}$ (eV)[a]	v'	$\sigma_{3/2\to v'}$ (Å^2)	$X_{3/2\to v'}$	$\sigma_{1/2\to v'}$ (Å^2)[d]	$X_{1/2\to v'}$	$\sigma_{3/2\to v'}$ (Å^2)	$X_{3/2\to v'}$	$\sigma_{1/2\to v'}$ (Å^2)[d]	$X_{1/2\to v'}$
0.25	0	$0.00^{+1.3}_{-0.0}$	$0.00^{+0.10}_{-0.00}$ 0.13 ± 0.10[e]	~0.0	0.0	...	...	...	...
	1	$12.9^{+0.6}_{-1.5}$	$1.00^{+0.00}_{-0.10}$ 0.87 ± 0.10[e]	~0.9(~0.9)	$0.14^{+0.35}_{-0.14}$	...	...	...	...
	2	...	...	~5.7(~5.8)	$0.86^{+0.14}_{-0.35}$	...	...	...	...
1.2	0	$0.0^{+1.5}_{-0.0}$	$0.00^{+0.10}_{-0.00}$	...	...	0.00	0.000	0.00	0.000
	1	12.3 ± 2.2	0.85 ± 0.15	...	...	8.28	0.998	0.90	0.019
	2	2.2 ± 2.2	0.15 ± 0.15	~4.5(8.5)[g]	~1.0[g]	0.02	0.002	4.68	0.977
	3	...	...	...	...	0.00	0.000	0.02	0.004
1.7	0	...	...[f]	...	...	...	...	...	...
	1	...	1.0[f]	...	...	...	...	...	...

4.1	0	$0.0^{+1.5}_{-0.0}$	$0.00^{+0.10}_{-0.00}$	...	...	<0.01	0.000	0.00	0.000
	1	12.7 ± 2.2	0.85 ± 0.15	...	...	12.06	0.995	0.56	0.196
	2	2.2 ± 2.2	0.15 ± 0.15	~3.3(7.2)[g]	~1.0[f] ~1.0[g]	<0.06	0.005	2.27	0.794
	3	...	...	...	...	0.00	0.000	0.03	0.010
10.3	0	$0.0^{+1.3}_{-0.0}$	$0.00^{+0.10}_{-0.00}$	...	...	0.08	0.006	0.01	0.045
	1	$12.8^{+0.4}_{-2.0}$	$0.97^{+0.03}_{-0.15}$	...	...	12.18	0.987	1.87	0.570
	2	$0.4^{+2.0}_{-0.4}$	$0.03^{+0.15}_{-0.003}$	...	...	0.08	0.007	1.24	0.378
	3	...	...	...	...	0.00	0.000	0.02	0.006
41.2	0	2.4 ± 1.1	0.22 ± 0.10	...	...	1.69	0.133	0.46	0.104
	1	7.2 ± 1.9	0.67 ± 0.18	...	...	7.60	0.855	4.29	0.799
	2	$1.2^{+1.9}_{-1.2}$	$0.11^{+0.18}_{-0.11}$	...	...	0.11	0.012	0.51	0.095
	3	...	...	...	...	0.00	0.000	0.01	0.002

[a]Center-of-mass collision energy.

[b]This work.

[c]Reference 32.

[d]The values for $\sigma_{1/2}$ in column 5 of Table I are used to calculate $\sigma_{1/2 \to v'}$. The values in parentheses are deduced using the values for $\sigma_{1/2}$ determined in this work (column 4 of Table I).

[e]Reference 16.

[f]Reference 17.

[g]Estimated values.

CONCLUSIONS

Absolute spin-orbit-state-selected total cross sections for reactions (1) and (2) over the $E_{c.m.}$ range of 0.25-115.3 eV have been measured using the newly developed tandem photoionization mass spectrometer. The theoretical values for $\sigma_{3/2}$ and $\sigma_{1/2}$ in the $E_{c.m.}$ range of 1.2-41.2 eV are approximately a factor of two smaller than those obtained in this experiment. A simple model analysis, which takes into account possible spin-orbit transitions in the rf octopole reaction gas cell, reveals that the measured values for $\sigma_{3/2}$ using the ion beam-gas cell arrangement are reliable, whereas the values for $\sigma_{1/2}/\sigma_{3/2}$ can be strongly affected by reactions (6) and (7) if high $P(N_2)(\geq 5 \times 10^{-4}$ Torr) is used in the absolute cross section measurement. Values for $\sigma_{1/2}$ are also deduced by using the measured values for $\sigma_{3/2}$ and the corresponding values for $\sigma_{1/2}/\sigma_{3/2}$ obtained in the crossed ion-neutral beam experiment. The values for $\sigma_{1/2}$ thus deduced are in reasonable agreement with the theoretical cross sections. The kinetic energy dependences for $\sigma_{3/2}$, $\sigma_{1/2}$ and $\sigma_{1/2}/\sigma_{3/2}$ predicted by the multi-state calculation [33] are in qualitative accord with the experimental observations. The values for $\sigma_{3/2}$ and $\sigma_{1/2}$ are found to increase at higher $E_{c.m.}$ (>41.2 eV). This observation is rationalized as due to the formation of N_2^+ in the $\tilde{A}^2\Pi_u$ state at high $E_{c.m.}$.

Combining the measured values for $\sigma_{3/2}$, $\sigma_{1/2}$, and the measured vibrational distributions for $N_2^+(\tilde{X},v')$, $X_{3/2\rightarrow v'}$ and $X_{1/2\rightarrow v'}$, formed by reactions (1) and (2) in a crossed ion-neutral beam experiment, the absolute state-to-state total cross sections, $\sigma_{3/2\rightarrow v'}$ and $\sigma_{1/2\rightarrow v'}$, for reactions (1) and (2) have also been determined.

The discrepancies observed between the experimental and theoretical results can be partly attributed to the estimated PES used in the semi-classical multi-state calculation. The recent theoretical study shows that the assumption of isotropic coupling used by Spalburg and Gislason is incorrect. At higher $E_{c.m.}$ it is necessary to include the $\tilde{A}^2\Pi_u$ state of N_2^+ in the calculation. A new calculation which used realistic PES for the [Ar + N_2]$^+$ system is expected to improve the theoretical predictions. We hope the experiment findings presented here will provide the impetus for a more rigorous theoretical study in the future.

APPENDIX

Possible N_2 Gas Cell Pressure Effects on the Measured Values for $\sigma_{3/2}$, σ_m, and $\sigma_{1/2}/\sigma_{3/2}$.

In the following analysis, a coordinate system is chosen such that the x-axis coincides with the central axis of the rf octopole gas cell. The entrance and the exit of the gas cell correspond to x=0 and x=l, respectively. The changes in the $Ar^+(^2P_{3/2})$ and $Ar^+(^2P_{1/2})$ beam intensities, $dI_{3/2}$ and $dI_{1/2}$, are proportional to the change in target thickness, dx,

$$dI_{3/2} = -n(\sigma_{3/2} + \sigma_E)I_{3/2}dx + n\sigma_D I_{1/2}dx \tag{A1}$$

$$dI_{1/2} = -n(\sigma_{1/2} + \sigma_D)I_{1/2}dx + n\sigma_E I_{3/2}dx \tag{A2}$$

The general solutions of the coupled differential equations are

$$I_{3/2}(x) = \left(\frac{k_1+a_1+a_4}{k_1+a_2+a_3}\right)C_1\exp(k_1x) + \left(\frac{k_2+a_1+a_4}{k_2+a_2+a_3}\right)C_2\exp(k_2x)$$

$$= b_1C_1\exp(k_1x) + b_2C_2\exp(k_2x) \tag{A3}$$

$$I_{1/2}(x) = C_1\exp(k_1x) + C_2\exp(k_2x) \tag{A4}$$

where $a_1 = n\sigma_D$, $a_2 = n(\sigma_{3/2} + \sigma_E)$, $a_3 = n\sigma_E$, $a_4 = n(\sigma_{1/2} + \sigma_D)$, $k_{1,2} = [-(a_2 + a_4) \pm \sqrt{[(a_2 - a_4)^2 + 4a_1a_3)]}/2$, and C_1 and C_2 are arbitrary constants. At

the entrance of the rf octopole gas cell, we assume that the fraction (X) for $Ar^+(^2P_{3/2})$ in the reactant Ar^+ ion beam is the same as that produced by photoionization. This requires that

$$I_{3/2}(x=0) = b_1C_1 + b_2C_2 = XI_o \tag{A5}$$

$$I_{1/2}(x=0) = C_1 + C_2 = (1-X)I_o \tag{A6}$$

$$C_1 = I_o[b_2(1 - X) - X]/(b_2 - b_1) = f_1I_o \tag{A7}$$

$$C_2 = I_o[X - b_1(1 - X)]/(b_2 - b_1) = f_2I_o, \tag{A8}$$

where I_o is the total intensity of the unattenuated reactant Ar^+ beam. Therefore, Eqs. (A3) and (A4) become

$$I_{3/2}(x) = [b_1f_1\exp(k_1x) + b_2f_2\exp(k_2x)]I_o \tag{A9}$$

$$I_{1/2}(x) = [f_1\exp(k_1x) + f_2\exp(k_2x)]I_o \tag{A10}$$

The total intensity of product $N_2^+(\tilde{X})$ formed in the rf octopole gas cell can be calculated as

$$I_{N_2^+}(l) = \int_o^l [nI_{3/2}(x)\sigma_{3/2} + nI_{1/2}(x)\sigma_{1/2}]dx$$

$$= nI_o\{[\frac{b_1 f_1}{k_1}(\exp(k_1 l) - 1) + \frac{b_2 f_2}{k_2}(\exp(k_2 l) - 1)]\sigma_{3/2}$$
$$+ [\frac{f_1}{k_1}(\exp(k_1 l) - 1) + \frac{f_2}{k_2}(\exp(k_2 l) - 1)]\sigma_{1/2}\} \qquad (A11)$$

The measured cross section is

$$\sigma(X) = \frac{-1}{nl} \ln(1 - \frac{I_{N_2^+}}{I_o}) \qquad (A12)$$

The values for $\sigma_{3/2}$ and σ_m are equal to $\sigma(X=1)$ and $\sigma(X=2/3)$, respectively.

References

1. N. G. Adams, A. G. Dean, and D. Smith, Int. J. Mass Spectrom. Ion Phys. 10, 62 (1972).

2. P. Warneck, J. Chem. Phys. 46, 513 (1967).

3. J. B. Laudenslager, W. T. Huntress, and M. T. Bowers, J. Chem. Phys. 61, 4600 (1974).

4. F. Howorka, J. Chem. Phys. 68, 804 (1978).

5. R. Thomas, A. Barassin, and R. R. Burke, Int. J. Mass Spectrom. Ion Phys. 28, 275 (1978).

6. D. Hyatt and P. F. Knewstubb, J. Chem. Soc. Faraday Trans. 68, 202 (1972).

7. N. G. Adams, D. K. Bohme, D. B. Dunkin, and F. C. Fehsenfeld, J. Chem. Phys. 52, 1851 (1970).

8. Y. Kaneko, N. Kobayashi, and I. Kanomata, J. Phys. Soc. Jpn. 27, 982 (1969).

9. F. C. Fehsenfeld, E. E. Furguson, and A. L. Schmeltekopf, J. Chem. Phys. 45, 404 (1966).

10. D. Smith and N. G. Adams, Phys. Rev. A 23, 2327 (1981).

11. W. Lindinger, F Howorka, P. Lukal, S Kuhn, H. Villinger, E. Alge, and H. Ramler, Phys. Rev. A 23, 2819 (1981).

12. T. Kato, K. Tanaka, and I. Koyano, J. Chem. Phys. 77, 337 (1982).

13. T. Kato, K. Tanaka, and I. Koyano, J. Chem. Phys. 77, 837 (1982).

14. B. B. Mahan, C. Martner, and A. O'Keefe, J. Chem. Phys. 76, 4433(1984).

15. T. R. Govers, P.-M. Guyon, T. Baer, K. Cole, H. Fröhlich, and M. Lavollée, Chem. Phys. 87, 373 (1984).

16. L. Hüwel, K. R. Guyer, G. H. Lin, and S. R. Leone, J. Chem. Phys. 81, 3520 (1984).

17. B. Friedrich, W Trafton, A. L. Rockwood, S. L. Howard, and J. Futrell, J. Chem. Phys. 80, 2537 (1984).

18. A. L. Rockwood, S. L. Howard, W.-H. Du, P. Tosi, W. Lindinger, and J. Futrell, Chem. Phys. Lett. 114, 486 (1985).

19. C.-L Liao, R. Xu, and C. Y. Ng, J. Chem. Phys. 84, 1948 (1986).

20. P.-M. Guyon and T. Govers, Université Paris-Sud, to be published.

21. R. Xu, C.-L. Liao, J. D. Shao, G. D. Flesch, and C. Y. Ng, J. Chem. Phys., to be published.

22. W. Federer, H. Ramler, H. Villinger, and W. Lindinger, Phys. Rev. Lett. 54, 540 (1985).

23. P.-M. Guyon, and T. R. Govers, Université Paris-Sud, to be published.

24. E. W. Kaiser, A. Crowe, and W. E. Falconer, J. Chem. Phys. 61, 2720 (1974).

25. R. L. Champion and L. D. Doverspike, J. Chem. Phys. 49, 4321 (1968).

26. T. L. Budzynski and T. L. Bailey, Int. J. Mass Spectrom. Ion Phys. 18, 317 (1975).

27. W. L. Hodge, A. L. Goldberger, M. Vedder, and E. Pollack, Phys. Rev. A 16, 2360 (1977).

28. Y. T. Lee, Ber. Bunsenges. Physik. Chem. 86, 378 (1982).

29. D. M. Neumark, A. M. Wodtke, G. N. Robinson, C. C. Hayden, and Y. T. Lee, Phys. Rev. Lett. 53, 226 (1984).

30. D. M. Neumark, A. M. Wodtke, G. N. Robinson, C. C. Hayden, and Y. T. Lee, J. Chem. Phys. 82, 3045 (1985).

31. D. M. Neumark, A. M. Wodtke, G. N. Robinson, C. C. Hayden, K. Shobatake, R. K. Sparks, T. P. Schafer, and Y. T. Lee, J. Chem. Phys. 82, 3067 (1985).

32. M. R. Spalburg and E. A. Gislason, Chem. Phys. 94, 339 (1985).

33. M. R. Spalburg, J. Los, and E. A. Gislason, Chem. Phys. 94, 327 (1985).

34. G. Parlant and E. A. Gislason, Chem. Phys. 101, 227 (1986).

35. P. Archirel and B. Levy, J. Chem. Phys., to be published.

36. R. E. Olson, F. T. Smith, and E. Bauer, Appl. Opt. 10, 1848 (1971).

37. J. D. Shao and C. Y. Ng, Chem. Phys. Lett. 118, 481 (1985).

38. J. D. Shao and C. Y. Ng, J. Chem. Phys. 84, 4317 (1986).

39. C.-L Liao and C. Y. Ng, J. Chem. Phys. 81, 5672 (1984).

40. C.-L Liao and C. Y. Ng, J. Chem. Phys. 82, 5489 (1985).

41. C.-L. Liao and C. Y. Ng, J. Chem. Phys. 84, 197 (1986).

42. J. A. R. Samson and R. B. Cairns, Phys. Rev. 173, 80 (1968).

43. H. B. Gilbody and J. B. Hasted, Proc. Roy. Soc. 238, 334 (1957).

44. A. Galli, A. Giardini-Guidoni, and G. G. Volpi, Nuovo Cimento 31, 1145 (1964).

45. S. N. Ghosh and W. F. Sheridan, J. Chem. Phys. 26, 480 (1957).

46. E. Gustafsson and E. Lindholm, Arkiv Fysik 18, 219 (1961).

47. R. C. Amme and H. C. Hayden, J. Chem. Phys. 42, 2011 (1965).

48. J. B. Homer, R. S. Lehrle, J. C. Robb, and D. W. Thomas, Trans. Faraday Soc. 62, 619 (1966).

49. P. Mahadevan and G. D. Magnuson, Phys. Rev. 171, 103 (1968).

50. Y. Kaneko, N. Kobayashi, and I. Konomata, J. Phys. Soc. (Japan) 27, 922 (1969).

51. I. Dotan and W. Lindinger, J. Chem. Phys. 76, 4972 (1982).

52. H. Böhringer, M. Durup-Ferguson, D. W. Fahey, F. C. Fehsenfeld, and E. E. Ferguson, J. Chem. Phys. 79, 4201 (1983).

53. W. Federer, W. Dobler, F. Howorka, W. Lindinger, M. Durup-Ferguson, and E. E. Ferguson, J. Chem. Phys. 83, 1032 (1985).

54. H. H. Teng and D. C. Conway, J. Chem. Phys. 59, 2316 (1973).

55. C.-Y. Lee and A. E. DePristo, J. Chem. Phys. 80, 1116 (1984).

56. C.-L. Liao, J. D. Shao, R. Xu, G. D. Flesch, Y.-G. Li, and C. Y. Ng, J. Chem. Phys., to be published.

SECTION III.

ABSOLUTE STATE-TO-STATE TOTAL CROSS SECTIONS FOR THE REACTION

$$N_2^+(\tilde{X},v'=0\text{-}2) + Ar(^1S_0) \longrightarrow N_2(\tilde{X},v) + Ar^+(^2P_{3/2\ 1/2})$$

Introduction

The state-selected cross section measurements[1-5] for the reaction

$$N_2^+(\tilde{X},v') + Ar(^1S_0) \longrightarrow N_2(\tilde{X},v) + Ar^+(^2P_{3/2\ 1/2}) \qquad (1)$$

and its reverse

$$Ar^+(^2P_{3/2\ 1/2}) + N_2(\tilde{X},v=0) \longrightarrow Ar(^1S_0) + N_2^+(\tilde{X},v') \qquad (2)$$

have stimulated many theoretical studies[2,3,5-9] of the $[N_2 + Ar]^+$ electron transfer system. Reliable theoretical state-to-state total cross sections, $\sigma_{v'\to Jv}$ and $\sigma_{Jv\to v'}$, for reactions (1) and (2) are now available from semi-classical multi-state calculations.[6-8] The most recent multi-state calculation[8] uses the ab initio potential energy surfaces (PES) at the linear and perpendicular approaches of Ar to N_2 and obtains the cross

sections from weighted averages of calculations using the two geometries. The procedure for obtaining the cross sections from weighted averages should be accurate if the cross section varies smoothly from the linear to the perpendicular configurations. Furthermore, the ab initio PES used have been calculated assuming a constant N-N distance equal to the equilibrium bond distance. Therefore, impulsive interactions and the dynamical effects induced by vibrational motion have not been accounted for in the multi-state calculation.[8] In spite of these approximations, it is gratifying to find[8] that the predicted state-selected total cross sections, $\sigma_{v'}$, $v' = 0$-4, for reaction (1) at the center-of-mass collision energies ($E_{c.m.}$) of 8 and 20 eV are in agreement with the experimental results.[3]

Since the product state distributions are expected to be sensitive to the geometry of the atom-diatom colliding pair, state-to-state cross sections obtained at a wide $E_{c.m.}$ range will provide a test for the multi-state calculation and the ab initio PES. Detailed absolute state-to-state cross section data for reaction (2)[10] and the spin-orbit-state distributions of reaction (1)[11] have been measured recently in our laboratory. Here, we report absolute values for $\sigma_{v'}$, $v' = 0$-2, and partial state-to-state cross sections $\sigma_{v'\rightarrow J}$ ($=\sum_{v}\sigma_{v'\rightarrow Jv}$), $v' = 0$-2, at $E_{c.m.}$ = 1.2-140 eV, and compare these values with the predictions of multi-state calculations. The consistency of the measured absolute state-to-state cross sections for reactions (1) and (2) is examined from the consideration of microscopic reversibility.

EXPERIMENTAL

The triple-quadrupole double-octopole photoionization apparatus used in this study has been developed from the tandem photoionization mass spectrometer.[12,13] The detailed design of this apparatus will be described in a separate publication.[14] Figure 1 shows the cross sectional view of the apparatus. It consists essentially of a 0.2 m vacuum ultraviolet (VUV) monochromator (McPherson 234) a discharge lamp, a tungsten photoelectric VUV light detector, three quadrupole mass filters (QMF), two radio frequency (rf) octopole ion guide[15] reaction gas cells, a supersonic free jet production system and a variant of the Daly-type scintillation ion detector.[16]

The experimental procedures for the measurement of σ_0 are similar to those described previously.[12,13] The photoionization efficiency (PIE) spectrum for N_2^+ in the wavelength region of 769 - 800 Å obtained using a wavelength resolution of 3.5 Å (FWHM) is shown in Fig. 2. The reactant $N_2^+(\tilde{X})$ ions in the $v' = 0$ state are prepared by photoionization of a N_2 molecular beam at the wavelength (λ) of 791.5 Å, which corresponds to the position of the first strong autoionization peak in the PIE spectrum. The N_2 molecular beam is produced by supersonic expansion through a 50 μm diameter quartz nozzle, at a N_2 stagnation pressure of 40 Torr. The photoionization chamber is pumped by a freon-trapped 6 in. diffusion pump (DP) which maintains a pressure of $<1\times10^{-5}$ Torr during the experiment. As pointed out previously[10], the use of a sufficiently low nozzle stagnation pressure, to maintain a low background pressure in the photoionization

Figure 1. Cross-sectional view of the triple-quadrupole double-octopole photoionization apparatus. (1) Photoionization region, (2) nozzle, (3) to freon-trapped 6 in. diffusion pump (DP), (4) the first quadrupole mass filter (QMF), (5) to liquid-nitrogen (LN_2)-trapped 6 in. DP, (6) the first QMF chamber, (7) the first ratio frequency (rf) octopole ion guide chamber, (8) the first reaction gas cell, (9) the first rf octopole ion guide, (10) to LN_2-trapped 6 in. DP, (11) the second QMF, (12) to LN_2-trapped 4 in. DP, (13) the second reaction gas cell, (14) the second rf octopole ion guide, (15) the second rf octopole ion guide chamber, (16) the third QMF, (17) detector chamber, (18) plastic scintillator window, (19) photomultiplier tube, (20) aluminum ion target, (21) to LN_2-trapped 2 in. DP

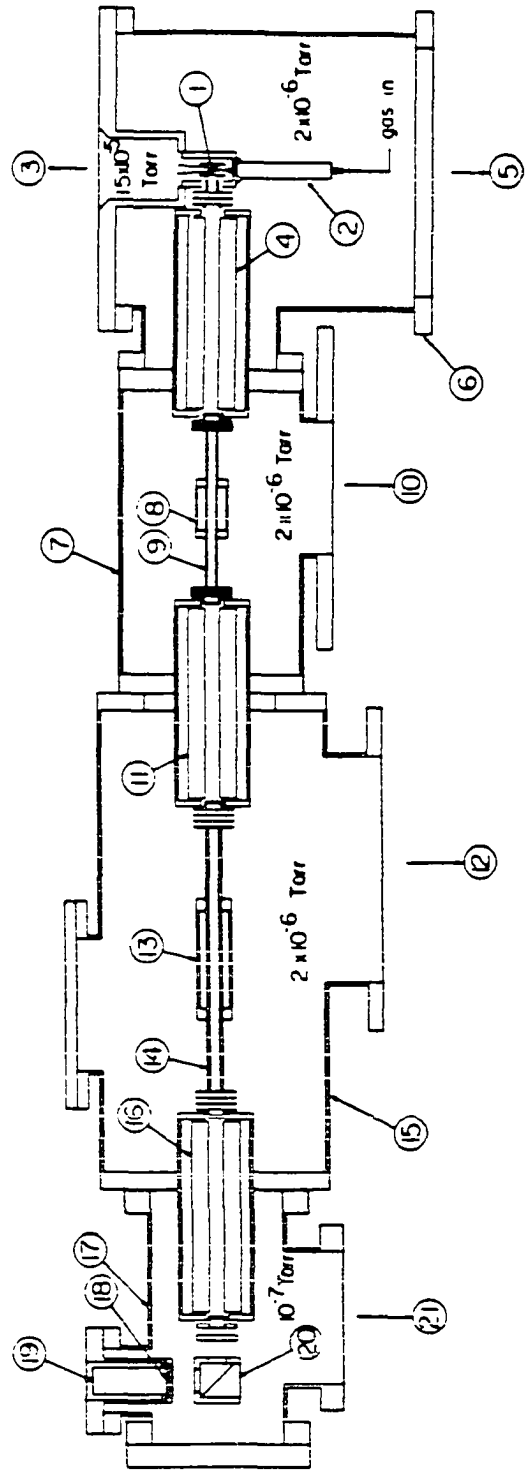
2 x 10⁻⁶ Torr
gas in
1.5 x 10⁻⁵ Torr
2 x 10⁻⁶ Torr
2 x 10⁻⁶ Torr
10⁻⁷ Torr
1
2
3
4
5
6
7
8
9
10
11
12
13
14
15
16
17
18
19
20
21

chamber, is essential to avoid a change in the vibrational state distribution of reactant N_2^+ ions due to collisions of reactant N_2^+ ions with background N_2 in the photoionization chamber. The reactant $N_2^+(\tilde{X},v'=0)$ ions formed at the photoionization region are extracted perpendicular to the N_2 molecular beam and selected by the first QMF (4) before reacting with Ar according to reaction (1) in the second rf octopole ion guide reaction gas cell (13). The first rf octopole ion guide (9) and the second QMF (11) are only used as ion lenses in this measurement. During this measurement, the second QMF is tuned to the mass of N_2^+ (m/e = 28) and the first rf octopole ion guide reaction gas cell (8) is empty.

The second rf octopole ion guide is constructed of eight molybdenum rods, with a diameter of 3.16 mm and a length of 28.5 cm, symmetrically spaced in a circle of 1.27 cm diameter. The second reaction gas cell is 13 cm long and is positioned at the center of the second rf octopole ion guide. The frequency and peak-to-peak voltage used are ~10 MHz and 450 V, respectively.[13,14] The Ar gas cell pressure is monitored with a Baratron manometer (MKS Model 390HA SP05) and a Ar gas cell pressure of 8×10^{-5} Torr is used in this experiment.

The Ar^+ product ions formed in the second rf octopole ion guide reaction gas cell are mass selected by the third QMF (16) and detected by the scintillation detector (18-20). The laboratory collision energy (E_{lab}) is determined by the difference in potential between the photoionization region and the second rf octopole ion guide reaction gas cell. The product Ar^+ ion intensity is maximized carefully at each $E_{c.m.}$.

The PIE spectra for the reactant N_2^+ ions and the product Ar^+ ions formed at E_{lab} = 10 eV, and the ratio of their intensities, $i(Ar^+)/I_0(N_2^+)$, are shown in Fig. 2. The composition of $N_2^+(\tilde{X})$ in the v' = 0 and 1 states produced at the autoionization peak, λ = 781 Å has been determined previously at wavelength resolutions of 0.3[17], 1[18], and 1.4 Å[10] (FWHM). Because of the lower wavelength resolution used here, the minor autoionization peak for N_2^+ at λ = 781 Å appears as a shoulder (see the arrow in Fig. 2) of the strong autoionization peak at λ = 784 Å. The autoionization peak at λ = 781 Å is evident in the PIE spectrum for product Ar^+ ions. The value for $i(Ar^+)/I_0(N_2^+)$ at λ = 781 Å is substantially higher than that at 791.5 Å. This is consistent with the previous experimental finding that $\sigma_1 >> \sigma_0$ at E_{lab} = 10 eV.

The absolute value for σ_0 at a given $E_{c.m.}$ is determined by the relation

$$\sigma_0 = \frac{-1}{nl} \ln\left[1 - \frac{i(Ar^+)}{I_0(N_2^+)}\right] \qquad (3)$$

Here $I_0(N_2^+)$ is sum of the intensities of Ar^+ and N_2^+; and n and l represent the number density of Ar and the length of the second reaction gas cell, respectively. The value for $i(Ar^+)$ has been corrected for background Ar^+ formed outside of the reaction gas cell using the procedures described in Ref. 15. We find that within experimental uncertainties, $I_0(N_2^+)$ is equal to the intensity of reactant N_2^+ observed when the gas cell is empty.

Using the same procedures, the cross section, σ_m, characteristic of reactant N_2^+ formed at 781 Å can be determined. Assuming the fraction of

Figure 2. (----) PIE curve for reactant N_2^+; (——) PIE curve for product Ar^+ at E_{lab} = 10 eV; (--•--) the ratio, $i(Ar^+)/I(N_2^+)$, of the intensity for product Ar^+ to that for reactant N_2^+.

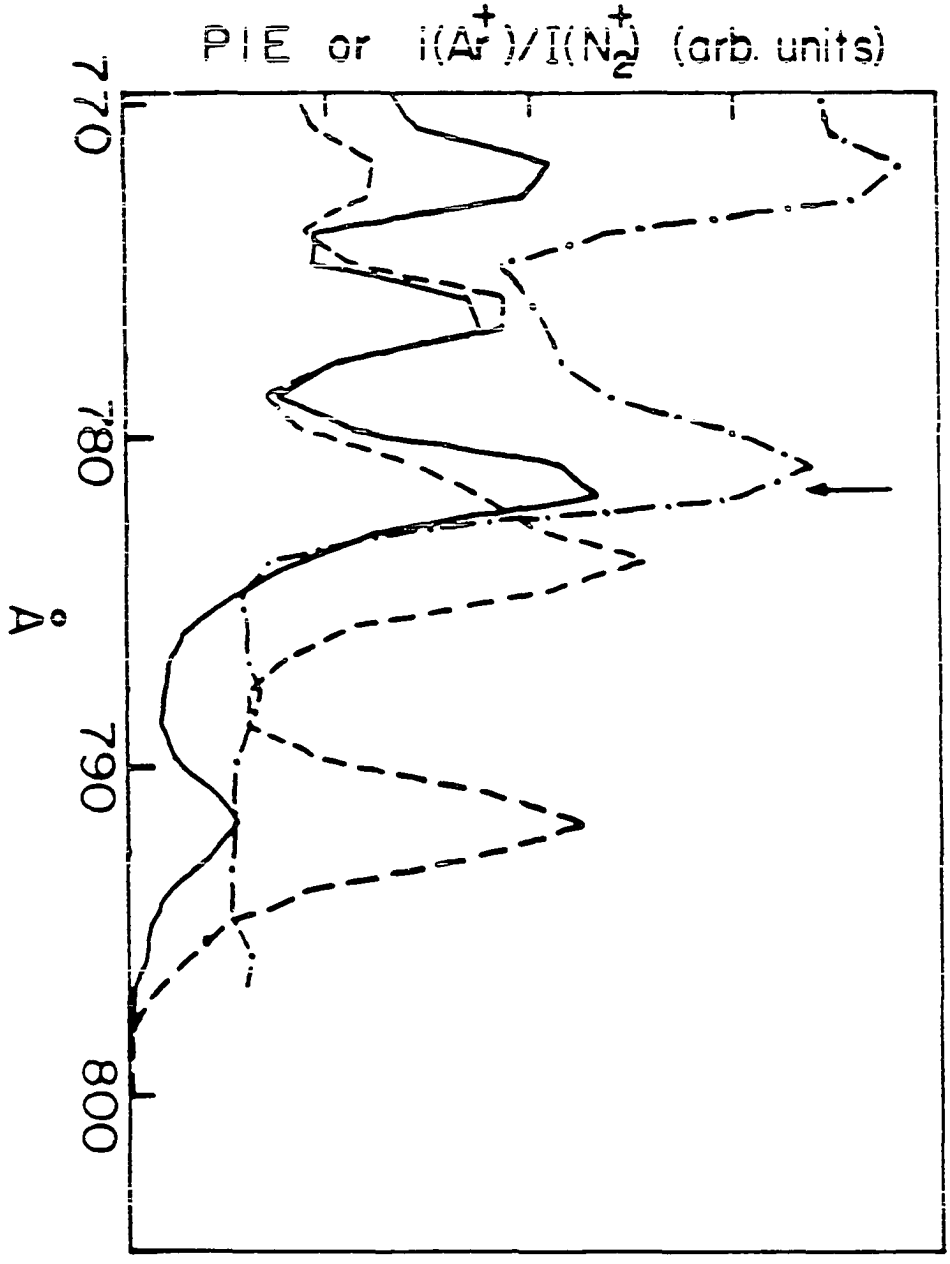
PIE or I(Ar+)/I(N2+) (arb. units)
770
780
790
800
A°

reactant $N_2^+(\tilde{X})$ in the v' = 0 and 1 states to be X_0 and X_1, respectively, the values for σ_0, σ_1, and σ_m are related to X_0 and X_1 by the relation

$$X_0\sigma_0 + X_1\sigma_1 = \sigma_m \tag{4}$$

Since the sum of X_0 and X_1 is equal to one, X_0 and X_1 can be calculated when σ_0 and σ_1 are known or σ_1 can be determined by measuring σ_0, σ_m, X_0, and X_1.

In order to calculate the value for σ_1 using Eq. (4), it is necessary first to determine the values for X_0 and X_1. The experiment of Liao et al.[10] has shown that the product $N_2^+(\tilde{X})$ ions of the electron transfer reaction $Ar^+(^2P_{3/2}) + N_2(\tilde{X},v=0)$ at $E_{c.m.}$ = 1.2-4.1 eV are formed predominantly (85±15%) in the v' = 1 state. We have prepared $N_2^+(\tilde{X})$ ions in the first rf octopole ion guide reaction gas cell using the reaction $Ar^+(^2P_{3/2}) + N_2(\tilde{X},v=0)$ at $E_{c.m.}$ = 4.1 eV. The Ar^+ ions are produced in the pure $^2P_{3/2}$ state by photoionization at λ = 786 Å. The $N_2^+(\tilde{X})$ ions formed in the first reaction gas cell are guided into the second rf octopole ion guide reaction gas cell and further react with Ar according to reaction (1) at $E_{c.m.}$ = 4.1 eV. The measurements of the intensity of product Ar^+ formed in the second reaction gas cell and that of N_2^+ formed in the first reaction gas cell using the third QMF allow the determination of the total cross section at $E_{c.m.}$ = 4.1 eV characteristic of $N_2^+(\tilde{X})$ ions produced by the reaction $Ar^+(^2P_{3/2}) + N_2(\tilde{X},v=0)$ at $E_{c.m.}$ = 4.1 eV. Knowing the vibrational distribution of $N_2^+(\tilde{X})$ and the value for σ_0 at $E_{c.m.}$ = 4.1 eV, we have calculated the value for σ_1 at $E_{c.m.}$ = 4.1 eV using an equation

similar to Eq. (4). In principle, σ_1 at other $E_{c.m.}$ of interest can be determined by the same method. Since the intensity for $N_2^+(\tilde{X})$ produced by the reaction $Ar^+(^2P_{3/2}) + N_2(\tilde{X},v=0)$ is low, the determination of σ_1 at each $E_{c.m.}$ requires considerable counting time. The value for σ_1 at $E_{c.m.}$ = 4.1 eV determined by this method, together with the measured values for σ_0 and σ_m at $E_{c.m.}$ = 4.1 eV, makes possible the calculation of X_0 and X_1 at λ = 781 Å using Eq. (4) The values for X_0 and X_1 are found to be 0.65±0.06 and 0.35±0.06, respectively. The experiment has also been performed by preparing $N_2^+(\tilde{X})$ in the first rf octopole ion guide reaction gas cell at $E_{c.m.}$ = 4.1 eV and then colliding it with Ar in the second rf octopole ion guide reaction gas cell at $E_{c.m.}$ = 5.88 eV. The values for X_0 and X_1 obtained in the two experiments are in agreement. These values for X_0 and X_1 have been used to calculate σ_1 from the values of σ_0 and σ_m measured at other $E_{c.m.}$.

RESULTS

Absolute state-selected cross sections, $\sigma_{v'}$, v' = 0-2, for reaction (1)

The absolute values for $\sigma_{v'}$, v' = 0-2, at $E_{c.m.}$ = 1.2-140 eV determined in this experiment are listed in Table I. The relative values for $\sigma_{v'}$, v' = 0-2, at $E_{c.m.}$ = 1.2-320 eV have been reported by Liao et al.[10] The previous values for σ_0/σ_1 at $E_{c.m.}$ = 20-140 eV are consistent with those determined here, whereas the values for σ_0/σ_1 at $E_{c.m.} \leq 14$ eV obtained by Liao et al. are lower than those of this experiment. The absolute values for σ_2 listed in Table I have been calculated using the known values for σ_2/σ_1 and σ_1. Since the values for σ_2/σ_0 at $E_{c.m.} \leq 20$ eV are large and the measured values for σ_0 have high uncertainties, the values for σ_2 at $E_{c.m.} \leq 20$ eV calculated using the values for σ_2/σ_0 and σ_0 are not accurate. However, absolute values for σ_2 at $E_{c.m.}$ = 20-140 eV determined by multiplying the values of σ_2/σ_0 with the corresponding values for σ_0 (see Table I) are in accord with those calculated using the values for σ_1 and σ_2/σ_1.

The results obtained in the threshold photoelectron secondary ion coincidence (TESICO) experiment of Govers et al.[3] are also shown in Table I. The absolute values for $\sigma_{v'}$, v' = 0-2, obtained by Govers et al. were determined indirectly by using the known absolute total cross sections for the symmetric electron transfer reaction $Ar^+ + Ar$ [19] and the relative total cross sections for the electron transfer reactions $Ar^+ + Ar$ and $N_2^+ + Ar$

Table I. Absolute vibrational-state-selected total cross sections, $\sigma_{v'}$, $v' = 0$–2, at $E_{c.m} = 1.2$–1.4 eV for the reactions $N_2^+(\tilde{X}, v'=0\text{–}2) + Ar(^1S_0) \longrightarrow N_2 + Ar^+$

$E_{c.m.}$ (eV)	σ_v (Å^2)					
	Experiment[a,b]			Theory[c,d]		
	$v' = 0$	$v' = 1$	$v' = 2$[e]	$v' = 0$	$v' = 1$	$v' = 2$
1.2	0.28 ± 0.08	26.3 ± 4.2	22.9 ± 4.3	0.00	17.46	14.41
4.1	1.01 ± 0.25	21.9 ± 3.4	21.7 ± 4.0	0.01	24.31	19.90
5.8	1.41 ± 0.35	21.7 ± 3.3	23.9 ± 4.3	...	...	...
8.0	1.59 ± 0.40 ($\leq$0.9)	18.8 ± 2.8 (18.7 ± 1.6)	22.7 ± 4.1 (23.1 ± 1.9)	0.1[g] (0.9)	26.0[g] (22.9)	30.8[g] (28.5)
14.0	1.93 ± 0.40 ($\leq$0.9)	16.6 ± 2.4 (15.6 ± 1.2)	23.1 ± 4.1 (24.2 ± 2.8)	...	...	...
20.0	2.17 ± 4.3 (1.6 ± 0.2)	14.3 ± 2.1 19.7 ± 4.4[f] (14.3 ± 2.4)	20.6 ± 3.6 28.4 ± 6.3[f] (17.8 ± 2.9)	1.0[g] (3.2)	25.0[g] (20.4)	29.6[g] (28.0)
40.0	4.3 ± 0.4	11.6 ± 1.8 13.1 ± 1.8[f]	16.4 ± 3.0 18.5 ± 2.6	3.0[h]	21.2[h]	30.8[h]
80.0	8.8 ± 0.67	11.5 ± 1.5 13.6 ± 1.7[f]	15.5 ± 2.5 18.3 ± 2.3[f]	...	...	...
140.0	14.9 ± 1.1	15.6 ± 1.5 17.0 ± 2.1[f]	14.3 ± 2.1 16.3 ± 2.0[f]	...	...	...

[a]This work.

[b]The values in parentheses are obtained from Ref.3.

[c]Reference 7.

[d]The values in parentheses are obtained from Ref.8.

[e]Values determined using the absolute values for σ_1 and values for σ_2/σ_1 obtained from Ref.11.

[f]Values determined using the absolute values fro σ_0 and values fro σ_1/σ_0 obtained from Ref.11.

[g]Values quoted in Ref. 8.

[h]Values calculated at $E_{c.m.} = 41.2$ eV.

measured in the TESICO experiment. We find that the results of the TESICO experiment and this work are in excellent agreement, except for σ_0 at $E_{c.m.}$ = 8 and 14 eV, where our values are slightly higher than theirs.

The absolute value for σ_0 increases monotonically from 0.28 $\mathring{A}^2$ at $E_{c.m.}$ = 1.2 eV to 14.9 $\mathring{A}^2$ at $E_{c.m.}$ = 140 eV. The absolute value for σ_1 decreases gradually from 26.3 $\mathring{A}^2$ at $E_{c.m.}$ = 1.2 eV to 11.5–13.6 $\mathring{A}^2$ at $E_{c.m.}$ = 80 eV and then increases to 15.6–17.0 $\mathring{A}^2$ at $E_{c.m.}$ = 140 eV. The absolute value for σ_2 at $E_{c.m.}$ = 1.2–20 eV are nearly equal. A decreasing trend for σ_2 is observed as $E_{c.m.}$ is increased from 20 eV to 140 eV. The values for $\sigma_{v'}$, v' = 0–2, at $E_{c.m.}$ = 140 eV are equal within experimental uncertainties.

Absolute partial state-to-state cross sections, $\sigma_{v'\to J}$, v' = 0–2, for reaction (1)

The fractions, $X_{v'\to J}$, v' = 0–2, of product $Ar^+(^2P_J)$ formed by reaction (1) at $E_{c.m.}$ = 4–320 eV have been measured by Liao et al.[10] Using the values of $X_{v'\to J}$ and absolute values for $\sigma_{v'}$, measured in this experiment, absolute partial state-to-state cross sections, $\sigma_{v'\to J}$, v' = 0–2, have been determined and are listed in Table II. The values for $\sigma_{v'\to 3/2}$ are substantially greater than those for $\sigma_{v'\to 1/2}$.

Table II. Absolute partial state-to-state total cross sections, $\sigma_{v;v'\to J}$. $v' = 0-2$, at $E_{c.m} = 1.2-140$ eV for the reactions $N_2^+(\tilde{X}, v'=0-2)\ Ar(^1S_0) \longrightarrow N_2(\tilde{X},v) + Ar^+(^2P_J)$

$E_{c.m.}$ eV	$\sigma_{v'\to J}$(Å) Experiment[a,b]					
	$\sigma_{0\to 3/2}$	$\sigma_{0\to 1/2}$	$\sigma_{1\to 3/2}$	$\sigma_{1\to 1/2}$	$\sigma_{2\to 3/2}$	$\sigma_{2\to 1/2}$
1.2	0.28±0.08	0.0	26.3±4.2	~0.0	...	...
4.1	1.01±0.25	0.0	21.4±3.4	0.5±0.6	...	...
5.8	1.41±0.35	0.0	20.2±3.1	1.5±0.5	...	...
8.0	1.53±0.39	0.06±0.04	16.8±2.5	2.0±0.6	18.8±3.6	3.9±1.3
10.3	1.61±0.38[e]	0.09±0.04[e]	15.8±2.4[e]	2.3±0.6[e]	18.6±3.6[e]	4.0±1.3[e]
14.0	1.84±0.38	0.09±0.04	14.6±2.2	2.0±0.5	19.1±3.6	3.8±1.4
20.0	2.00±0.40	0.17±0.06	2.2±1.8	2.1±0.4	16.9±3.8	3.7±1.2
			(16.8±3.8)	(2.9±0.8)	(23.3±5.2)	(5.1±1.8)
40.0	4.0±0.4	0.4±0.1	9.8±1.6	1.8±0.4	13.6±2.6	2.8±0.9
			(11.2±1.6)	(2.0±0.4)	(15.3±2.3)	(3.1±1.0)
80.0	8.0±0.6	0.8±0.2	9.7±1.3	1.8±0.4	12.6±2.2	2.9±0.9
			(11.4±1.6)	(2.2±0.4)	18.4±2.1	(3.4±1.0)
140.0	13.2±1.0	1.7±0.4	13.0±1.4	2.6±0.6	(11.4±1.8)	2.9±0.8
			(14.2±1.9)	(2.8±0.7)	(13.0±1.8)	(3.3±0.9)

[a]This work.

[b]The values in parentheses are obtained from values of σ_1 and σ_2 determined using the values for σ_0 of this work and σ_1/σ_0 and σ_2/σ_0 obtained form Ref.1.

[c]Reference 7.

[d]The vlues in parentheses are obtained from Ref. 8.

[e]Values estimated using the estimated values for $\sigma_{v'}$, $v'=0\pm2$ at $E_{c.m.}$ = 10.3 eV which are interpolated using the $\sigma_{v'}$ values at $E_{c.m.}$ = 8 and 14 eV.

[f]Values calculated at $E_{c.m.}$ = 41.2 eV.

Theory[c,d]					
$\sigma_{0\to3/2}$	$\sigma_{0\to1/2}$	$\sigma_{1\to3/2}$	$\sigma_{1\to1/2}$	$\sigma_{2\to3/2}$	$\sigma_{2\to1/2}$
0.00	0.00	17.37	0.09	9.06	5.35
0.00	0.00	24.31	0.56	16.56	3.34
0.00	0.00	0.00	0.00	0.00	0.00
(0.08)	(0.1)	(19.3)	(3.6)	(23.5)	(5.0)
0.15	0.01	24.86	1.89	25.2	3.94
0.00	0.00	0.00	0.00	0.00	0.00
(2.6)	(0.6)	(16.1)	(4.3)	(21.5)	(6.5)
2.40[f]	0.57[f]	16.52[f]	4.63[f]	24.43[f]	6.40[f]
0.00	0.00	0.00	0.00	0.00	0.00
0.00	0.00	0.00	0.00	0.00	0.00

DISCUSSION

Absolute state-selected cross sections, $\sigma_{v'}$, v' = 0-2, for reaction (1)

The theoretical values for $\sigma_{v'}$, v' = 0-2, at $E_{c.m.}$ = 8 and 20 eV obtained by Parlant and Gislason[8] and the theoretical cross sections at $E_{c.m.}$ = 1.2, 4.1, 8, 20 and 41.2 eV calculated by Spalburg and Gislason[7] are compared to the experimental results in Table I. Due to the fact that the former multi-state calculation uses more accurate PES for the $[N_2 + Ar]^+$ system, its predictions are expected to be more reliable than those of the latter study. We find that the predictions of Parlant and Gislason are in satisfactory agreement with the experimental values. The values calculated by Spalburg and Gislason for σ_1 and σ_2 at $E_{c.m.}$ = 8 and 20 eV, as quoted in Ref. 8, appear to be too high, an observation consistent with a previous conclusion.[8] It has been pointed out that the higher cross sections are the results of the stronger estimated coupling potential used in Ref. 7. The small values for σ_0 at low $E_{c.m.}$ are consistent with the fact that the formation of the least energetic channel $Ar^+(^2P_{3/2}) + N_2(\tilde{X},v=0)$ from $N_2^+(\tilde{X},v'=0) + Ar(^1S_0)$ is endothermic by 0.179 eV. The theory correctly predicts the increasing trend for σ_0 as $E_{c.m.}$ is increased. However, the theoretical values for σ_0 at $E_{c.m.}$ = 1.2-41.2 eV obtained by Spalburg and Gislason are lower than the experimental values and the values predicted in Ref. 8. The theoretical values[7] for σ_1 and σ_2 at $E_{c.m.}$ = 1.2 eV are substantially lower than the experimental values. The observed

trends for σ_1 and σ_2 as a function of $E_{c.m.}$ also are different from those predicted in Ref. 7. The predicted value for σ_1 exhibits a maximum at $E_{c.m.}$ = 8 eV, while the theoretical value for σ_2 increases as $E_{c.m.}$ is increased at $E_{c.m.}$ = 1.2-8 eV and it remains approximately constant for $E_{c.m.}$ = 8-41.2 eV. At $E_{c.m.} \geq 8$ eV, the calculated values for σ_1 and σ_2 of Ref. 7 are greater than the experimental cross sections.

The multi-state calculation of Spalburg and Gislason[7] used estimated isotropic PES. They argue that since the most important transitions take place at large atom-diatom distances, the anisotropy of the potential is relatively unimportant. This argument has been found to be incorrect in the recent calculation of Ref. 8, which shows that the cross sections for reactions (1) and (2) depend strongly on the orientation of the atom-diatom pair.

The binding energy of the $(Ar \cdot N_2)^+$ complex is ~1 eV.[20] Recent studies on the vibrational relaxation of diatomic ions reveal that the relaxation rate constant scales with the binding energy of the collision pair.[21,22] At low $E_{c.m.}$, the strong binding energy between N_2^+ and Ar should have a significant effect on the cross section of reaction (1). The ab initio PES used in the calculation of Ref. 8 assume a constant N-N distance at all atom-diatom distances. At higher $E_{c.m.}$, if electron transfer is mostly due to transition at large atom-diatom distance, the perturbation introduced by varying the N-N distance may not be important. However, the dynamical effects induced by the vibrational motion is expected to be more important at low $E_{c.m.}$. In order to account for the binding energy effect and the dynamic effects induced by the vibrational motion, and to improve the

theoretical predictions at low $E_{c.m.}$, it is necessary to use accurate PES which have been calculated by varying the N-N bond distance as well as the distance between Ar and N_2 at many atom-diatom geometries.

Absolute partial state-to-state cross sections,

$\sigma_{v'\to J}$, v' = 0-2, for reaction (1)

The theoretical values for $\sigma_{v'\to 3/2}$ and $\sigma_{v'\to 1/2}$, v' = 0-2, at $E_{c.m.}$ = 8 and 20 eV reported in Ref. 8 and those at $E_{c.m.}$ = 1.2, 4.1, 10.3, and 41.2 eV predicted in Ref. 7 are included in Table II. We find satisfactory agreement between our experimental observations and the theoretical predictions of Ref. 8 at $E_{c.m.}$ = 8 and 20 eV. The theoretical values for $\sigma_{0\to 3/2}$ of Ref. 7 are lower than the experimental values. Similar to the comparison between the experimental and theoretical values for σ_1 and σ_2, the theoretical values for $\sigma_{1\to 3/2}$ and $\sigma_{2\to 3/2}$ at $E_{c.m.}$ =10.3 and 41.2 eV are higher than the experimental results, while the theoretical value for $\sigma_{1\to 3/2}$ at $E_{c.m.}$ = 1.2 eV is substantially lower than the experimental value.

Consistency of measured absolute state-to-state cross sections for reactions (1) and (2) from the consideration of microscopic reversibility

From the consideration of microscopic reversibility,[23] we have

$$E_1 g_1 \sigma_{v'\to Jv}(E_1) = E_2 g_2 \sigma_{Jv\to v'}(E_2) \qquad (5)$$

Here E_1 is the asymptotic reactant relative kinetic energy, E_2 is the asymptotic product relative kinetic energy, g_1 is the degeneracy for the reactant state, g_2 is the degeneracy for the product state, and $\sigma_{v'\to Jv}(E_1)$ and $\sigma_{Jv\to v'}(E_2)$ are the state-to-state cross sections for reaction (1) and its reverse at E_1 and E_2, respectively. If the degeneracies due to the rotational states of $N_2^+(\tilde{X})$ and $N_2(\tilde{X})$ are ignored, the values of g_1 and g_2 for reaction (1) are equal to the degeneracy of the electronic state ($^2\Sigma_g^+$) of N_2^+ and that of spin-orbit state (^2P_J) of Ar^+, respectively.

Absolute values for $\sigma_{3/2\ 0\to 1}$ at selected $E_{c.m.}$ have been determined by Liao et al.[10] with accuracy. According to theoretical studies, the values for $\sigma_{0\to 3/2}$ and $\sigma_{1\to 3/2}$ are overwhelmingly dominated by $\sigma_{0\to 3/2\ 0}$ and $\sigma_{1\to 3/2\ 0}$, respectively. Assuming $\sigma_{0\to 3/2\ 0} \simeq \sigma_{0\to 3/2}$ and $\sigma_{1\to 3/2\ 0} \simeq \sigma_{1\to 3/2}$, Eq. (5) becomes

$$\sigma_{3/2\ 0\to v'}(E_2) = (E_1/2E_2)\ \sigma_{0\to 3/2}(E_1) \qquad (6)$$

Using the values for $\sigma_{0\to 3/2}$ listed in Table II, we have calculated values for $\sigma_{3/2\ 0\to v'}$, $v' = 0$ and 1, at $E_{c.m.}$ = 1-41.2 eV. Tables III compares the values for $\sigma_{3/2\ 0\to v'}$, $v' = 0$ and 1, calculated using Eq.(6) and the experimental values obtained in Ref. 10. The predicted and experimental values are in good agreement except at $E_{c.m.}$ = 10.3 eV where the predicted value for $\sigma_{3/2\ 0\to 1}$ is slightly higher than the experimental value.

The theoretical calculation of Ref. 7 also reveals that at $E_{c.m.}$ = 8-41.2 eV, $Ar^+(^2P_{3/2}) + N_2(\tilde{X},v=1)$ is the predominant (>95%) product channel in the reaction of $N_2^+(\tilde{X},v'=2) + Ar(^1S_0)$. Assuming $\sigma_{2\to 3/2} \simeq \sigma_{2\to 3/2\ 1}$,

Table III. Comparison of experimental values and predicted values[a] for $\sigma_{3/2\to v'}$, $v' = 0-1$, at $E_{c.m.} = 1.2-41.3$ eV from the consideration of microscopic reversibility

	$\sigma_{3/2\ 0\to0}$ (Å^2)		$\sigma_{3/2\ 0\to1}$ (Å^2)	
$E_{c.m.}$ (eV)	Predicted	Experimental[b]	Predicted	Experimental[b]
1.2	0.16 ± 0.05[c]	$0.0 + 1.5 - 0.0$	12.2 ± 2.0[d]	12.3 ± 2.2
4.1	0.53 ± 0.13[e]	$0.0 + 1.5 - 0.0$	10.5 ± 1.7[f]	12.7 ± 2.2
10.3	0.82 ± 0.19	$0.0 + 1.3 - 0.0$	7.9 ± 1.2	$12.8 + 0.4 - 2.0$
41.2	2.0 ± 0.2	2.4 ± 1.1	4.9 ± 0.8 5.6 ± 0.8	7.2 ± 1.9

[a]Values calculated using Eq. (6) (see text).

[b]Reference 10.

[c]The predicted value at $E_{c.m.} = 1.04$ eV.

[d]The predicted value at $E_{c.m.} = 1.29$ eV.

[e]The predicted value at $E_{c.m.} = 3.94$ eV.

[f]The predicted value at $E_{c.m.} = 4.19$ eV.

the values for $\sigma_{3/2\ 1\to2}$ at $E_{c.m.}$ = 8, 20, and 40 eV have been calculated using Eq. (5) and compared to the theoretical predictions of Ref. 7 in Table IV. The theoretical predictions are found to be higher than the calculated values.

Table IV. Comparison of theoretical and predicted values[a] for $\sigma_{3/2\ 1\to2}$ at $E_{c.m.} \approx 8$, 20, 40 eV from the consideration of microscopic reversibility

$E_{c.m.}$ (eV)	$\sigma_{3/2\ 1\to2}$ (Å^2)	
	Predicted	Theoretical[b]
8	9.3 ± 1.8	12.2
20	8.4 ± 1.5 11.6 ± 2.7	...
40	6.8 ± 1.3 7.7 ± 1.2	11.6

[a]Values calculated using Eq. (6) (see text).

[b]Reference 7.

CONCLUSIONS

Absolute values for $\sigma_{v'}$, and $\sigma_{v'\rightarrow J'}$, v' = 0-2, have been determined over the $E_{c.m.}$ range of 1.2-140 eV. The state selected cross sections at $E_{c.m.}$ = 8, 14, and 20 are in agreement with the results of the previous TESICO experiment.[3] The absolute partial state-to-state cross sections obtained in this experiment are found to be consistent with the absolute state-to-state cross sections for reaction (2) at $E_{c.m.}$ = 1.2-41.2 eV reported recently by Liao et al.[10] The experimental results at $E_{c.m.}$ = 8 and 20 eV are in better agreement with the results of the calculation of Parlant and Gislason[8] than with the predictions of the earlier calculation[7] which used estimated isotropic PES for the $[N_2 + Ar]^+$ system.

This study, together with the recent measurements by Liao et al.[10,11] has provided detailed experimental data over a wide $E_{c.m.}$ range for the $[N_2 + Ar]^+$ electron transfer system. We hope these experimental studies will stimulate a more rigorous theoretical study in the future. A major improvement of the future theoretical calculation can be attained by using more accurate PES for the $[N_2 + Ar]^+$ system at many atom-diatom interaction geometries.

References

1. T. Kato, K. Tanaka, and I. Koyano, J. Chem. Phys. 77, 337 (1982).
2. T. Kato, K. Tanaka, and I. Koyano, J. Chem. Phys. 77, 837 (1982).
3. T. R. Govers, P.-M. Guyon, T. Baer, K. Cole, H. Frohlich, and M. Lavollée, Chem. Phys. 87, 373 (1984).

4. C.-L. Liao, R. Xu, and C. Y. Ng, J. Chem. Phys. 84, 1948 (1986).

5. P.-M. Guyon and T. R. Govers, Université Paris-Sud, to be published.

6. M. R. Spalburg, J. Los, and E. A. Gislason, Chem. Phys. 94, 327 (1985).

7. M. R. Spalburg, and E. A. Gislason, Chem. Phys. 94, 339 (1985).

8. G. Parlant and E. A. Gislason, Chem. Phys. 101, 227 (1986).

9. P. Archirel and B. Levy, J. Chem. Phys. (in press).

10. C.-L. Liao, J. D. Shao, R. Xu, G. D. Flesh, Y.-G. Li, and C. Y. Ng, J. Chem. Phys. 85, xxxx (1986).

11. C.-L. Liao, R. Xu, and C. Y. Ng, J. Chem. Phys. (submitted).

12. J. D. Shao and C. Y. Ng, Chem. Phys. Lett. 118, 481 (1985).

13. J. D. Shao and C. Y. Ng, J. Chem. Phys. 84, 4317 (1986).

14. J. D. Shao, Y.-G. Li, G. D. Flesh, and C. Y. Ng, J. Chem. Phys., to be published.

15. E. Teloy and D. Gerlich, Chem. Phys. 4, 417 (1974).

16. H. M. Gibbs and E. D. Commins, Rev. Sci. Instr. 37, 1385 (1966).

17. J. Berkowitz and W. A. Chupka, J. Chem. Phys. 51, 2341 (1969).

18. K. Tanaka, T. Kato, and I. Koyano, Chem. Phys. Lett. 97, 562 (1983).

19. P. Mahadevan and G. D. Magnuson, Phys. Rev. 171, 103 (1968).

20. H. H. Teng and D. C. Conway, J. Chem. Phys. 59, 2316 (1973).

21. H. Böhringer, M. Durup-Ferguson, D. W. Fahey, F. C. Fehsenfeld, and E. E. Ferguson, J. Chem. Phys. 79, 4201 (1983).

22. W. Federer, W. Dobler, F. Howorka, W. Lindinger, M. Durup-Ferguson, and E. E. Ferguson, J. Chem. Phys. 83, 1032 (1985).

23. J. Ross, J. C. Light, and K. E. Schuler, in "Kinetic Processes in Gases and Plasma", ed. A. R. Hochstim (Academic, New York, 1969), Chap.8.

PART II.

ABSOLUTE SPIN-ORBIT-STATE EXCITATION CROSS SECTIONS FOR THE REACTIONS $Ar^+(^2P_{3/2}) + Ar(^1S_0)$ AND $Ar^+(^2P_{3/2}) + N_2(\tilde{X}, v=0)$

INTRODUCTION

Energy transfer plays an important role in nearly all aspects of fundamental and applied research. Due to the advancements of molecular beam and laser technology, microscopic state-to-state cross sections for many inelastic scattering processes involving neutral atoms and molecules have been measured.[1-3] Although important strides[4-6] have also been made in this area in ion chemistry, the progress of state-to-state energy transfer studies in ion-molecule collisions is still behind that in neutral experiments. Recent flow tube experiments[4] using the monitor ion method have provided extensive rate data on the vibrational relaxation collisions of many diatomic molecular ions with various quenching gases as a function of collision energy. Nevertheless, detailed microscopic state-to-state inelastic cross section data for ion-molecule collisions remain scarce.

One of the difficulties in state-to-state studies of ion-molecule interactions is the preparation of state-selected reactant ions. The intensity of state-selected ions produced by single-photon ionization using laboratory vacuum ultraviolet (VUV) discharge lamps of synchrotron radiation is low ($\lesssim 10^5$ ions/sec), making the final product state detection experiment very difficult. Recently, Liao et al.[7-10] have developed an internal state sensitive charge exchange detector. By measuring the reactivities of simple product atomic or molecular ions with different probing gases, they have been able to perform state-to-state studies on the electron transfer reactions of $H_2^+(v'=0-1) + H_2(v=0)$,[7,8] $Ar^+(^2P_{3/2,1/2}) + Ar(^1S_0)$,[9] $Ar^+(^2P_{3/2,1/2}) + N_2(\tilde{X},v=0)$,[10] $N_2^+(\tilde{X},v'=0-2) + Ar(^1S_0)$,[11,12]

$Ar^+(^2P_{3/2,1/2}) + H_2(v=0)$,[13] and $H_2^+(v'=0-4) + Ar(^1S_0)$.[14] The charge exchange detector is highly sensitive, which allows the vibrational state distribution of electron transfer product ions to be measured with as low as 2-10 product ions formed per sec.[10,11]

In order to extend this method for state-to-state excitation and relaxation cross section measurements in ion-molecule collisions, we have developed a new triple-quadrupole double-octopole photoionization apparatus. In this communication, we present preliminary results on the absolute state-to-state total cross section measurements of the reactions

$$Ar^+(^2P_{3/2}) + Ar(^1S_0) \longrightarrow Ar^+(^2P_{1/2}) + Ar(^1S_0) \qquad (1)$$

$$Ar^+(^2P_{3/2}) + N_2(\tilde{X},v=0) \longrightarrow Ar^+(^2P_{1/2}) + N_2(\tilde{X},v) \qquad (2)$$

Absolute cross sections, $\sigma_{3/2\rightarrow1/2}$, for reaction (1) have been reported previously.[15] The comparison of experimental results of this study and Ref. 15 allows the performance of the apparatus to be evaluated. The recent multi-state calculation[16] finds the cross sections, $\sigma_{3/2\rightarrow1/2}$, for reaction (2) to be surprising large. The high value for $\sigma_{3/2\rightarrow1/2}$ of reaction (2) has been attributed to the mutual interactions of electron transfer $Ar + N_2^+$ states with the spin-orbit states of Ar^+. The cross sections obtained for reaction (2) in this experiment provide a test of the theoretical findings.

EXPERIMENTAL

The triple-quadrupole double-octopole photoionization apparatus used in this study has been developed from the tandem photoionization mass spectrometer.[17,18] The detailed design of this apparatus will be described in a separate publication. Figure 1 shows the cross sectional view of the apparatus. It consists essentially of a 0.2 m VUV monochromator (McPherson 234), a VUV discharge lamp, a tungsten photoelectric VUV light detector, three quadrupole mass filter (QMF), two ratio frequency (rf) octopole ion guide[19] reaction gas cells, a supersonic jet production system, and a variant of the Daly-type scintillation ion detector.[20]

The reactant $Ar^+(^2P_{3/2})$ ions are prepared by photoionization of an Ar atomic beam at the wavelength (λ) of 785 Å. The wavelength resolution used is 3.5 Å (FWHM). The neutral Ar beam is produced by supersonic expansion through a 50 μm diameter quartz nozzle at a stagnation pressure of ~68 Torr. The $Ar^+(^2P_{3/2})$ ions formed at the photoionization region are extracted perpendicular to the neutral Ar beam and selected by the first QMF (4) before colliding with Ar or N_2 in the first rf octopole ion guide reaction gas cell (8). The laboratory collision energy (E_{lab}) is defined to be the difference in potential between the photoionization region and the first rf octopole reaction gas cell. After the collisions of $Ar^+(^2P_{3/2})$ with Ar or N_2 in the first reaction gas cell, a small fraction of $Ar^+(^2P_{3/2})$ ions have been excited to the $^2P_{1/2}$ state according to reactions (1) and (2). Here we denote the fractions of Ar^+ in the $^2P_{3/2}$ and $^2P_{1/2}$ states to be $X_{3/2}$ and $X_{1/2}$, respectively. The Ar^+ ions in a mixture of

Figure 1. Cross-sectional view of the triple-quadrupole double-octopole photoionization apparatus. (1) Photoionization region, (2) nozzle, (3) to freon-trapped 6 in. diffusion pump (DP), (4) the first quadrupole mass filter (QMF), (5) to liquid-nitrogen (LN_2)-trapped 6 in. DP, (6) the first QMF chamber, (7) the first ratio frequency (rf) octopole ion guide chamber, (8) the first reaction gas cell, (9) the first rf octopole ion guide, (10) to LN_2-trapped 6 in. DP, (11) the second QMF, (12) to LN_2-trapped 4 in. DP, (13) the second reaction gas cell, (14) the second rf octopole ion guide, (15) the second rf octopole ion guide chamber, (16) the third QMF, (17) detector chamber, (18) plastic scintillator window, (19) photomultiplier tube, (20) aluminum ion target, (21) to LN_2-trapped 2 in. DP

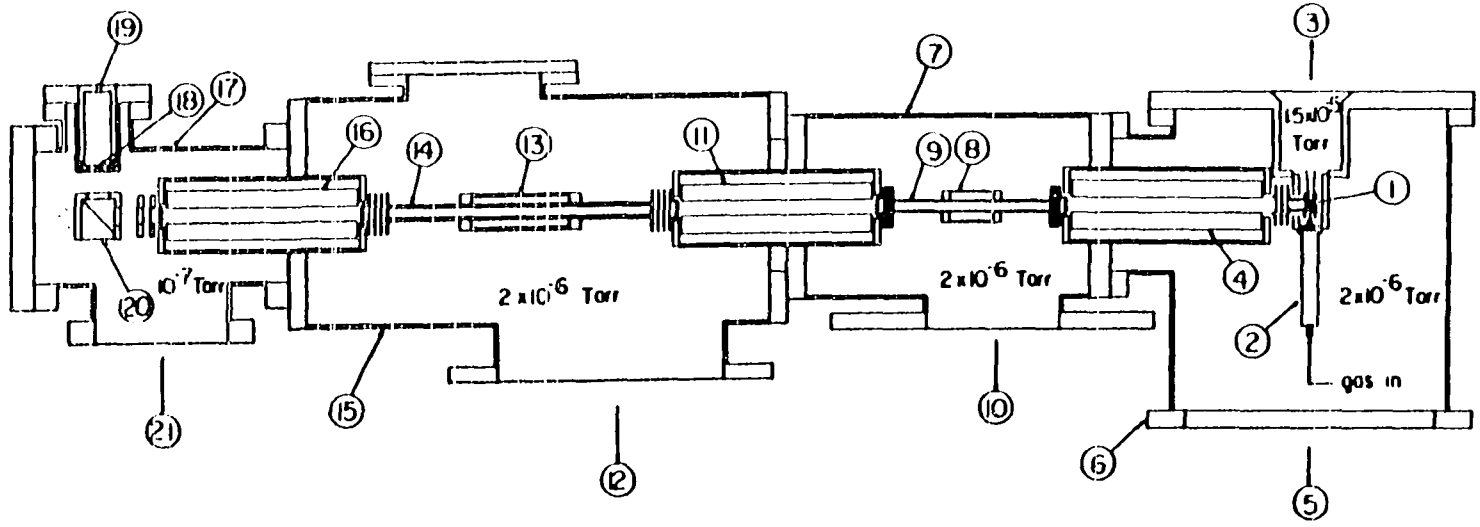
19
18
17
16
14
13
11
7
3
9
8
1
4
2
gas in
20
15
21
12
10
6
5
10^{-7} Torr
2×10^{-6} Torr
2×10^{-6} Torr
2×10^{-6} Torr

$^2P_{3/2}$ and $^2P_{1/2}$ states are then selected by the second QMF (11) and further react with the H_2 probing gas according to the reaction

$$Ar^+(^2P_J) + H_2 \longrightarrow Ar + H_2^+ \qquad (3)$$

at E_{lab} = 10 eV in the second reaction gas cell (13); and the total cross section, σ_m, of reaction (3), characteristic of $Ar^+(^2P_J)$ passing through the first reaction gas cell, is measured using the procedures described previously.[10,12,17,18] The value for the E_{lab} of the probing reaction (3) is determined by the potential difference between the photoionization region and the second reaction gas cell. The spin-orbit-state-selected cross sections, $\sigma_{3/2}$ and $\sigma_{1/2}$, for reaction (3), have been shown[13,21,22] to be substantially different at E_{lab} = 10 eV.

For the direct excitation processes, such as reactions (1) and (2), at sufficiently high E_{lab}, the laboratory velocities for product $Ar^+(^2P_{1/2})$ ions are expected to be only slightly different from those of $Ar^+(^2P_{3/2})$, where product $Ar^+(^2P_J)$ of $N_2^+(\tilde{X},v')$ ions resulting from the electron transfer processes

$$Ar^+(^2P_{3/2}) + Ar(^1S_0) \longrightarrow Ar(^1S_0) + Ar^+(^2P_J) \qquad (4)$$

$$Ar^+(^2P_{3/2}) + N_2(\tilde{X},v=0) \longrightarrow Ar(^1S_0) + N_2^+(\tilde{X},v') \qquad (5)$$

will have slow velocities, close to thermal velocities. For a E_{lab} of >10 eV for reactions (1) or (2), slow electron transfer product ions formed in the first reaction gas cell cannot enter the second reaction gas cell

because the second reaction gas cell is biased at a positive potential with respect to the first reaction gas cell.

Since, under the thin target conditions, we have the relation,

$$X_{3/2} + X_{1/2} = 1 \tag{6}$$

$$X_{3/2}\sigma_{3/2} + X_{1/2}\sigma_{1/2} = \sigma_m \tag{7}$$

$Ar^+(^2P_{1/2})$. $X_{3/2}$ can be calculated by the equation

$$X_{3/2} = (\sigma_m - \sigma_{1/2}) / (\sigma_{3/2} - \sigma_{1/2}) \tag{8}$$

The values for $\sigma_{3/2}$ and $\sigma_{1/2}$ have been determined using the second reaction gas cell when the first reaction cell is empty.

Furthermore, we have the relation

$$I - i_{1/2} = I_0\exp[-nl(\sigma_{CT} + \sigma_{3/2\to1/2})]$$
$$= I\exp(-nl\sigma_{3/2\to1/2}) \tag{9}$$

or $$1 - (i_{1/2}/I) = X_{3/2}$$
$$= \exp(-nl\sigma_{3/2\to1/2}) \tag{10}$$

Here I_0 is the intensity of Ar^+ observed when the first and second gas cell are empty. I is the intensity of Ar^+ after Ar or N_2 is introduced into the first reaction gas cell (I includes the intensity, $i_{1/2}$, of product $Ar^+(^2P_{3/2})$ resulting from reactions (1) or (2) but not that of electron transfer product $Ar^+(^2P_J)$); σ_{CT} represents the electron transfer cross

section of reactions (3) or (4); n is the number density of Ar (or N_2) in the first reaction gas cell; and l is the length of the first reaction gas cell. By measuring $X_{3/2}$, we have calculated $\sigma_{3/2\rightarrow 1/2}$ using Eq. (11a)

$$\sigma_{3/2\rightarrow 1/2} = (-1/nl)\ln(X_{3/2}) \tag{11a}$$

$$\simeq X_{1/2}/nl \tag{11b}$$

Equation (11b) is valid for thin target conditions.

The Ar or N_2 pressure used in the first reaction gas cell ranges from ~2 to 5×10^{-4} Torr. The H_2 probing gas pressure used in the second reaction gas cell is ~2×10^{-4} Torr.

The most important condition for the success of this experiment is the use of the rf octopole ion guides which make possible the collection of nearly all product $Ar^+(^2P_{3/2})$ ions of reaction (1) or (2). We find that the attenuation of reactant $Ar(^2P_{3/2})$ ions, when N_2 is introduced into the first reaction gas cell, is consistent with the estimate calculated using the electron transfer cross section measured previously in our laboratory.

RESULTS AND DISCUSSION

The absolute values for $\sigma_{3/2\rightarrow1/2}$ of reaction (1) measured in this study at E_{lab} = 60, 130, and 200 eV are compared to the experimental results obtained by Itoh et al.[15] in Table I. Both experiments show that $\sigma_{3/2\rightarrow1/2}$ of reaction (1) increases as E_{lab} is increased, an observation consistent with the theoretical prediction.[23] In the experiment of Itoh et al. the value for $\sigma_{3/2\rightarrow1/2}$ is measured by observing the energy loss of Ar^+ along the reactant Ar^+ beam direction with an acceptance angle of 0.45°. At low E_{lab}, where the angular spread of inelastic scattered $Ar^+(^2P_{1/2})$ ions is >0.45°, the values for $\sigma_{3/2\rightarrow1/2}$ obtained previously are likely to be lower limits. As E_{lab} is increased and the angular spread of product $Ar^+(^2P_{1/2})$ ions becomes narrower, the value measured in the energy loss experiment is expected to be closer to the true value for $\sigma_{3/2\rightarrow1/2}$. This expectation is in accord with the values for $\sigma_{3/2\rightarrow1/2}$ determined here are higher than those of Ref. 15 and that the difference between the two measurements decreases as E_{lab} is increased. Although our values for $\sigma_{3/2\rightarrow1/2}$ are higher, they are still lower than the theoretical predictions. As pointed out previously,[9] the theoretical predictions will be improved if accurate ab initio potential energy curves for Ar_2^+ are used in the calculation.

Table II listed the values for $X_{3/2}$ and $\sigma_{3/2\rightarrow1/2}$ at E_{lab} = 25 eV for reaction (2) obtained in the N_2 gas cell pressure (P) range of 2.38-4.65x10^{-4} Torr. The average value for $\sigma_{3/2\rightarrow1/2}$ at E_{lab} = 25 eV is 2.18±0.25 $Å^2$ which is found to be substantially greater than the excitation

Table I. Absolute spin-orbit-state excitation cross sections, $\sigma_{3/2\to1/2}$, for the reaction $Ar^+(^2P_{3/2}) + Ar(^1S_0) \longrightarrow Ar^+(^2P_{1/2}) + Ar(^1S_0)$ E_{lab} = 60, 130, and 200 eV

	E_{lab}(eV)		
	60	130	200
$\sigma_{3/2\to1/2}(\mathring{A}^2)$[a,b]	0.61 ± 0.06 (0.31)	1.58 ± 0.28 (1.1)	2.14 ± 0.30 (2.0)

[a]This work.

[b]The values in the parentheses are obtained from Ref. 15.

Table II. Absolute spin-orbit-state excitation cross sections, $\sigma_{3/2\to1/2}$, for the reaction $Ar^+(^2P_{3/2}) + N_2(\tilde{X},v=0) \longrightarrow Ar^+(^2P_{1/2}) + N_2(\tilde{X},v)$ at E_{lab} = 25 eV

$P(10^{-4}$ Torr)[a]	$X_{3/2}$[b]	$\sigma_{3/2\to1/2}(\text{Å}^2)$
2.38	0.9894	2.42
2.79	0.9865	2.53
3.31	0.9845	2.09
4.06	0.9877	1.34
4.65	0.9738	2.53
		$\langle\sigma_{3/2\to1/2}\rangle = 2.18 \pm 0.25$ (1.98[c]; 3[d])

[a]The N_2 pressure used in the first reaction gas cell.
[b]The fraction of Ar^+ in the $^2P_{3/2}$ state.
[c]The theoretical value obtained from Ref. 16.
[d]The theoretical value obtained from Ref. 24.

cross section for reaction (1) at E_{lab} = 60 eV. The experimental value is in agreement with the calculated values (see Table II) obtained by Spalburg and Gislason[16] and Parlant and Gislason.[24] The calculation of Parlant and Gislason used ab initio potential energy surfaces for the $[Ar + N_2]^+$ system and is expected to be more accurate.

The value for $\sigma_{3/2\rightarrow 1/2}$ at E_{lab} = 25 eV of reaction (2) has also been obtained from the slope of a $\ln(X_{3/2})$ vs P plot. The value of 2.31 $\mathring{A}^2$ thus determined is in good accord with the average value.

CONCLUSIONS

We have demonstrated a new experimental method which allows the determination of absolute state-to-state excitation cross sections of reactions (1) and (2). The detailed fine structure excitation and relaxation cross section measurements for the reactions $Ar^+(^2P_{3/2,1/2})$ + N_2(CO,O_2,NO,Kr, and Ne) are in progress. With the similar experimental arrangement and procedures, it is possible to determine absolute state-to-state vibrational relaxation cross sections for many simple molecular ions in collisions with various quenching gases.

APPENDIX

The Design for Quantum State Excitation or Deexcitation Experiments with the Double-Gas-Cell Arrangement of the Tandem Mass Spectrometer

The following procedures are designed for experiments and the corresponding data analysis for the measurement of absolute collision induced excitation or deexcitation total cross sections using the triple-quadrupole double-octopole photoionization tandem mass spectrometer. This appendix is divided into four parts, based on the four possible reactions of interest. The first part involves all four possible reactions, and the equations used in general form throughout this paper are derived therein. The remaining three parts are special cases where one or more of the possible reactions is not involved. All variables which are assumed given can be measured by the method mentioned when they first appear in the text.

Consider the following reactions

$$A^{+*} + B \xrightarrow{\sigma_{r*}} C^{+} + D \qquad \text{(R1)}$$

$$A^{+} + B \xrightarrow{\sigma_{r}} E^{+} + F \qquad \text{(R2)}$$

$$A^{+*} + B \xrightarrow{\sigma_{R}} A^{+} + B \qquad \text{(R3)}$$

$$A^{+} + B \xrightarrow{\sigma_{E}} A^{+*} + B \qquad \text{(R4)}$$

where (R1) and (R2) are the reaction channels for the primary ions in the excited state and the ground state respectively, and which include the charge transfer; (R3) is the quantum state relaxation channel; and (R4) is the quantum state excitation channel.

The probing reactions are

$$A^+ + M \xrightarrow{\sigma_{pr}} M^+ + A \qquad (R5)$$

$$A^{+*} + M \xrightarrow{\sigma_{pr*}} M^+ + A \qquad (R6)$$

Values for the cross sections for reactions (R1), (R2), (R5) and (R6) must be available for the following experiments.

Case 1 : Measurement of σ_R with all of the reactions involved

When the upper gas cell is filled with the probing gas and the lower gas cell is empty the measurements result in a mixed cross section for reactions (R5) and (R6) multiplied by an arbitrary constant

$$\begin{aligned} Y_{m,w/o} &= C\sigma_{m,w/o} \\ &= C(X_g\sigma_{pr} + X_e\sigma_{pr*}) \end{aligned} \qquad (1a)$$

When the test gas is sent into the lower gas cell and measurements made under the same conditions as before, the result is also a mixed cross section for both reactions (R5) and (R6) multiplied by the same constant as in Eq. (1a)

$$\begin{aligned} Y_{m,w} &= C\sigma_{m,w} \\ &= C(X'_g\sigma_{pr} + X'_e\sigma_{pr*}) \end{aligned} \qquad (2a)$$

The distribution coefficients X_g and X_e are for the reactant ions at ground state and excited state respectively before the collision in the lower gas cell, while X'_g and X'_e are for after the collision. Values for X_g and X_e

must be available for carrying out this experiment. They have the relationship

$$X_g + X_e = 1 \tag{3a}$$

$$X_g' + X_e' = 1 \tag{4a}$$

Dividing (2a) by (1a) yields

$$\frac{Y_{m,w}}{Y_{m,w/o}} = \frac{C(X_g'\sigma_{pr} + X_e'\sigma_{pr*})}{C(X_g\sigma_{pr} + X_e\sigma_{pr*})} \tag{5a}$$

where X_g', considering Eq. (4a), is the only unknown, and which can be calculated by

$$X_g' = \frac{\frac{Y_{m,w}}{Y_{m,w/o}}(X_g\sigma_{pr} + X_e\sigma_{pr*}) - \sigma_{pr*}}{\sigma_{pr} - \sigma_{pr*}} \tag{6a}$$

The flux of the reactant in the ground state after the collision in the lower gas cell, $i(A^+)$, can be expressed as

$$i(A^+) = i_o(A^+)\exp[-(\sigma_I + \sigma_E)nl] + i_o(A^{+*})(1 - \exp(-\sigma_R nl)) \tag{7a}$$

where $i_o(A^+)$ and $i_o(A^{+*})$ are the fluxes of the reactant at the ground state and the excited state entering the lower gas cell, and the excitation cross section, σ_E, can be measured by the method discussed in Case 4.

After dividing (7a) by the total primary ion flux after the collision in the lower gas cell, I, the new distribution coefficient can also be written as

$$X_g' = X_g(I_o/I)\exp[-(\sigma_r + \sigma_E)nl] + X_e(I_o/I)[1 - \exp(-\sigma_R nl)] \tag{8a}$$

where I_o is the total flux of reactant before the collision with the neutral gas B in the lower gas cell. Hence I_o and I can be expressed as

$$I_o = i_o(A^+) + i_o(A^{+*}) \tag{9a}$$

$$I = i(A^+) + i(A^{+*})$$

$$= X_g I_o \exp(-\sigma_r nl) + X_e I_o \exp(-\sigma_{r*} nl) \tag{10a}$$

Substituting Eq. (10a) into Eq. (8a), we obtain

$$X_g' = \frac{X_g\exp[-(\sigma_r + \sigma_E)nl] + X_e[1 - \exp(-\sigma_R nl)]}{X_g\exp(-\sigma_r nl) + X_e\exp(-\sigma_{r*} nl)} \tag{11a}$$

Rearranging Eq. (11a) yields Eq. (12a) from which the quantum state relaxation cross section can be calculated.

$$\sigma_R = \frac{-1}{nl}\ln\{1 - \frac{1}{X_e}[X_g'(X_g\exp(-\sigma_r nl) + X_e\exp(-\sigma_{r*} nl)) - X_g\exp[-(\sigma_r+\sigma_E)nl]]\} \tag{12a}$$

Case 2 : Measurement of σ_E with only (R2) and (R4) involved

In this case the primary ion is prepared in the pure ground state. When the upper gas cell is filled with the probing gas and the lower gas cell is empty, the measurements result in the cross section of reaction (R5) multiplied by an arbitrary constant

$$Y_{m,w/o} = C\sigma_{pr} \tag{13a}$$

The measurements with the gas B in the lower gas cell give the same result as expressed by Eq. (2a).

Since X_g equals unity in this case, Eqs. (5a) and (6a) can be rewritten as

$$\frac{Y_{m,w}}{Y_{m,w/o}} = \frac{C(X_g'\sigma_{pr} + X_e'\sigma_{pr*})}{C\sigma_{pr}} \tag{14a}$$

$$X_g' = \frac{(Y_{m,w}/Y_{m,w/o})\sigma_{pr} - \sigma_{pr*}}{\sigma_{pr} - \sigma_{pr*}} \tag{15a}$$

Since the reactions (R2) and (R4) are the only channels which affect the flux of the primary ion

$$\begin{aligned} i(A^+) &= i_o(A^+)\exp[-(\sigma_r + \sigma_E)nl] \\ &= I_o\exp[-(\sigma_r + \sigma_E)nl] \end{aligned} \tag{16a}$$

Dividing (16a) by the total primary ion flux after the collision in the lower gas cell, I, the new distribution coefficient can be written as

$$X_g' = (I_o/I)\exp[-(\sigma_r + \sigma_E)nl] \tag{17a}$$

where

$$I = I_o\exp(-\sigma_r nl) \tag{18a}$$

Simplifying Eq. (17a) gives

$$X_g' = \exp(-\sigma_E nl) \tag{19a}$$

From Eq. (19a) we obtain

$$\ln(X_g') = -\sigma_E nl \tag{20a}$$

Therefore, the quantum state excitation cross section can be calculated from either of the following equations

$$\sigma_E = \frac{-1}{nl}\ln(X_g') \tag{21a}$$

$$\sigma_E = \frac{-1}{l}\frac{d\ln(X_g')}{dn} \tag{22a}$$

Case 3 : Measurement of σ_R with only (R1) and (R3) involved

Following the same arguments as were used in Case 2, the quantum state relaxation cross section can be calculated from either of the following equations.

$$\sigma_R = \frac{-1}{nl} \ln(X_g') \tag{23a}$$

$$\sigma_R = \frac{-1}{l} \frac{d\ln(X_g')}{dn} \tag{24a}$$

Case 4 : Measurement of σ_R with (R1), (R3) and (R4) involved

Since reaction (R2) does not exist, Eq. (12a) can be modified with $\sigma_r = 0$ to get the following equation to calculate the quantum state relaxation cross section.

$$\sigma_R = \frac{-1}{nl} \ln\{1 - \frac{1}{X_e}[X_g'(X_g + X_e\exp(-\sigma_{r*}nl)) - X_g\exp(-\sigma_E nl)]\} \tag{25a}$$

References

1. J. T. Yardley, "Introduction to Molecular Energy Transfer"(New York: Academic, 1980).

2. M. Faubel, Adv. Atomic Molec. Phys. 19, 345 (1983).

3. G. Hall, K. Liu, M. J. McAuliffe, C. F. Giese, and W. R. Gentry, J. Chem. Phys. 78, 5260 (1983); ibid. 81, 5577 (1984); ibid. 80, 3494

(1984); ibid. 84, 1402 (1986); and G. Hall, C. F. Giese, and W. R. Gentry, J. Chem. Phys. 83, 5343 (1985).

4. T. Ellenbroek, U. Gierz, and J. P. Toennies, Chem. Phys. Lett. 70, 459 (1980); T. Ellenbroek and J. P. Toennies, Chem. Phys. 71, 309 (1982); T. Ellenbroek, U. Gierz, M. Noll, and J. P. Toennies, J. Phys. Chem. 86, 1153 (1982); and U. Gierz, M. Noll, and J. P. Toennies, J. Chem. Phys. 83, 2259 (1985).

5. H. Bohringer, M. Durup-Ferguson, D. W. Fahey, F. C. Fehsenfeld, and E. E. Ferguson, J. Chem. Phys. 79, 4201 (1983); W. Dobler, H. Ramler, H. Villinger, F. Howorka, and W. Lindinger, Chem. Phys. Lett. 97, 553 (1983); I. Dotan, S. E. Barlow, and E. E. Ferguson, Chem. Phys. Lett. 121, 38 (1985); W. Federer, W. Dobler, F. Howorka, W. Lindinger, M. Durup-Ferguson, and E. E. Ferguson, J. Chem. Phys. 83, 1032 (1985); M. Durup-Ferguson, F. Bohringer, D. W. Fahey, F. C. Fehsenfeld, and E. E. Ferguson, J. Chem. Phys. 81, 2657 (1984); W. Federer, H. Ramler, H. Villinger, and W. Lindinger, Phys. Rev. Lett. 54, 540 (1985); D. Smith and N. G. Adams, Phys. Rev. A23, 2327 (1981); and W. Lindinger, F. Howorka, P. Lukac, S. Kuhn, H. Villinger, E. Alge, and H. Ramler, Phys. Rev. A23, 2319 (1981).

6. A. O. Langford, V. M. Bierbaum, and S. R. Leone, J. Chem. Phys. 84, 2158 (1986); ibid. 83, 3913 (1985); G.-H. Lin, Jurgen Maier, and S. R. Leone, J. Chem. Phys. 84, 2180 (1986); ibid. 82, 5527 (1985); C. E. Hamilton, V. M. Bierbaum, and S. R. Leone, J. Chem. Phys. 83, 601 (1985); ibid. 83, 2284 (1985); ibid. 80, 1831 (1984); L. Huwel, D. R. Guyer, G.-H. Lin, and S. R. Leone, J. Chem. Phys. 79, 1259 (1983); V. E. Bondybey and T. A. Miller, J. Chem. Phys. 69, 3597 (1978); and D. H. Katayama, T. A. Miller, and V. E. Bondybey, J. Chem. Phys. 72, 5469 (1980).

7. C.-L. Liao, C.-X. Liao, and C. Y. Ng, J. Chem. Phys. 81, 5672 (1984).

8. C.-L. Liao and C. Y. Ng, J. Chem. Phys. 84, 197 (1986).

9. C.-L. Liao, C.-X. Liao, and C. Y. Ng, J. Chem. Phys. 82, 5489 (1985).

10. C.-L. Liao, J. D. Shao, R. Xu, G. D. Flesch, Y.-G. Li, and C. Y. Ng, J. Chem. Phys. 85, xxxx (1986), in press.

11. C.-L. Liao, R. Xu, and C. Y. Ng, J. Chem. Phys. Submitted.

12. J. D. Shao, Y.-G. Li, G. D. Flesch, and C. Y. Ng, J. Chem. Phys. Submitted.

13. R. Xu, C.-L. Liao, J.-H. Guo, and C. Y. Ng, J. Chem. Phys., to be published.

14. R. Xu, C.-L. Liao, J.-H. Guo, and C. Y. Ng, J. Chem. Phys., to be published.

15. Y. Itoh, N. Kobayashi, and Y. Kaneko, J. Phys. Soc. Jpn. 50, 3541 (1981).

16. M. R. Spalburg and E. A. Gislason, Chem. Phys. 94, 339 (1985).

17. J. D. Shao and C. Y. Ng, Chem. Phys. Lett. 118, 481 (1985).

18. J. D. Shao and C. Y. Ng, J. Chem. Phys. 84, 4317 (1986).

19. E. Teloy and D. Gerlich, Chem. Phys. 4, 417 (1974).

20. H. M. Gibbs and E. D. Commins, Rev. Sci. Instr. 37, 1385 (1966).

21. C. J. Latimer and F. M. Campbell, J. Phys. B15, 1765 (1982).

22. K. Tanaka, J. Durup, T. Kato, and I. Koyano, J. Chem. Phys. 74, 5561 (1981).

23. R. E. Johnson, J. Phys. B3, 539 (1970).

24. G. Parlant and E. A. Gislason, Dept. of Chem., University of Illinois at Chicago, to be published.

CONCLUSIONS

A new ion-molecule reaction apparatus, which consists of a photoionization source, a tandem mass spectrometer, and a radio frequency (rf) octopole reaction cell, has recently been developed. Absolute total cross sections for the reaction $H_2^+(v_0') + H_2(v_0''=0) \longrightarrow H_3^+ + H$, have been measured as a function of the vibrational state of reactant H_2^+, where $v_0'=0-4$, over the center-of-mass collision energy range of 0.04-15eV. The experimental results are compared with phenomenological cross sections obtained in previous single gas cell studies, the quasiclassical trajectory calculations of Stine and Muckerman, and the recent similar calculations of Eaker and Schatz. The absolute total cross sections measured for $v_0'=0$ and 3 at $E_{c.m.}=0.5$, 1, 3, and 5 eV are found to be in agreement with "trajectory surface hopping" calculations which include nonadiabatic surface hopping throughout the reaction.

Absolute spin-orbit-state-selected total cross sections for charge transfer reactions $Ar^+(^2P_{3/2}) + N_2(\tilde{X},v=0)$ and $Ar^+(^2P_{1/2}) + N_2(\tilde{X},v=0)$, $\sigma_{3/2}$ and $\sigma_{1/2}$, respectively, at the $E_{c.m.}$ range of 0.25-115.3 eV have also been measured using the same apparatus. The measured values for $\sigma_{3/2}$ at $E_{c.m.}$ = 4.1, 10.3, and 41.2 eV and $\sigma_{1/2}$ at 41.2 eV are in reasonable agreement with the theoretical cross sections. However, the experimental values for $\sigma_{3/2}$ at 1.2 eV and $\sigma_{1/2}$ at 1.2, 4.1, and 10.3 eV are approximately a factor of two higher than the theoretical predictions. A model analysis, which takes into account possible collision induced spin-orbit mixings of the reactant Ar^+ states in the rf octopole gas cell, shows that the values for $\sigma_{1/2}/\sigma_{3/2}$

and $\sigma_{1/2}$ determined using the ion beam-rf octopole gas cell arrangement can be strongly susceptible to gas cell pressure effects whereas the experimental values for $\sigma_{3/2}$ are reliable. The values for $\sigma_{1/2}$ deduced by multiplying the values for $\sigma_{3/2}$ and the ratios $\sigma_{1/2}/\sigma_{3/2}$ determined in the crossed ion-neutral beam experiment are in agreement with the theoretical cross sections. Both $\sigma_{3/2}$ and $\sigma_{1/2}$ are found to increase as $E_{c.m.}$ is increased from 41.2 eV. This observation is interpreted as due to the formation of N_2^+ in the $\tilde{A}^2\Pi_u$ state at high $E_{c.m.}$.

With the triple-quadrupole double-octopole photoionization tandem mass spectrometer, absolute state-selected total cross sections, $\sigma_{v'}$, v' = 0 and 1, for reaction $N_2^+(\tilde{X},v'=0,1) + Ar(^1S_0) \longrightarrow N_2(\tilde{X},v) + Ar^+(^2P_{3/2,1/2})$ (reaction (1)) over $E_{c.m.}$ range of 1.2-140 eV have been measured. These measurement, together with the relative values for $\sigma_{v'}$, v' = 0-2, and spin-orbit-state distributions of product Ar^+ ions determined using the crossed ion-neutral beam photoionization apparatus, allow the determination of the absolute values for σ_2 and partial state-to-state cross sections, $\sigma_{v'\rightarrow J}$, v' =0-2, for reaction (1). Absolute values for $\sigma_{v'}$, v' = 0-2, at $E_{c.m.}$ = 8 and 20 eV are in good agreement with those determined previously by the threshold photoelectron secondary ion coincidence method. Absolute values for $\sigma_{v'\rightarrow J}$, v' = 0-2, at $E_{c.m.}$ = 8 and 20 eV are also found to be in satisfactory accord with the predictions of the semi-classical multi-state calculation which uses the ab initio potential energy surfaces of the $[N_2 + Ar]^+$ system. Experimental state-to-state cross sections obtained in this study are consistent with those for the reaction, $Ar^+(^2P_{3/2}) + N_2(\tilde{X},v=0) \longrightarrow Ar(^1S_0) + N_2^+(\tilde{X},v')$, from the consideration of microscopic reversibility.

Using the triple-quadrupole double-octopole apparatus, absolute fine-structure transition cross sections for the reactions $Ar^+(^2P_{3/2}) + Ar$ and $Ar^+(^2P_{3/2}) + N_2(\tilde{X},v=0)$ at laboratory collision energies of 25-200 eV have been measured. The results are in satisfactory agreement with theoretical prediction and a previous experimental study.

The experimental approach discussed in this dissertation can be further improved by coupling with laser and coincidence techniques. The detailed experimental cross-sectional data obtained by using the tandem photoionization mass spectrometer provide more information to complement theoretical consideration.

APPENDIX A.

SELECTED COMPUTER PROGRAMS

I. The programs for the operation of the photoionization mass spectrometer.

1. Take single data point.

```
C TDATA.FOR takes data points n(I) times at given wavelengthes WL(I) and
C mass MASS(J). The dimensions of array WL and N are the same and no
C larger than 50. The format for input of the number of elements and the
C values of WL and N is defined in file NONAME.FOT. The input data should
C exist in file NONAME.DAT. The output data will be found in file
C NONAME.LOG.
C
C At every stop for continue or exit, the content of file NONAME.DAT can
C be C changed to obtain different data composition.
C
C Program :
      INTEGER RTNCOD, N(50), MASS(50)
      REAL WL(50)
      INTEGER CLIN, CLOUT, FLAG
      BYTE BUFFER(60), BUFER1(60), STRING(60), DA
      OPEN(UNIT=33, NAME='DAT:TDATA.LOG', TYPE='NEW',
     F CARRIAGECONTROL='FORTRAN')
      CALL IMRINI(CLIN,CLOUT,BUFFER,BUFER1,60,RTNCOD)
150   OPEN(UNIT=22, NAME='TDATA.DAT', TYPE='OLD')
      READ(22,3) DA
      READ(22,*) NMASS
      READ(22,*) (MASS(I), I=1,NMASS)
      READ(22,*) NUM
      READ(22,*) (N(I), I=1,NUM)
      READ(22,*) (WL(I), I=1,NUM)
      TYPE 2
      ACCEPT 3, STRING
      WRITE(33,4) STRING
      TYPE 4, STRING
      WRITE(33,*) ' '
      TYPE*, ' '
      DO 300 K = 1,NUM
          CALL IMRWL(CLIN, CLOUT, BUFFER, BUFER1, 60, WL(K))
          DO 100 I = 1,NMASS
          CALL IMRMAS(CLIN, CLOUT, BUFFER, BUFER1, STRING,
     F    60,DA,MASS(I), 33)
              DO 200 J = 1,N(K)
                  CALL IMRSDP(CLIN, CLOUT, BUFFER,BUFER1, STRING,
     F            60, 33)
200           CONTINUE
100       CONTINUE
```

```
300     CONTINUE
        CLOSE(UNIT=22)
        CALL BELL
2       FORMAT(//X,'Enter the conditions (< 60 characters) : ')
3       FORMAT(60A1)
4       FORMAT(X,60A1)
130     TYPE 1
1       FORMAT(' ','Choose one by number :',//7x,'1. Continue.',
     F /7x,'2. Exit.'//x,'Number : ',$)
        ACCEPT*, FLAG
        IF(FLAG .EQ. 2) GOTO 120
        GOTO 150
120     CLOSE(UNIT=33)
        END
```

2. Scan mass spectrum.

```
C MASCAN.FOR sans the mass spectrum.
      INTEGER CLIN, CLOUT, FLAG, STARTM, RTNCOD
      BYTE BUFFER(60), BUFER1(60), STRING(60), DA
      OPEN(UNIT=33, NAME='MASCAN.LOG', TYPE='NEW')
      CALL IMRINI(CLIN,CLOUT,BUFFER,BUFER1,60,RTNCOD)
14    OPEN(UNIT=22, NAME='MASCAN.DAT', TYPE='OLD')
      READ(22,206) DA
301   READ(22,*,END=302) STARTM, LASTM, INT
      DO 300 MASS = STARTM, LASTM, INT
          CALL IMRMAS(CLIN,CLOUT, BUFFER,BUFER1,
     F    STRING,60,DA,MASS,33)
          CALL IMRSDP(CLIN, CLOUT, BUFFER,BUFER1,
     F    STRING, 60,33)
300   CONTINUE
      GOTO 301
302   CLOSE(UNIT=22)
      CALL BELL
130   TYPE 201
      ACCEPT*, FLAG
      IF(FLAG .EQ. 2) GOTO 120
      GOTO 14
201   FORMAT(/X,'Choose one by number :',//7x,'1. Continue.',
     F ' point.'/7x,'2. Exit.'
     F //x,'Number : ',$)
203   FORMAT(/X,'Starting number for the mass scan : ',$)
204   FORMAT(/X,'Ending number : ',$)
205   FORMAT(/X,'Interval of the numbers : ',$)
206   FORMAT(1A1)
120   CLOSE(UNIT=33)
      END
```

3. Subroutines.

```
C SUBROUTINE CLEAR clears the character string STRING. The dimension of
C the string should be given by the calling program.
C
C Program :
      SUBROUTINE CLEAR(STRING,N)
      BYTE STRING(N)
      DO 100 I = 1,N
          STRING(I) = 0
100   CONTINUE
      RETURN
      END
```

```
C SUBROUTINE IMRMAS sets the mass for the lower, middle, upper
C quadrupoles by sending integer numbers to the corresponding D/A's. The
C range of the numbers is 0 to 4095.
C The following characters are used to indicate the quadrupoles :
C      DA = 'L' - lower quadrupole.
C      DA = 'M' - middle quadrupole.
C      DA = 'U' - upper quadrupole.
C
C Program :
      SUBROUTINE IMRMAS(CLIN, CLOUT, BUFFER, BUFER1, STRING, N, DA,
     F MASS, UNIT)
      BYTE BUFER1(N), BUFFER(N), STRING(N), TERM(2), DA, MSCHAR(5)
      INTEGER CLIN, CLOUT, TRIGER, UNIT
      DATA TERM,MSCHAR(5) /1,13,13/
      CALL CLEAR(STRING, N)
      IF(DA .EQ. 'L') TRIGER = 'L'
      IF(DA .EQ. 'M') TRIGER = 'M'
      IF(DA .EQ. 'U') TRIGER = 'U'
      ENCODE(4,1,MSCHAR) MASS
      DO 100 I = 1,4
          IF(MSCHAR(I) .EQ. ' ') MSCHAR(I) = '0'
100   CONTINUE
      CALL LPUTLN(CLOUT,TRIGER,1)
      CALL LRECEV(CLIN,,,RTNCOD,RESET)
      CALL LPUTLN(CLOUT,MSCHAR,5)
      CALL LGETLN(CLIN,STRING,60,RTNCOD,1,TERM)
      WRITE(7,2) STRING
      IF(UNIT .GT. 0) WRITE(UNIT,2) STRING
1     FORMAT(I4)
2     FORMAT('+',60A1/)
      RETURN
      END
```

```
C SUBROUTINE IMRINI is used to initialize the working conditions. It
C enables the I/O for the console terminal and the M6809 microprocessor,
C which are assigned to unit 0 and 1, and 2 and 3 respectively. If there
C is anything wrong, the error message will be displayed on the screen C
and the program will be halted.
C
C Program :
      SUBROUTINE IMRINI(CLIN,CLOUT,BUFFER,BUFER1,N)
      INTEGER RTNCOD, CLIN, CLOUT
      BYTE BUFFER(N), BUFER1(N)
      CLIN = 2
      CLOUT = 3
      IF(LENABL(0,,,RTNCOD)) GOTO 10
      IF(LENABL(1,,,RTNCOD)) GOTO 10
      GOTO 11
10    CALL LERROR(RTNCOD,10,'Console failed to enable.',25)
      STOP
11    IF(LENABL(CLIN,BUFFER,N,RTNCOD) .EQ. 0) GOTO 12
      CALL LERROR(RTNCOD,11,'M6809 failed to enable.',23)
      STOP
12    IF(LENABL(CLOUT,BUFER1,N,RTNCOD) .EQ. 0) GOTO 13
      CALL LERROR(RTNCOD,12,'M6809 failed to enable.',23)
      STOP
13    RETURN
      END
```

```
C SUBROUTINE IMRSDP triggers the M6809 to take a single data point. The
C output from M6809 has to be manipulated in the calling program.
C
C Program :
      SUBROUTINE IMRSDP(CLIN, CLOUT, BUFFER,BUFER1, STRING,
     F N, UNIT)
      BYTE BUFER1(N), BUFFER(N), STRING(N), TERM(2)
      INTEGER CLIN, CLOUT, RTNCOD, RESET, UNIT
      RESET = "1000
      TRIGER = 'I'
      TERM(1) = 1
      TERM(2) = 10
      CALL CLEAR(STRING, N)
      CALL LRECEV(CLIN,,,RTNCOD,RESET)
      CALL LPUTLN(CLOUT,TRIGER,1)
      TYPE 2
      CALL LGETLN(CLIN,STRING,N,RTNCOD,1,TERM)
      WRITE(7,1) STRING
      IF(UNIT .GT. 0) WRITE(UNIT,1) STRING
1     FORMAT('+',60A1)
2     FORMAT('+','TRIGGER OK')
      RETURN
      END
```

```
C SUBROUTINE IMRWL changes the wavelength WL from REAL to BYTE, and
C then transmits them to M6809 microprocessor to set the grating at the
C wavelength.
C
C Program :
      SUBROUTINE IMRWL(CLIN, CLOUT, BUFFER, BUFER1, N, WL)
      BYTE WLCHAR(6), BUFFER(N), BUFER1(N), STRING(60), TRIGER
      BYTE TERM(2)
      INTEGER CLIN, CLOUT, RTNCOD, WLX100(2)
      DATA TERM,TRIGER/1,10,'S'/
      IF(WL .GE. 0 .OR. WL .LE. 6000) GOTO 10
      WRITE(7,*) 'The wavelength is out of the range. No action is',
     F ' undertaken.'
      GOTO 11
10    CALL CLEAR(STRING, 60)
      WLX100(1) = INT(WL / 10)
      WLX100(2) = INT(AMOD(WL,10.) * 100)
      ENCODE(6,1,WLCHAR) WLX100
      DO 100 I = 1,6
          IF(WLCHAR(I) .EQ. ' ') WLCHAR(I) = '0'
100   CONTINUE
      CALL LPUTLN(CLOUT,TRIGER,1)
      CALL LRECEV(CLIN,,,RTNCOD,RESET)
      CALL LPUTLN(CLOUT,WLCHAR,6)
      CALL LGETLN(CLIN,STRING,60,RTNCOD,1,TERM)
1     FORMAT(2I3)
11    RETURN
      END
```

II. Programs for data treatment.

1. Average the output file obtained by using TDATA.FOR.

```
C AVESD.FOR reads in data from SPECTR.DAT according to the format defined
C in AVESD.DAT, and calculates the average values and the standard
C deviations. Then it writes the results into AVESD.LOG.
C
C Program :
      REAL PIE(15,6,6)
      INTEGER N(6,6), NOREP(6)
      OPEN(22, FILE='SPECTR.DAT', STATUS='OLD')
      OPEN(23, FILE='AVESD.DAT', STATUS='OLD')
      OPEN(33, FILE='AVESD.LOG', STATUS='NEW',
     F CARRIAGECONTROL='FORTRAN')
      READ(23,*) NOCYCL
      READ(23,*) NOMASS
      READ(23,*) NOWL
      READ(23,*) (NOREP(I), I=1,NOWL)
      READ(23,*) PHOTBG
      DO 100 K = 1,NOCYCL
          DO 200 J = 1,NOWL
              DO 300 L = 1,NOMASS
                  DO 350 M = 1,NOREP(J)
                      N(J,L) = N(J,L) + 1
                      CALL READSD(WORD, WL, X, A, PHOTON)
                      PIE(N(J,L),J,L) = X / (PHOTON - PHOTBG)
350               CONTINUE
300           CONTINUE
200       CONTINUE
100   CONTINUE
      DO 400 J = 1,NOWL
          DO 500 L = 1,NOMASS
              AVE = AVERAG(PIE(1,J,L), N(J,L))
              S = STAND(PIE(1,J,L), N(J,L), AVE)
              IF(AVE .NE. 0) P = S * 100 / AVE
              WRITE(33,2) AVE, S, P
500       CONTINUE
400   CONTINUE
2     FORMAT(' ', G11.4, 7X, G11.4, 7X, F7.2,'%')
      CLOSE(33)
      END
```

2. Calculation of absolute cross section.

```
C ABSCS.FOR calculates the absolute cross section for reaction
C
C              A+ + B —> C+ + D
C
C with the following equation
C
C              ABSCS = Ln{I(A+) / [I(A+) - I(C+)]} / (n * l)
C
C where n is number density of the target gas B, l is the length of the
C collision path, and
C
C              I(C+) = PIE(C+) - PIE(BG of C+)
C              I(A+) = PIE(A+) + PIE(C+)
C
C where BG - background.
C
C Program :
      REAL ABSCS(20,7), PIEC(6), PIECBG(6), LENGTH, X(20)
      PARAMETER (LENGTH=0.13)
      OPEN(UNIT=22,NAME='SPECTR.DAT',TYPE='OLD')
      OPEN(UNIT=33,NAME='TEMP.DAT',TYPE='NEW')
      READ(22,*) NUM
      N = NUM + 1
      WRITE(33,*) NUM,' product(s)'
      READ(22,*) M
      READ(22,*) P
      DENSIT = 6.022E23 * P * 133.3 / 8.3143 / 298.
      READ(22,*) (X(K), K=1,M)
      READ(22,*) (PIECBG(K), K=1,N)
      DO 300 K = 1,M
          CALL PRECS(PIEC, PIECBG, PIEA, N, 22)
          DO 200 J = 1,NUM
              A = PIEA - PIEC(J)
              ABSCS(K,J) = 1E20*ALOG(PIEA/A)/DENSIT/LENGTH
200       CONTINUE
300   CONTINUE
      DO 500 I = 1,NUM
          WRITE(33,3) I
          DO 400 J = 1,M
              WRITE(33,4) X(J), ABSCS(J,I)
400       CONTINUE
500   CONTINUE
3     FORMAT(//X,'E(eV)',2X,'Product ',I1)
4     FORMAT(X,F5.1,2X,G11.4)
      CLOSE(UNIT=33)
      END
```

3. Draw PIE spectra.

```
C THIS PROGRAM PLOTS PIE SPECTRA OF REACTANT A+ BEFORE AND AFTER
C COLLISION, AND PRODUCT C+. IT ALSO PLOTS ATTENUATION CURVE AND RATIO
C CURVE OF REACTANT AND PRODUCT. ALL SPECTRA AND CURVES MUST BE UNIFORMLY
C DISTRIBUTED POINTS.
C      *            *            *
C NOTE: 1. This program is used for analyzing the PIE data without
C       any correction. If photoelectric yield should be used to
C       correct the PIE data detected with tungston detector, the
C       program AUTOPC.FOR should be used.
C
C      2. MARK is used to indicate the differente species in the reaction
C
C              A+ + B ---> C+ + D
C
C              MARK = 1        I0 : A+ BEFORE COLLISION
C              MARK = 2        I : A+ AFTER COLLISION
C              MARK = 3        Ic : PRODUCT
C              MARK = 4        (I0-I)/I0 : ATTENUATION
C              MARK = 5        Ic/I0 : CONSTANT * PRODUCT CROSS SECTION
C
C      3. The maximum dimentions in the arrays of wavelength and the
C      corresponding data is 100.
C
C Program :
       REAL XAXIS(100), Y(100,5), NOISE
       INTEGER KEY(5), KEYY(5)
       CHARACTER*11 DATE, FILENM, XTIT, YTIT, TIT(5)
       DATA XSIZE,YSIZE,KEY,YMIN,YMAX,NOISE/10.25,7.25,5*0,3*0./
       TIT(4) = 'Attenuation'
       TIT(5) = 'Ic/I0      '
       OPEN(UNIT=22, NAME='SPECTR.DAT', TYPE='OLD')
       OPEN(UNIT=9, NAME='PT:OUTPUT.DAT', TYPE='NEW')
       READ(22,1) DATE
1      FORMAT(A11)
       READ(22,1) FILENM
       READ(22,1) XTIT
       READ(22,1) YTIT
5      READ(22,4,ERR=5,END=7) SIGN, MARK
       IF(SIGN .EQ. 'AA') READ(22,*) PHOTBG
       IF(SIGN .EQ. 'BB') READ(22,*) PIEBG
       IF(SIGN .NE. 'MM') GOTO 5
       IF(MARK .EQ. 1 .OR. MARK .EQ. 2 .OR. MARK .EQ. 3) GOTO 10
       TYPE*, 'The MM# is wrong in the data file.'
       GOTO 11
10     READ(22,1) TIT(MARK)
       CALL GETDAT(XMAX,XMIN,XTIC,N,Y(1,MARK),100,YYMAX,PIEBG,PHOTBG)
       IF(YYMAX .GT. YMAX) YMAX = YYMAX
       KEY(MARK) = 1
```

```
      GOTO 5
4     FORMAT(A2,I1)
7     YMAX = YMAX * 1.2
      YTIC = YMAX / 4.
3     FORMAT(A1)
      CALL WL(XAXIS, N, XMIN, XMAX, XTIC)
C
C CHOOSE TERMINAL OR HIPLOTTER
C
123   CALL PROMP(Y, N, 5, KEY, KEYY)
12    TYPE 6
6     FORMAT(/X,'Choose one of the followings by number :',//7X,'1. ',
     F 'Change scale or frame size.',/7X,'2. Change values.',/7X,'3. ',
     F 'Normalization.',/7X,'4. Plot.',/7X,'5. Calculate cross section.',
     F /7X,'6. Choose other curves.',/7X,'7. Exit.',//X,'Number = ',$)
      ACCEPT*, NUM
      IF(NUM .EQ. 1) CALL SCALE1(XMIN,XMAX,XTIC, YMIN,YMAX,YTIC,
     F XSIZE,YSIZE)
      IF(NUM .EQ. 2) CALL ALGEB(Y, N, 5, KEYY)
      IF(NUM .EQ. 3 .AND. KEYY(1) .EQ. 1 .AND. KEYY(3) .EQ. 1)
     F CALL NORMLZ(XAXIS, Y(1,3), Y(1,1), N)
      IF(NUM .EQ. 3 .AND. KEYY(1) .NE. 1 .OR. NUM .EQ. 3 .AND.
     F KEYY(3) .NE. 1) TYPE*,'Cannot find data.'
      IF(NUM .EQ. 5) CALL CROSSN(XAXIS,Y(1,1),Y(1,3),N)
      IF(NUM .EQ. 6) GOTO 123
      IF(NUM .EQ. 7) GOTO 11
      IF(NUM .NE. 4) GOTO 12
      CALL CHOICE(IUNIT)
      CALL INIPLT(IUNIT, XSIZE, YSIZE)
      CALL SCALE(XMIN, XMAX, YMIN, YMAX)
      CALL AXIS(XTIC,YTIC, XTIT, 11,2,1, YTIT, 11,2,3)
      I = 1
13    IF(I .GT. 5) GOTO 14
      IF(KEYY(I) .EQ. 1) CALL LINE(XAXIS, Y(1,I), N, I,0,0,0)
      I = I + 1
      GOTO 13
C
C CONSTRUCT LEGEND
C
14    I = 1
      CALL INILGN(5.5, 7.5, 4., 5.5)
      CALL WRILGN(DATE, 8, 0,0,0,0)
      CALL WRILGN(FILENM, 11, 0,0,0,0)
15    IF(I .GT. 5) GOTO 16
      IF(KEYY(I) .EQ. 1) CALL WRILGN(TIT(I), 11, I,0,0,0)
      I = I + 1
      GOTO 15
16    CONTINUE
      CALL ENDLGN
      CALL ENDPLT
      GOTO 12
```

```
C
11      CONTINUE
        END
```

4. Subroutines.

```
C Subroutine READSD(WORD, WL, ION, BACKGD, PHOTON) reads data from
C SPECTR.DAT with the format of 6800 output as following repeatly:
C
C  :I (WL)****.**     (ION)********  (BACKGD)********  (PHOTON)********
C
C PROGRAM :
      SUBROUTINE READSD(WORD, WL, ION, BACKGD, PHOTON)
      REAL ION
10    READ(22,1,ERR=10) WORD, WL, ION, A, PHOTON
      IF(WORD .NE. ':I') GOTO 10
1     FORMAT(A2,X,F7.2,5X, 3(F8.0,2X))
      RETURN
      END
```

```
C SUBROUTINE MULTSC reads in the ion counts of n products for reaction
C
C      I0(A+) + B —> I(A+) + I1 + I2 + ... + In
C
C For product Ii, the cross section is calculated by using the following
C equation in the calling program :
C
C      ABSCS(i) = Ii / [I(i) * n * l]
C      ABSCS(i) = Ln{I(i) / [I(i) - Ii]} / (n * l)
C
C where n is number density of the target gas B, l is the length of the
C collision path, and
C
C      I(i) = I(A+) + I1' + ... + Ii-1' + Ii+1' + ... + In'
C
C where Ij' = Ij - Ij(Background).
C This subroutine calculates the I(i) and return Ij' and I(i) to the
C calling program. ION(i)=Ii', SUM(i)=I(i).
C
C Program :
      SUBROUTINE PRECS(ION, BG, SUM, NN, UNIT)
      INTEGER UNIT
      REAL ION(NN), BG(NN), SUM
      J = 0
      DO 100 I = 1,NN
          J = J + 1
          READ(UNIT,1) ION(J), SIGNAL
      TYPE*, ION(J)
          IF(SIGNAL .NE. 'PP') GOTO 10
          PION = ION(J) - BG(I)
          J = J - 1
          GOTO 100
10        ION(J) = ION(J) - BG(I)
100   CONTINUE
      SUM = PION
      N = NN - 1
      DO 300 J = 1,N
          SUM = SUM + ION(J)
300   CONTINUE
1     FORMAT(G11.4, 2X, A2)
      RETURN
      END
```

```
      SUBROUTINE PROMP(Y, N, NC, KEY, KEYY)
      REAL Y(100,5)
      INTEGER KEYY(NC), KEY(NC)
      DO 300 I = 1,NC
             KEYY(I) = 0
300   CONTINUE
10    TYPE 1
1     FORMAT(X,'FOR REACTION',//,8X,'A+ + B ---> C+ + D',//,
     F X,'CHOOSE THOSE YOU WANT TO PLOT BY NUMBER',//)
      IF(KEY(1) .EQ. 1) TYPE*,' 1. PIE of A+ before collision.'
      IF(KEY(2) .EQ. 1) TYPE*,' 2. PIE of A+ after collision.'
      IF(KEY(3) .EQ. 1) TYPE*,' 3. PIE of C+.'
      IF(KEY(1) .EQ. 1 .AND. KEY(2) .EQ. 1) TYPE*,' 4. Attenuation.'
      IF(KEY(1) .EQ. 1 .AND. KEY(3) .EQ. 1) TYPE*,' 5. Ic/I0.'
      TYPE*,' 6. NONE.'
11    TYPE 2
2     FORMAT(/X,'NUMBER = ',$)
      ACCEPT*, NUMBER
      IF(NUMBER .LT. 1 .OR. NUMBER .GT. 6) GOTO 10
      IF(NUMBER .EQ. 6) GOTO 12
      KEYY(NUMBER) = 1
      GOTO 11
12    IF(KEYY(4) .NE. 1) GOTO 13
      DO 100 I = 1,N
             Y(I,4) = (Y(I,1) - Y(I,2)) / Y(I,1)
100   CONTINUE
13    IF(KEYY(5) .NE. 1) GOTO 14
      DO 200 I = 1,N
             Y(I,5) = Y(I,3) / Y(I,1)
200   CONTINUE
14    RETURN
      END
```

APPENDIX B.

BLOCK DIAGRAM OF THE COMPUTER SYSTEM

Figure B.1 Block diagram of the computer system : 2030 bus is the main communication path in the M6809 microprocessor governed computer (6809 computer). The resident programs in 6809 computer control signal input and output between the 6809 computer and the electronic parts of the apparatus directly. The output signals go to the quadrupole mass filters (QMF) and motor sequencer (MOTOR SEQNCR) of the monochromator through the peripheral interface adapters (PIA), and digital-to-analog converters (D/A). The input signals are photon signal, ion signal, and DC voltages of the lens systems, QMFs, and octopole gas cells. The LSI-11 computer is the master in the whole system. The LSI-11 and 6809 computers communicate through an asynchronous communication interface adapter (ACIA). Through a modem, the LSI-11 can communicate with any other computer system (WORLD)

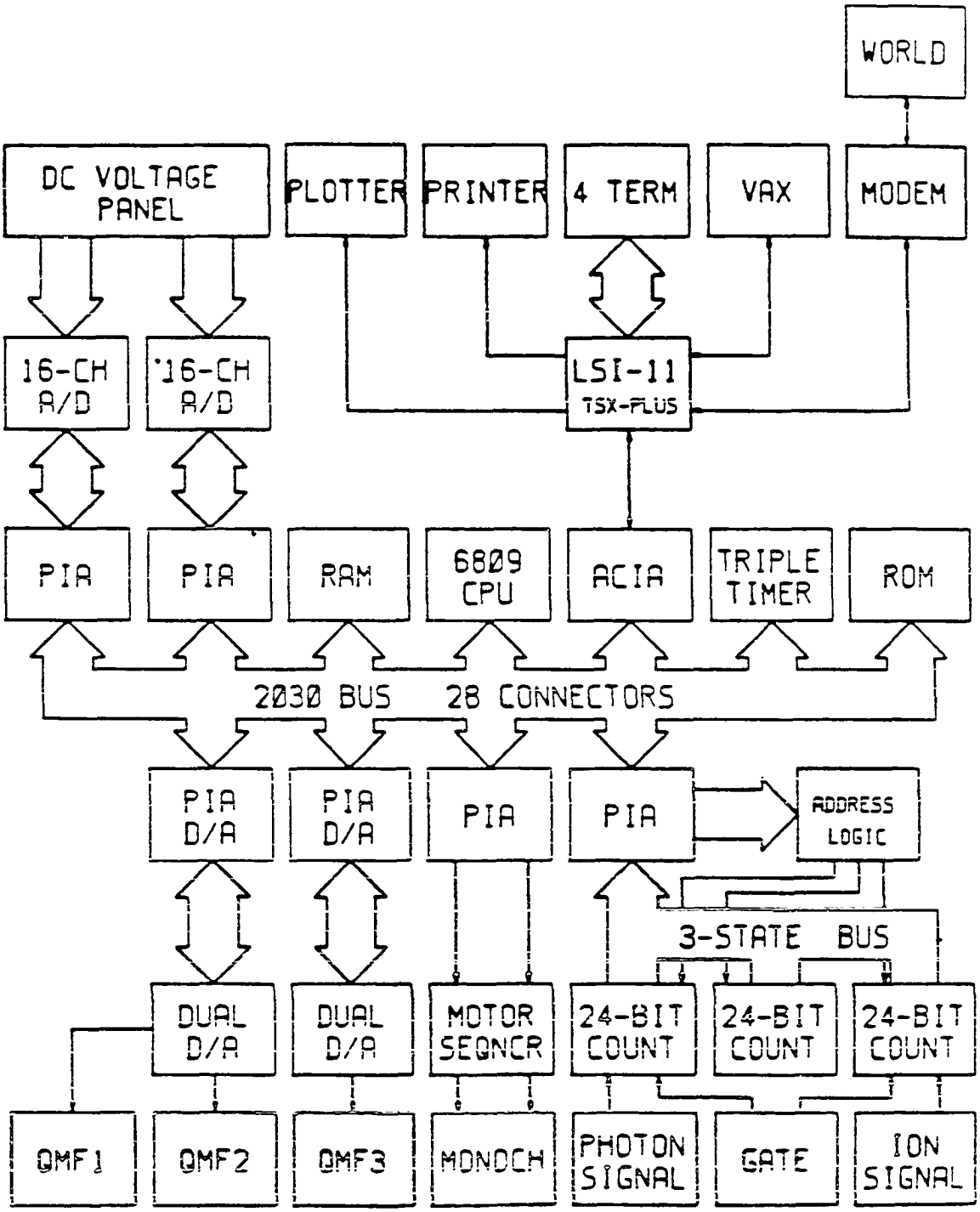
WORLD
DC VOLTAGE PANEL
PLOTTER
PRINTER
4 TERM
VAX
MODEM
16-CH A/D
16-CH A/D
LSI-11 TSX-PLUS
PIA
PIA
RAM
6809 CPU
ACIA
TRIPLE TIMER
ROM
2030 BUS
28 CONNECTORS
PIA D/A
PIA D/A
PIA
PIA
ADDRESS LOGIC
3-STATE BUS
DUAL D/A
DUAL D/A
MOTOR SEQNCR
24-BIT COUNT
24-BIT COUNT
24-BIT COUNT
QMF1
QMF2
QMF3
MONOCH
PHOTON SIGNAL
GATE
ION SIGNAL